CRANFIELD UNIVERSITY

CHRISTOS SKLIROS

SYSTEM DIAGNOSIS FOR AN AUXILIARY POWER UNIT

SCHOOL OF AEROSPACE, TRANSPORT AND MANUFACTURING
Integrated Vehicle Health Management Centre

Doctor of Philosophy
Academic Year: 2019 - 2020

Supervisor: Prof. Ian K. Jennions
Associate Supervisor: Dr. Fakhre Ali
August 2020

CRANFIELD UNIVERSITY

SCHOOL OF AEROSPACE, TRANSPORT AND MANUFACTURING
Integrated Vehicle Health Management Centre

Doctor of Philosophy

Academic Year 2019 - 2020

CHRISTOS SKLIROS

SYSTEM DIAGNOSIS FOR AN AUXILIARY POWER UNIT

Supervisor: Prof. Ian K. Jennions
Associate Supervisor: Dr. Fakhre Ali
August 2020

This thesis is submitted in fulfilment of the requirements for the degree of Doctor of Philosophy

ABSTRACT

Even though the Auxiliary Power Unit (APU) is a widely used system in modern aviation, the existing experimental, simulation and diagnostic studies for this system are very limited. The topic of this project is the System Diagnosis of an APU, and the case study that is used in this research is a Boeing 747 APU.

This APU was used to develop an experimental rig in order to collect performance data under a wide range of loading and environmental conditions. The development of the experimental rig consumed considerable time and required the design and installation of structures and parts related with the control of the APU, the adjustment of the electric and pneumatic load and the data acquisition. The validation of the rig was achieved by a repeatability test, which ensures that the collected measurements are repeatable under the same boundary conditions, and by a consistency test, which ensures that the performance parameters are consistent with the imposed ambient conditions. The experimental data that are extracted from the rig were used to calibrate a physics-based (0-D) model for steady-state conditions.

Data that correspond to faulty conditions were generated by injecting faults in the simulation model. Based on the most prominent APU faults, as reported by The Boeing Company, six components that belong to different sub-systems were considered in the diagnostic analysis, and for each one of them, a single fault mode was simulated. By using healthy and faulty simulation data, for each component under examination, a classification algorithm that can recognise the healthy and faulty state of the component is trained. A critical part of the diagnostic analysis is that each classifier was trained to recognise the healthy and the faulty state of the corresponding component, while other components can be either healthy or faulty. The test results showed that the proposed technique is able to diagnose both single and multiple faults, even though in many cases different component faults resulted in similar fault patterns.

Keywords:

Condition Based Maintenance; Experimental rig; Simulation model; Fault simulations; Diagnostics; System-level diagnostics

ACKNOWLEDGEMENTS

This work is dedicated to my family that supported me throughout the period of my studies.

My supervisor, Prof. Ian Jennions, has been an inspiration for me and through our collaboration, I have developed as an engineer and as a person. Prof. Jennions is an outstanding engineer and an excellent teacher, and I am very grateful for his guidance and advice throughout my PhD studies.

I would also like to thank my secondary supervisors, Dr. Manuel Esperon-Miguez and Dr. Fakhre Ali, for their guidance during this project as well as for the tips they gave me for the life of a PhD student in Cranfield.

Moreover, I would like to especially thank Mr. Scott Booden, who is the Senior Technician of the Gas Turbine Laboratories, for his significant contribution and advice during the development of the Boeing 747 APU rig. Scott is very knowledgeable technician and a very good person, and I really enjoyed working with him. Also, I appreciate the help provided by Mr. Norman Partridge and Mr. Sada Ram during the rig development.

I appreciate the fact that the University's Power and Propulsion Department allowed me to use their facilities to develop the experimental rig of the Boeing 747 APU that is a major part of this project.

Furthermore, I would like to thank The Boeing Company that funded this project and supported me with technical advice during my studies.

It was a very pleasant experience to be a PhD student in the IVHM Centre and I enjoyed the time I spent with the students and staff in the Centre.

Table of Contents

LIST OF FIGURES

LIST OF TABLES

LIST OF EQUATIONS

LIST OF ABBREVIATIONS

AANN	Auto Associative Neural Networks
ANN	Artificial Neural Networks
AHU	Air Handling Unit
APU	Auxiliary Power Unit
AVR	Automatic Voltage Regulator
BAV	Bleed Air Valve
BFSL	Best Fit Straight Line
CBM	Condition Based Maintenance
CI	Condition Indicator
CO	Carbon monoxide
COP	Compressor Outlet Pressure
COT	Compressor Outlet Temperature
CUSUM	Cumulative Sum
DD	Document D-matrix
DLM	Dynamic Linear Model
DRT	Diagnostic Reasoning Techniques
D-S	Dempster-Shafer

DX	Diagnostic Artificial Intelligence
ECS	Environmental Control System
ED	Engineering D-matrix
EFF_{com_final}	Compressor's map efficiency after scaling
$EFF_{com\_initial}$	Compressor's map efficiency before scaling
EFF_{tur_final}	Turbine's map efficiency after scaling
$EFF_{tur\_initial}$	Turbine's map efficiency before scaling
EGT	Exhaust Gas Temperature
EPI	Energy Performance Indices
ETC	Electronic Turbine Controller
EV	Excitation Voltage
$FADEC$	Full Authority Digital Engine Controller
FC	Fault Condition
FDI	Fault Detection and Isolation
FL	Fuzzy Logic
$FMECA$	Failure Mode Effect and Criticality Analysis
FMV	Fuel Metering Valve
GA	Genetic Algorithms
$GLRT$	General Likelihood Ratio Test
GPA	Gas Path Analysis
$HVAC$	Heat Ventilation and Air Condition
$IVHM$	Integrated Vehicle Health Management
KKT	Karush-Kuhn-Tucker
LCV	Load Control Valve
LRU	Line Replaceable Unit
MF_{com_final}	Compressor's map mass flow rate after scaling
$MF_{com\_initial}$	Compressor's map mass flow rate before scaling
MF_{tur_final}	Turbine's map mass flow rate after scaling
$MF_{tur\_initial}$	Turbine's map mass flow rate before scaling
ML	Machine Learning
MRO	Maintenance Repair Overhaul
$MSPCA$	Multi Scale Principal Component Analysis
$N\text{-}R$	Newton-Raphson

NO_X	Oxides of nitrogen
OEM	Original Equipment Manufacturer
PCA	Principal Component Analysis
$P\text{-}I$	Proportional - Integral
PI	Performance Indicators
PLS	Partial Least Square
PR_{com_final}	Compressor's map pressure ratio after scaling
$PR_{com\_initial}$	Compressor's map pressure ratio before scaling
PR_{hp_com}	Health parameter related with the compressor's map pressure ratio
PR_{tur_final}	Turbine's map pressure ratio after scaling
$PR_{tur\_initial}$	Turbine's map pressure ratio before scaling
RUL	Remaining Useful Life
SCV	Surge Control Valve
SF_MF_{com}	Scaling factor for compressor map mass flow rate
SF_PR_{com}	Scaling factor for compressor map pressure ratio
SF_EFF_{com}	Scaling factor for compressor map efficiency
SF_MF_{tur}	Scaling factor for turbine map mass flow rate
SF_PR_{tur}	Scaling factor for turbine pressure ratio
SF_EFF_{tur}	Scaling factor for turbine efficiency
$SPRT$	Sequential Probability Ratio Test
SS	Speed Sensor
SVM	Support Vector Machine
TD	Test Datasets
TIT	Turbine Inlet Temperature
UHB	Unburnt Hydrocarbons

List of Symbols

A	Area
A_{th}	Exhaust nozzle's throat area
$C_{p,air}$	Air specific heat at constant pressure
$C_{p,gas}$	Gas specific heat at constant pressure

D	Diameter
$h_{bur\_total\_in}$	Burner inlet total enthalpy
$h_{bur\_total\_out}$	Burner outlet total enthalpy
$h_{com\_isentropic\_out}$	Compressor's outlet isentropic enthalpy
$h_{com\_total\_in}$	Compressor inlet total enthalpy
$h_{com\_total\_out}$	Compressor outlet total enthalpy
H_f	Fuel lower heating value
h_{th_total}	Total enthalpy at the exhaust nozzle throat
h_{th_static}	Static enthalpy at the exhaust nozzle throat
$h_{tur\_isentropic\_out}$	Turbine's outlet isentropic enthalpy
$h_{tur\_total\_in}$	Turbine inlet total enthalpy
$h_{tur\_total\_out}$	Turbine outlet total enthalpy
I_{load}	Generator current output
J	Joule's constant
L_E	Entrance length
$\dot{m}$	Mass flow rate
$\dot{m}_{bleed}$	Mass flow rate extracted through the LCV
$\dot{m}_{bur\_in}$	Mass flow rate entering the burner
$\dot{m}_{bur\_out}$	Mass flow rate exiting the burner
$\dot{m}_{com\_in}$	Compressor's inlet mass flow rate
$\dot{m}_{com\_map}$	Mass flow rate that corresponds to the operating point on the compressor map
$\dot{m}_{ext}$	mass flow rate extracted from the compressor outlet
$\dot{m}_f$	Fuel flow
$\dot{m}_{hp\_com}$	Health parameter related with the compressor's map mass flow rate
$\dot{m}_{hp\_tur}$	Health parameter related with the turbine's map mass flow rate
$\dot{m}_{in}$	Inlet mass flow
$\dot{m}_{min}$	Minimum mass flow rate extracted to protect the compressor from surge
$\dot{m}_{noz\_in}$	Exhaust nozzle's inlet mass flow rate
$\dot{m}_{noz\_out}$	Exhaust nozzle's outlet mass flow rate
$\dot{m}_{rel}$	Relative mass flow

$\dot{m}_{surge}$	Mass flow rate extracted through the SCV
$\dot{m}_{tur\_in}$	Turbine's inlet mass flow rate
$\dot{m}_{tur\_map}$	Mass flow rate that corresponds to the operating point on the turbine map
N	APU shaft rotational speed
$\dot{N}$	APU shaft acceleration
N_{gen}	Generator rotational speed
P	Power
P_{bl}	Bleed air power
p_{bur_in}	Burner's inlet pressure
p_{bur_out}	Burner's outlet pressure
P_{com}	Compressor power
P_{gen}	Generator power demand
p_{com_in}	Compressor inlet pressure
p_{com_out}	Compressor outlet pressure
p_{in}	Compressor inlet pressure
p_{out}	Compressor outlet pressure
p_s	Static pressure
p_t	Total pressure
p_{tur_in}	Turbine inlet pressure
p_{tur_out}	Turbine outlet pressure
P_{tur}	Turbine power
r	Radial position in the circular duct
R	Circular duct radius
R_{arm}	Generator armature resistance
R_{gas}	Universal Gas Constant
R_{stat}	Generator stator resistance
Re	Reynolds number
T	Temperature
$T_{com\_total\_in}$	Compressor inlet total temperature
T_{in}	Compressor inlet temperature
T_{out}	Compressor outlet temperature
$T_{tur\_total\_in}$	Turbine inlet total temperature

$Torque_{com}$	Compressor's torque
$Torque_{tur}$	Turbine's torque
$Torque_{gen}$	Generator's torque
v	Air velocity
V	Air velocity at the entrance of the circular duct
V_{arm}	Generator armature voltage
V_{ex}	Generator excitation voltage
V_{out}	Generator output voltage
x	Distance from the entrance of the inlet section
X_{in}	Generator windings inductive reactance

List of Greek Symbols

γ	Air heat capacity
$\delta()$	Standard deviation of a quantity
Δp	Differential pressure, the difference between total and static pressure
ΔT	Temperature difference
η	APU efficiency
η_{bur}	Burner's efficiency
η_{hp_com}	Health parameter related with the compressor's map isentropic efficiency
η_{hp_tur}	Health parameter related with the turbine's map isentropic efficiency
η_{com_isen}	Compressor isentropic efficiency
η_{com_pol}	Compressor polytropic efficiency
η_{tur_isen}	Turbine isentropic efficiency
μ	Dynamic viscosity
ρ	Air density
φ	Generator internal magnetic flux

1 INTRODUCTION

All airliners aim to reduce operational costs and maximize profit. A major contributor to operational costs are Maintenance Repair and Overhaul (MRO) activities, as reported by Saxon and Weber [1]. Especially, unscheduled maintenance contributes significantly to airlines operational costs since it is the major cause of flight delays in Europe, as reported by Guest [2].

Aircraft maintenance activities are usually performed on predefined periods or depend on the hours of system operation (preventive maintenance strategy). Under the preventive maintenance strategy, even though maintenance actions are performed regularly, systems and components are not constantly monitored, thus faults can appear unexpectedly. A method to avoid unexpected faults is to monitor the health state of the aircraft components and perform maintenance actions when their performance drops below predefined thresholds (Condition Based Maintenance (CBM)). The application of CBM prevents unscheduled maintenance and can increase aircraft availability as reported by Jennions [3] and Vachtsevanos [4]. A prerequisite for CBM is the monitoring of systems and components performance through appropriately installed sensors. The collected data are processed by appropriate algorithms that can diagnose component faults and propose maintenance actions.

1.1 Project motivation

The topic of this project is the system diagnosis of an aircraft Auxiliary Power Unit (APU). This project has been motivated by The Boeing Company, which funds and supports this project, and considers the APU as a major driver for aircraft maintenance.

The APU is a system which is installed in all large commercial aircraft (normally in the tail section – Figure 1-1), and its purpose is to provide electric power and bleed air to other aircraft systems.

- Electric power is provided to the aircraft electrical system.
- Bleed air is used:
    - As input in the Environmental Control System (ECS).

- As input in the anti-ice system.
- To start the aircraft engines.

The APU is used as an alternative power source to the aircraft and is operated when the aircraft is at the gate or in cases of emergency during fights.

a. The APU on the aircraft [5]

b. The APU removed from the aircraft

Figure 1-1 The Auxiliary Power Unit – a. Boeing 747-200 [5], b. The Boeing 747 APU that was used to set the test rig for this project installed on its cradle

The APU consists of several sub-systems, which transform the fuel chemical energy, to electric energy and pneumatic energy (bleed air). The core subsystem of the APU is a gas turbine which is used to deliver bleed air and provide mechanical energy to an electric generator. Bleed air is either extracted directly from the gas turbine compressor or in modern APUs, is provided by an independent compressor, which is called “load” compressor and is mounted on the same shaft with the gas turbine. Lubrication to the APU bearings is provided by a lubrication system, which is protected from overheating by a cooling system. The fuel flow to the gas turbine is adjusted by the fuel system, which is controlled by the APU control unit. The APU control unit, apart from controlling the fuel flow, monitors the APU operation during starting and steady-state, and if a fault is sensed, it stops the APU in order to protect it from catastrophic damage. In modern systems, the control unit is a Full Authority Digital Engine Controller (FADEC), while in older systems, control units are either hydromechanical or analogue electronic. The electric generator, as well as the pumps of the fuel, lubrication, and cooling systems are mounted on a gearbox and mechanical torque is transmitted to them from the gas turbine shaft. Starting of the APU is

achieved by an electric motor (mounted on the gearbox), which spools up the gas turbine, and an ignition system that is used to initiate fuel combustion.

It can be seen that the APU is a complex system, which consists of numerous components, and can be subject to many different faults. It is noted that a fault in the APU results in the grounding of the entire aircraft. Therefore, the diagnosis of the APU is a topic of significant importance and it is worthy of study.

1.2 Gaps in the literature

The research gaps that are addressed in this project are identified by conducting a literature review on:

- The diagnostic approaches that have been applied to APUs, gas turbine systems, as well as in general complex systems.
- The experimental and simulation studies on APUs and the broader category of gas turbine systems.

This Thesis follows a paper-based format, and the literature review is distributed appropriately in the following chapters.

Chapter 2: The entire paper reviews the diagnostic methods that have been applied to complex systems emphasising the system-level diagnostic approaches.

Chapter 3: In this paper, a thorough review of the experimental studies that have been applied to APUs and gas turbine engines is conducted. Also, some representative simulation studies of the discussed systems are reviewed.

Chapter 4: In this paper, diagnostic and prognostic studies that have been applied specifically on APU systems are reviewed.

In this section, the gaps that have been identified in the literature are presented and following that, the aim and objectives of this project are defined.

Research Gap 1: Diagnostic studies for APU and gas turbine engines mainly focus on the gas turbine sub-system while the other sub-systems are ignored.

The APU belongs in the broader category of gas turbine systems and during the last decades, there have been developed numerous model-based and data-driven diagnostic methods for these systems.

An observation that is extracted by reviewing the various research efforts that have been applied on APU and gas turbine engine systems is that in most cases, the analysis focuses entirely on the gas turbine sub-system, while the rest sub-systems (e.g. fuel, control, lubrication, cooling and generator) are ignored. The public domain literature is missing studies that conduct system-level diagnostic analyses on the discussed systems.

In this project, a diagnostic analysis on a Boeing 747 APU is conducted, including components from the gas turbine, fuel, and control sub-systems as well as the electric generator.

Research Gap 2: Studies discussing experimental data collection from APU or gas turbines are very limited in the public domain literature.

All diagnostic methods that have been reviewed, develop diagnostic rules by comparing healthy and faulty data from the system under examination. These data are usually either collected directly from the aircraft or are generated from validated simulation models. Usually, the validation of the models that are used to simulate the system performance under healthy and faulty conditions is conducted against experimental data. However, research papers that discuss the experimental data collection from APU or gas turbine systems are very limited.

More specifically, the papers that discuss this issue are provided by:

- Siebel et al. [6] who developed a test rig of an APS3200 APU and collected performance, acoustic and exhaust emission data.
- Zanger et al. [7] who discuss the collection of performance and exhaust emission data from a GTCP36-28 APU.
- MacLeod et al. [8] who injected faults in the compressor and the turbine of an Allison T-56 engine and investigate the changes in the performance parameters under faulty conditions.

- Aus Der Wiesche [9] who developed a mobile test rig for a micro gas turbine SPM5 and collected performance data for various shaft loads.

Experimental studies from the discussed systems are not usually found in the public domain literature, for two main reasons:

- The development of experimental rigs for APU and gas turbine engines is an expensive task.
- The technical information that is required for the rig development is only available to system manufacturers.

This Thesis contributes to the literature by providing an experimental investigation of a Boeing 747 APU.

Research Gap 3: Most diagnostic methods for APUs and gas turbines are designed to identify the existence of single component faults, while research efforts that discuss the diagnosis of simultaneous faults are very limited.

By reviewing the relevant literature on APU and gas turbine diagnostics, it is observed that most diagnostic studies are designed to identify single component faults. Methods that are able to diagnose the simultaneous existence of multiple component faults have not been sufficiently discussed.

The most notable approaches regarding multiple fault diagnostics for the discussed systems are presented below.

- Sadough Vanini et al. [10], who used auto-associative neural networks to diagnose single component and sensor faults, as well as the simultaneous existence of a single component and a single sensor fault.
- Joly et al. [11] who proposed a technique for the diagnosis of single and selected multiple faults, by training a neural network for each fault combination that is examined.
- Lee et al. [12] who developed a technique that is able to diagnose the simultaneous existence of a fault in the compressor and the fuel flow sensor.

- Sampath and Singh [13] who applied a technique that combines neural networks with genetic algorithms that is able to diagnose single component or sensor faults and detect the existence of simultaneous component faults (without being able to identify the specific degraded components).
- Guralnik et al. [14] who used Dempster-Shafer (D-S) to integrate the results of independent single-fault diagnostic algorithms in order to calculate the probability of the existence of simultaneous faults in an APU system.

The simultaneous existence of multiple component faults is a common problem in industry; thus, this topic is worthy to study.

In this project, there is proposed a diagnostic technique that is designed to diagnose single and more importantly the simultaneous existence of multiple component faults in a Boeing 747 APU.

1.3 Aim and Objectives

Based on the gaps that have been identified in the literature, the aim and objectives of this project are defined below.

Aim

The aim of this PhD is to diagnose system-level faults, in the presence of multiple other faults, in a Boeing 747 Auxiliary Power Unit (APU).

Objectives

In order to achieve the aim of the project, a series of objectives that include experimentation, simulations, and data analysis need be satisfied. These objectives are described below:

1. Literature review on:
    i. APU, gas turbines and complex systems diagnostics.
    ii. Experimental and simulation studies on APU and gas turbines.
2. Selection of the B747 APU fault modes that will be investigated.
3. Development and validate a test rig of a Boeing 747 APU.

4. Run the APU rig and obtain experimental data under various loads.
5. Calibration of a 0-D simulation model against experimental data collected from the Boeing 747 APU test rig.
6. Run the simulation model with injected faults and assess the sensitivity under the influence of the selected faults.
7. Training of diagnostic classifiers that can diagnose the components health states under single and multiple faults.
8. Testing of the diagnostic classifiers and identification of the strengths and weaknesses of the proposed diagnostic technique.

1.4 Research Methodology and Structure of the Thesis

1.4.1 Research Methodology

The overall research methodology is constructed in order to:

- Set the context of the research by identifying the research gaps.
- Define the aim and objectives.
- Address the project objectives.

The tasks that are performed in this project are split into four stages as shown in Figure 1-2.

The **1st phase** of this project aims to set the research context. This is achieved by reviewing the relevant literature, and by identifying the research gaps that will be addressed in this project. Following that, the aim of the project and the objectives that should be covered are defined. Based on the project objectives, the 2nd and 3rd phases of the project are constructed.

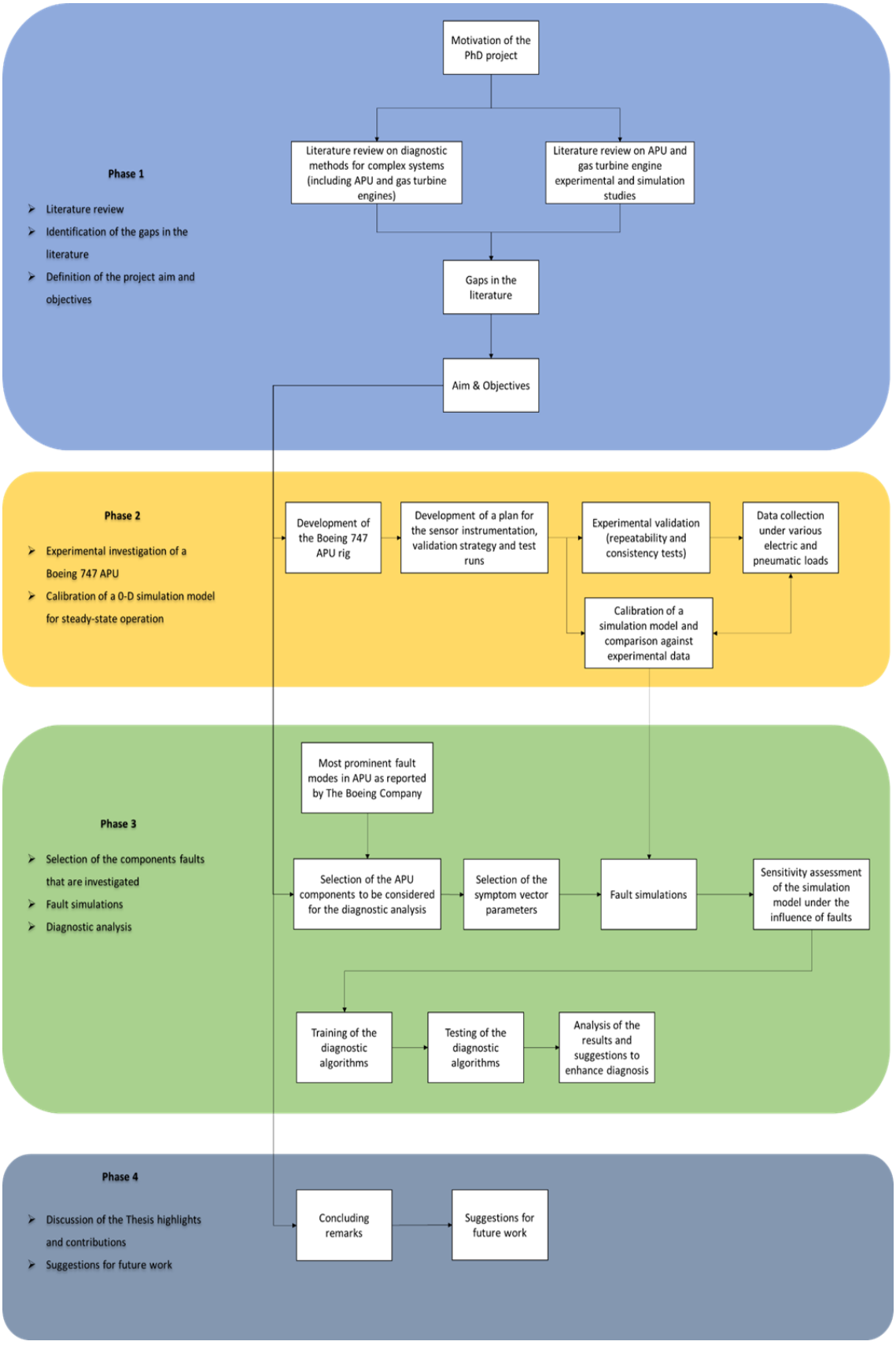

Figure 1-2 Methodology Flowchart

The **2nd phase** of this project discusses the experimental investigation of a Boeing 747 APU and the development of a simulation model for this APU. The aspects that are discussed during the experimental investigation involve:

- The tasks that are required to start, stop, and monitor the rig.
- The components that were installed on the rig to adjust the bleed flow and electric power.
- The instrumentation and testing strategy.
- The rig's validation process.
- The data collection and uncertainty analysis.
- The changes in the APU performance parameters under varying power settings.

Furthermore, during the validation process, a 0-D simulation model of the APU is calibrated against experimental data. One of the purposes of this task is to contribute in the validation of the experimental rig by comparing the experimental and simulation data. Also, since the calibrated model is based on physics, it can be trusted to emulate component faults, and for this reason, it is used in the 3rd phase of this project to simulate healthy and faulty conditions.

In the **3rd phase** of the project, the simulation model that was previously calibrated is used to simulate the APU performance under faulty conditions. The healthy and faulty datasets that are generated from the simulation model are used to develop a diagnostic technique that is able to identify single and multiple faults.

The selection of the components that are considered in the fault simulations and diagnostic analysis is driven by two factors:

- The selected components are included in a list of the most prominent APU faults, as reported by The Boeing Company.
- The selected components belong to various subsystems (gas turbine, fuel and control sub-system and the electric generator), in order to conduct a system-level diagnostic analysis.

The model's sensitivity under the influence of the component faults is assessed. Based on the sensitivity analysis, the degradation ranges of the simulated component faults are selected.

The healthy and faulty datasets that are generated form the simulation model are used to train a classification algorithm for each component under examination. Each classification algorithm is designed to identify the health state of the corresponding component, while other components can be either healthy or faulty. Finally, the results of the proposed technique are tested against datasets that have been generated independently from the training datasets and the strengths and weaknesses of this analysis are discussed.

In the **4th phase** of the Thesis, the most important parts of this research are highlighted and areas for future research are proposed.

1.4.2 Structure of the Thesis

This Thesis follows the paper-based format and includes five chapters. Chapters 2-4 are reformatted versions of published papers (no text changes). The concluding remarks of this work and suggestions for future research are included in Chapter 5. In this section, brief overviews of Chapters 2-5 are given.

Chapter 2: A Review of Model-Based and Data-Driven Methods Targeting Hardware Systems Diagnostics

This chapter covers a major part of the literature review. It provides a comprehensive literature review of the various diagnostic methods and techniques that have been applied to complex systems.

In this chapter, a taxonomy of the various diagnostic methods is proposed, and the advantages and limitations of each method are discussed. Also, special emphasis is given on the discussion of system-level diagnostic approaches.

The outcomes of this chapter:

- Aid in the identification of the gaps in the literature.
- Contribute to the selection of the most appropriate diagnostic technique to be applied in this project.

This chapter is a reformatted version of the paper:

Skliros, C., Esperon Miguez, M., Fakhre, A., and Jennions, I. (2019). A review of model-based and data-driven methods targeting hardware systems diagnostics. Diagnostyka, 20(1), pp.3-21. https://doi.org/10.29354/diag/99603

Chapter 3: Experimental Investigation and Simulation for a Boeing 747 Auxiliary Power Unit

This chapter describes the experimental investigation of a Boeing 747 APU and the calibration of a 0-D simulation model. This chapter covers the 2nd stage of the methodology that is described above. This chapter is a reformatted version of the paper:

Skliros, C., Fakhre, A., and Jennions, I. K. (July 13, 2020). "Experimental Investigation and Simulation of a Boeing 747 Auxiliary Power Unit." ASME. J. Eng. Gas Turbines Power. doi: https://doi.org/10.1115/1.4047771

Chapter 4: Fault Simulations and Diagnostics of a Boeing 747 Auxiliary Power Unit

This chapter describes the fault simulations and the diagnostic analysis that is applied to the Boeing 747 APU. This chapter covers the 3rd stage of the methodology that is described above. This chapter is a reformatted version of the paper:

Skliros, C., Fakhre, A., and Jennions, I. K. (2020) "Fault Simulations and Diagnostics of a Boeing 747 Auxiliary Power Unit." (Submitted to Expert Systems with Applications)

Chapter 5: Concluding remarks

This chapter includes the conclusion of the Thesis and proposes areas for future research.

1.5 References

[1] S. Saxon and M. Weber, “A Better Approach to airline costs,” *McKinsey & Company Travel, Transport & Logistics*. McKinsey&Company, 2017, available at: https://www.mckinsey.com/industries/travel-transport-and-logistics/our-insights/a-better-approach-to-airline-costs.

[2] T. Guest, “A Matter of Time : Air Traffic Delay in Europe,” *Eurocontrol*. Eurocontrol, 2007.

[3] I. K. Jennions, Ed., *Integrated Vehicle Health Management - Perspectives on an Emerging Field*. SAE International, 2011.

[4] G. Vachtsevanos, F. Lewis, M. J. Roemer, A. Hess, and B. Wu, *Intelligent Fault Diagnosis and Prognosis for Engineering Systems*. John Wiley & Sons, Inc., 2006.

[5] Boeing 747-200 By Aldo Bidini, August 1990, accessed at 13 October 2020, available at: http://www.airliners.net/photo/Alitalia/Boeing-747-243B/1200648/L/&sid=f499b3169d12a0d4f410846e6512443a, GFDL 1.2, https://commons.wikimedia.org/w/index.php?curid=27438693.

[6] T. Siebel, J. Zanger, A. Huber, M. Aigner, K. Knobloch, and F. Bake, “Experimental investigation of cycle properties, noise, and air pollutant emissions of an APS3200 auxiliary power unit,” *J. Eng. Gas Turbines Power*, vol. 140, no. 6, pp. 1–9, 2018.

[7] J. Zanger, T. Krummrein, T. Siebel, and J. Roth, “Characterization of an Aircraft Auxiliary Power Unit Test Rig for Cycle Optimization Studies,” *J. Eng. Gas Turbines Power*, vol. 141, no. 1, pp. 1–9, 2019.

[8] J. D. MacLeod, V. Taylor, and M. J. C. G. Laflamme, “Implanted component faults and their effects on gas turbine engine performance,” *J. Eng. Gas Turbine Power*, vol. 114, no. 174, 1992.

[9] S. Aus Der Wiesche, “A mobile test rig for micro gas turbines based on a thermal power measurement approach,” *J. Eng. Gas Turbines Power*, vol.

134, pp. 467–477, 2012.

[10] Z. N. Sadough Vanini, N. Meskin, and K. Khorasani, “Multiple-model sensor and components fault diagnosis in gas turbine engines using autoassociative neural networks,” *J. Eng. Gas Turbines Power*, vol. 136, no. 9, pp. 1–16, 2014.

[11] R. B. Joly, S. O. T. Ogaji, R. Singh, and S. D. Probert, “Gas-turbine diagnostics using artificial neural-networks for a high bypass ratio military turbofan engine,” *Appl. Energy*, vol. 78, no. 4, pp. 397–418, 2004.

[12] Y. K. Lee, D. N. Mavris, V. V. Volovoi, M. Yuan, and T. Fisher, “A fault diagnosis method for industrial gas turbines using Bayesian data analysis,” *J. Eng. Gas Turbines Power*, vol. 132, no. 4, pp. 1–6, 2010.

[13] S. Sampath and R. Singh, “An integrated fault diagnostics model using genetic algorithm and neural networks,” *J. Eng. Gas Turbines Power*, vol. 128, no. 1, pp. 49–56, 2006.

[14] V. Guralnik, D. Mylaraswamy and H. Voges, "On handling dependent evidence and multiple faults in knowledge fusion for engine health management," 2006 IEEE Aerospace Conference, Big Sky, MT, 2006, pp. 9 pp.-, doi: 10.1109/AERO.2006.1656100.

2 A REVIEW OF MODEL-BASED AND DATA-DRIVEN METHODS TARGETING HARDWARE SYSTEMS DIAGNOSTICS

System health diagnosis serves as an underpinning enabler for enhanced safety and optimized maintenance tasks in complex assets. In the past four decades, a wide range of diagnostic methods have been proposed, focusing either on system or component level. Currently, one of the most quickly emerging concepts within the diagnostic community is system-level diagnostics. This approach targets in accurately detecting faults and suggesting to the maintainers a component to be replaced in order to restore the system to a healthy state. System-level diagnostics is of great value to complex systems whose downtime due to faults is expensive. This paper aims to provide a comprehensive review of the most recent diagnostics approaches applied to hardware systems. The main objective of this paper is to introduce the concept of system-level diagnostics and review and evaluate the collated approaches. In order to achieve this, a comprehensive review of the most recent diagnostic methods implemented for hardware systems or components is conducted, highlighting merits and shortfalls.

2.1 Introduction

Integrated Vehicle Health Management (IVHM), as reported by Jennions [1], is a capability that enables condition monitoring of high value industrial assets and offers numerous services to stakeholders. IVHM outputs can be applied to optimize individual project plans as well as an organization's overall business plan. The understanding of a system's fault modes can provide feedback for the design of new products that can then be made to be more robust to faults and embed intelligent fault detection features.

As reported by Mobley [2] and Evans and Annunziata [3], maintenance costs contribute significantly to the overall operational cost of high value industrial assets. Thus, optimization of maintenance activities can substantially contribute to overall operational cost reduction. One of the most important services that IVHM can provide is a provision of Condition Based Maintenance (CBM) as

reported by Esperon-Miguez [4]. As discussed by Pelham et al. [5], CBM targets in suggesting maintenance actions before the performance of an asset has deteriorated to a level that will lead to an unscheduled interruption of its operation as reported by. This leads to improved and more robust maintenance plans and potential cost reduction strategies. CBM is based on the implementation of intelligent diagnostic and prognostic methods. Diagnostics is a process of accurately detecting system faults and isolating their root cause. Prognostics moves a step further and targets in identifying the Remaining Useful Life of a system or a component before its replacement. There has been a profound interest from both Original Equipment Manufacturers (OEMs) and operators to advance their level of scientific understanding in the subject area in order to provision optimized maintenance scheduling of high value assets as well as to better align their business models to market needs [1].

The main contribution of this paper is a review and discussion of system-level diagnostics. A literature review of publications developed under this approach is conducted. A discussion is offered that identifies the main features of this approach, merits it can provide, limitations it faces and areas of further research.

In order to set the framework for system diagnostics, a review of existing diagnostic methods is presented. An algorithm-based taxonomy of existing methods is proposed. A literature review of the most recent and representative techniques of its respective category is conducted. Advantages and disadvantages of each category are outlined and the way these techniques were applied to system-level diagnostics is discussed.

2.1.1 Scope of the present chapter

System level diagnostics approach is especially beneficial in applications of high value industrial assets whose downtime for unscheduled maintenance is expensive. This approach suggests quickly and accurately to a system’s maintainer the component that should be replaced to restore the asset to operational condition.

A definition of “system” in engineering terms is quite generic. In this paper, the concept of a system will be limited to a hardware system which consists of components that can be physically replaced. Approaches as the examples discussed by Piel Eric et al. [6], that consider a computer software as a system and the lines of the code as its components will not be considered.

Diagnostic methods developed so far focus on the component level and, sometimes, on the system level. In order to clarify this distinction, an example of a compressor (component) in a gas turbine engine (system) is considered. Applying a diagnostic analysis on the engine (system level), the major interest is detecting a fault in the system and identifying the component (e.g. compressor) that if replaced will restore the system to the healthy state. Under a system level diagnostic analysis, the root cause of the component’s fault is not the main concern. In the example of the compressor fault as reported by Ogaji et al. [7], the root cause could be related to fouling, tip clearance, erosion, corrosion, foreign object damage.

In the light of the aforementioned background, the main objective of this paper is to review and discuss the work conducted on system-level diagnostics. The main features of this approach are introduced, methods that were developed under this approach are presented along with their advantages and limitations.

The discussion of system-level diagnostics prerequisites a review and discussion of the main features, advantages, and shortfalls of existing diagnostic methods. The quest for each stakeholder is to employ the most suitable diagnostic method(s) that will enable the optimum utilization of the data acquired from their asset of interest to optimize maintenance. Therefore, knowledge of the key pros and cons of each available method plays a vital role on provision the implementation of the most suitable diagnostic method. Thus, another contribution of this paper is a review and discussion of the most recent public domain literature dedicated towards the diagnostic problems. A taxonomy that categorizes diagnostic methodologies based on the algorithms they use is proposed. Initially, diagnostic reasoning techniques that can be used individually or in combination with other diagnostic methodologies are presented. This paper

details model-based, and data-driven methods. Methodologies based on expert systems are outlined since they offer a unique approach, but the discussion conducted is limited. Finally, applications of combining model based and data driven methods and creating hybrid techniques are described.

It is to be noted that the aim of this work is not to conduct an exhaustive search of publications of each category but to discuss the most recent work conducted under each respective approach. This work refers to methods that have been developed in order to apply diagnostics in a systematic way. However, it should be mentioned that since diagnostics is an engineering problem, heuristic methods can always be part of the solution (e.g. cracks or leaks at mechanical systems can be discovered with visual inspections or non-destructive inspections as reported by Staszewski et al. [8]).

The remaining part of this paper is organized as follows. In section 2, a taxonomy of diagnostic methods is proposed, and fault reasoning techniques are presented. In section 3, rule and case-based reasoning methods are presented. In section 4, model-based diagnostic techniques are illustrated, while in section 5 data-driven techniques are described. In section 6, hybrid techniques that combine model-based and data-driven methods are outlined. In Section 7, the system-level diagnostic concept is presented, and a literature review of the most important publications is conducted. In Section 8 and 9, a detailed discussion and concluding remarks are elaborated, respectively.

2.2 Taxonomy of diagnostic methods and diagnostic reasoning techniques

Categorization of diagnostic methods can be conducted in many ways depending on predefined criteria. For example, a taxonomy of diagnostic algorithms can target to categorize methods based on their application to various fault severity modes (e.g. minor degradation, major degradation, complete destruction). Another categorization of diagnostic methods can separate them in qualitative methods that conduct the analysis using qualitative criteria of system parameters (e.g. increase in a temperature, decrease in mass flow), or in quantitative methods that extract their results by comparing system parameters on predefined

thresholds (e.g. component electrical resistant higher that 10 kΩ). In this paper, a taxonomy of diagnostic methods is proposed using an algorithm-based perspective. Figure 2-1 presents a taxonomy of the compiled diagnostic methods. Under this approach diagnostic methods are categorized based on the features of the algorithms they are using, regardless of qualitative or quantitative characteristics. Existing diagnostic methods in the literature can be characterized into three main categories:

1. Model-Based Methods (Physics based)
2. Data-Driven Methods (Artificial intelligence, Statistics)
3. Expert System Methods (Rule-based or Case-based reasoning)

A discussion that is conducted for each respective category informs the reader for the inputs each one requires and compares their advantages and disadvantages. Also, the analysis of each respective category compares the advantages and shortfalls of various algorithms in each category (e.g. accuracy, response time, ease of application).

At this section, techniques that can be used in combination with the diagnostic methods and will be referred in this paper as “Diagnostic Reasoning Techniques (DRT)” will be presented. DRT can either be used individually when conducting a diagnostic analysis or can be used as a pre-processor in order to enhance the accuracy and response time of the results. The most widely used DRT are Failure Mode Effect and Criticality Analysis (FMECA), Decision (Fault) Trees, Directed Graphs and Decision Matrices (D-Matrices).

A FMECA breaks down the system into its subsystems and components and works in a bottom-up way starting from the failure modes each component can present and propagates its effects upwards to the higher system levels. As it is described by Ben-Daya et al. [9], a system’s FMECA analysis answers the questions: “what problems could arise?”, “how likely are these problems to occur and how serious are they if they happen?”, “how can these problems be prevented?”. Mehdi et al. [10] conducted a FMECA study on an industrial gas turbine. The analysis conducted had two branches. Two separate FMECA are conducted on the gas generator subsystem and on the lubrication subsystem.

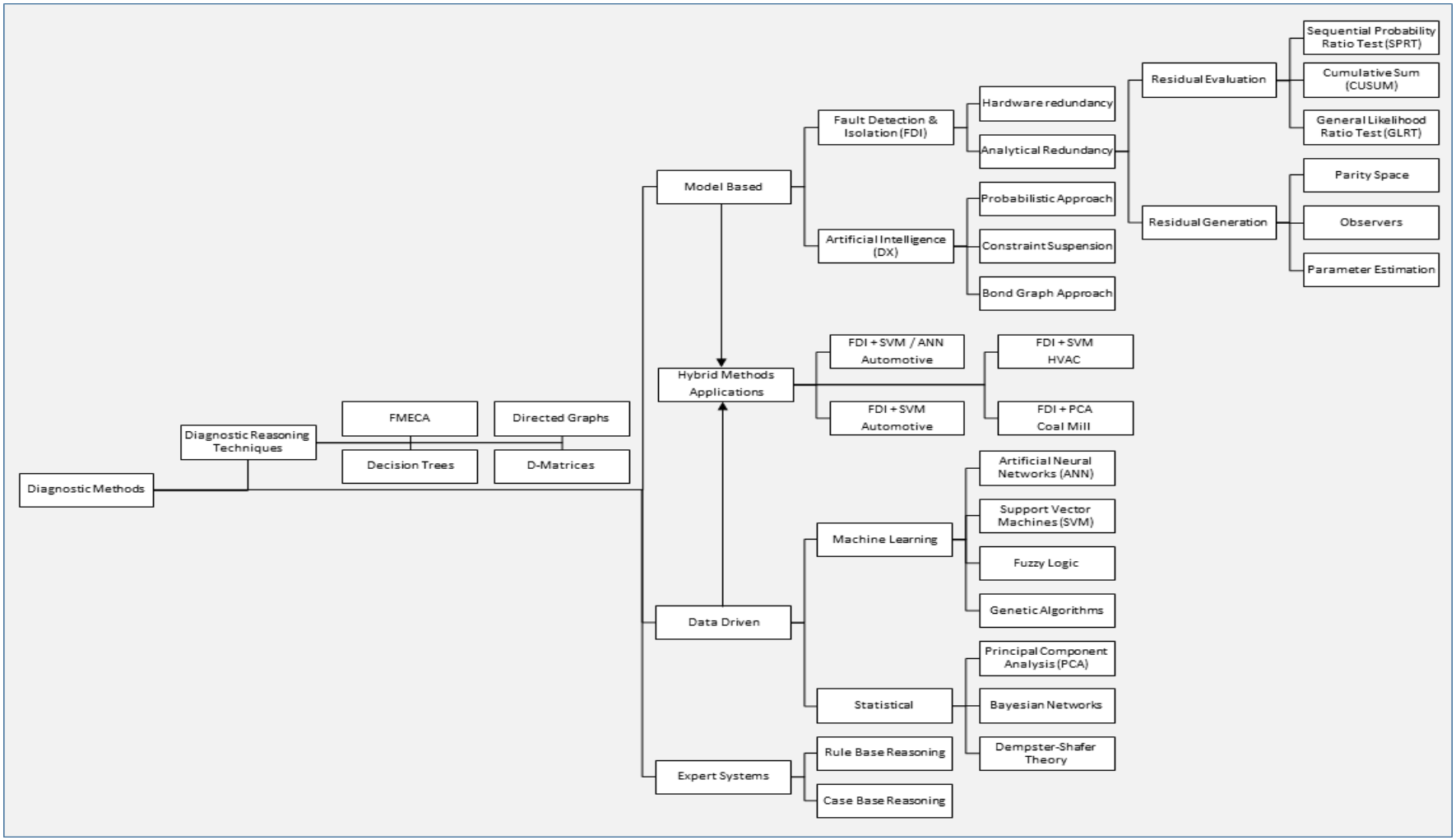

Figure 2-1 Taxonomy of Diagnostic Methods & Diagnostic Reasoning Techniques

The FMECA was based on one-dimensional models of the respective subsystems. The results of this study could identify failure modes in components in each respective subsystem, based on their effect on the overall system performance. Another application of FMECA, as suggested by Saha and Vachtsevanos [11], is that it can provide a database of system fault modes, which a diagnostic method should target to identify.

A Decision Tree models the system in the same way as a FMECA (higher levels-major subsystems, lower levels-components). However, the diagnostic analysis is conducted by traversing the tree top-down. Higher level nodes are related to major subsystems and lower level nodes correspond to components or different failure modes in the same component. At every node of the tree, a system's parameter is compared to a baseline value and depending on the result of the comparison lower branches of the tree are being excluded. The algorithm terminates when it reaches the lowest nodes of the tree. Depending on the fault modes that the analysis targets to capture, different architectures can be developed. For example, in a pipe fault case, the decision tree should be constructed differently depending if the analysis just targets to capture the faulty pipe or it targets to capture the root cause of the pipe failure (e.g. leakage, blockage). Bartlett et al. [12] and Papadopoulos [13], developed two similar fault tree methods of an aircraft fuel system. Fuel tank imbalance faults were considered at higher levels of the trees, and faults such as pump failure or pipe leakage were modelled on the lower levels. The proposed methodologies could capture the injected faults. Ambiguity groups among some components were developed in few cases.

Another way of identifying possible system and component fault modes is the Directed Graph analysis. The nodes of the directed graph represent the system components failure modes and are connected with directed and weighted edges. The edges indicate the effect that a component fault has on other components that are connected with. Starting from a node where the observed values deviate from normal, the algorithm back-traces the directed graph and all possible fault combinations can be identified. Bartlett et al. [12] conducted a diagnostic analysis

on an aircraft fuel system, using a directed graph. In this case study, a blocked valve node is connected to a fuel flow node with a weight of “-10”, while nodes of pipes that have normal fuel flow operation are connected with a weight of “+1”.

Considering a system with its corresponding sensors, a Decision Matrix (D-Matrix) is a table with its columns and rows corresponding to the system failure modes and sensors, respectively. The values of the matrix can be either binary or real numbers and represent the way each failure mode is reflected to each sensor. Singh et al. [14] review different techniques for creating and integrating D-matrices. The D-matrices are separated into three categories; Engineering D-matrix (ED), which is extracted from a physics based analysis of the system; Document D-matrix (DD), which is extracted from maintenance logs and Historic D-matrix, which can be built utilizing historic knowledge that correlates various symptoms to their corresponding failure modes. Integration of diverse types of D-matrices requires expert or domain knowledge of the application under examination. By using a D-Matrix, the designer understands the critical measurements that reflect each component’s health state. This can result in the development of more accurate and faster diagnostic rules.

2.3 Expert systems

Expert system methods contain the rule-based reasoning approach and the case-based reasoning approach. Rule based reasoning is a technique in which the diagnostic results are extracted by propagating the system’s observations through a set of rules. The embedded rules are derived from the knowledge of an expert or a group of experts. An expert system is defined by Durkin [15] as: “A computer program designed to model the problem solving ability of a human expert”. There are two ways of building an expert system, forward chaining reasoning and backward chaining reasoning. The forward chaining technique propagates the system observations through the expert system’s rules and has diagnostic results as its output. In the backward chaining, a fault hypothesis is initially suspected, and the expert system investigates if the hypothesis can be supported from the observations, using a predefined set of rules.

Case base reasoning is a methodology of solving an existing problem based on the knowledge acquired by solving the same or similar problems in the past. Under the case base reasoning approach, old solutions and outputs of old problems that are similar to the case under examination are collected. Selecting the old case that most resembles the case under examination, based on predefined criteria, an initial solution is proposed. Through a series of steps involving adjustment and modification of the initial solution, the final solution is extracted. In the case of diagnostics, the solution may have the form of a specific failure mode on a system.

The methods of rule and case-based reasoning require the system expert knowledge of experienced personnel or a large historic database of solutions of various cases. Both prerequisites are hard to acquire in many cases. When a diagnostic analysis is conducted based on limited experience of the system failure modes, the corresponding symptoms or successful troubleshooting actions, the rule and case base reasoning methods are not applicable. This paper focuses on reviewing the developed diagnostic methods in applications where little or no historic knowledge of the system failures and troubleshooting is available. To this end, the next sections discuss model based and data driven methods in more detail.

2.4 Model-based methods

Model-based methods use a physics model of the system or component under examination, to conduct the analysis. Physical parameters calculated by the model are compared with system observations and by using various techniques, faults can be detected, and their root cause can be isolated. Model based methods can be further separated into two major categories, an approach developed by the Control Engineering community, Fault Detection and Isolation (FDI), and an approach developed by the Diagnostic Artificial Intelligence (DX) community.

2.4.1 Scope of the present chapter

Considering a physical system, the FDI approach considers two alternative methods, hardware redundancy and analytical redundancy. The methodology used by both techniques is based on creating redundant information for a system under examination. By analysing the residual vector created by comparing the redundant system information to the observed measurements, faults can be detected. In hardware redundancy, redundant information is generated from a hardware module (component or sensor) that operates in parallel with the main hardware module. In analytical redundancy, a system simulation model generates the redundant information.

2.4.1.1 Hardware redundancy

Hardware redundancy is a method that has been applied mostly in the designing of fault tolerant systems. The main target of hardware redundancy is to guarantee the safety of the system when a component or sensor fails. This is accomplished by installing redundant hardware (components or sensors) operating in parallel. A major disadvantage of hardware redundancy is that increases in system size, weight, power consumption and cost as reported by Dubrova [16].

Hardware redundancy has fault detection capabilities as reported by Ferrara [17]. This is accomplished by considering two system modules (components or sensors) that work in parallel and a comparator box that compares the modules values. A fault can be detected when an inconsistency is observed. As discussed by Dubrova [16], this technique cannot isolate the faulty module, but it can detect a fault in one of the two compared modules as reported by.

2.4.1.2 Analytical redundancy

Analytical redundancy methods conduct an analysis on the residual between a system's observations to its simulation model. An analysis is conducted on the generated residual in order to detect faults in the system (residual evaluation). Analytical redundancy algorithms target in creating residuals insensitive to sensor and process noise but sensitive to system faults (residual generation). The generated residual must be close to zero at a system's healthy state and greater

than zero when faults exist. The main advantage of analytical redundancy compared to hardware redundancy is that this technique does not require additional hardware. On the other hand, a limitation of this method is that diagnostic accuracy is highly dependent on the fidelity of the simulation model.

Residual evaluation targets in decreasing the false alarm rates and building algorithms robust to noise. Statistical hypothesis testing techniques are used for residual evaluation. As explained by Shi and Tao [18], the null hypothesis is defined as the fault free case. Observing the system parameters, if the null hypothesis is considered to hold, no faults are detected. When the null hypothesis is no longer valid, a fault is detected. Rejecting or confirming the null hypothesis is based on rules derived from probability theory. For example, if a 95% confidence rule is set, having a dataset of pressure measurements against time and 95% of the measurements are within a predefined healthy threshold the system can be considered healthy, otherwise, a fault is detected. The most popular hypothesis testing algorithms used in diagnostics are: Sequential Probability Ratio Test (SPRT) [19], Cumulative Sum (CUSUM) algorithm [20] and General Likelihood Ratio Test (GLRT) [18]. Hypothesis testing algorithms can be designed to detect either single faults or multiple faults as reported by Basseville and Nikiforov [21].

The residual (parity) space method is a residual generation technique. Under this approach, system inputs and outputs are represented by vectors. Using a simulation model that is built on mathematical equations, output system values are predicted. Thus, the residual is the algebraic difference of the observed and the simulated output vector. The simulated output vector depends on constants defined in the system's mathematical equations. As discussed by Patton and Chen [22], these constants are selected in such a way that produce a residual close to zero at a fault free case and residuals higher than zero when faults exist. A fault diagnostic analysis based on parity space method was conducted by Höfling and Isermann [23] on a brushless DC motor. The proposed methodology considered the mechanical and the electrical system of the motor operating in

isolation (no interconnection between them) and could accurately detected injected faults in each one of them.

An alternative technique for residual generation is based on optimal estimation algorithms (observers). As reported by Patton and Chen [24], the difference this technique has compared to parity space method is that a system's simulation model is not based on mathematical equations but on optimal estimation algorithms (Kalman filter, weighted least square, etc.) that can estimate a system's outputs based on its inputs. Under this approach, selected faults can be isolated. This can be done by considering all other faults as noise and selecting the constants of the simulation model appropriately in order to produce residual higher than zero only in the presence of a predefined fault Case studies that apply the discussed method have been provided by White and Speyer [25], Frank [26], [27], Hwang et al. [28] and Patton et al. [29].

Isermann [30], [31] used another residual generation technique which is called parameter estimation. Under this technique, a system is modelled using mathematical equations and deviation of its nominal operation (healthy state) can be modelled by adjusting properly equations parameters. These parameters represent features of the physical components, e.g. resistance for electrical components, or effectiveness for mechanical components. Based on the observed input and output measurements, the physical parameters can be estimated using optimal estimation techniques (Kalman filter [32], [33], weighted least squares [34]). Faults are detected by correlating parameters that deviated from their nominal baseline to system components. For example, a decrease in the value of a parameter representing a heat exchanger's efficiency in an air conditioning system, suggests degradation in the heat exchanger component. Moseler and Isermann [35] used the parameter estimation technique to diagnose faults on an D.C. motor, by considering separately the mechanical subsystem and the electrical subsystem of the motor. Two faults were injected into each respective subsystem and the proposed methodology could capture the deviations on the physical parameter values and attribute the faults to the respective components. Parameter estimation, has been widely applied in gas

turbine diagnostics (Gas Path Analysis - GPA), initially by Urban [36] and further developed by Doel [34], [37], [38], Stamatis et al. [39], [40], and Volponi [41].

2.4.2 Diagnostic Artificial Intelligence (DX)

A model based approach to detect and isolate systems faults was developed by Davis [42] in the Diagnostic Artificial Intelligence (DX) community. This approach models a system as a network of interconnected components and each component is modelled by physical equations (constraints) that describe its nominal operation. Providing input values to the model, physical parameters can be calculated at the input and output of all components. As described by Kolcio et al. [43], a fault is detected when the estimated physical parameter values (model) deviate from observed physical parameter values (sensors).

2.4.2.1 Fault detection challenges

Fault detection is highly dependent on the model's accuracy. Kolcio et al. [43] developed a method of adjusting properly the component equations to be insensitive to noise and disturbances, but sensitive to faults. Based on the complexity of the modelled system and the model's capability of incorporating noise and disturbances, there can be used either fixed thresholds, as proposed by Fesq [44], or adaptive thresholds as proposed by Kolcio et al. [45] and Rossi et al. [46], [47].

A major obstacle observed in general in all fault diagnostic applications is a trade-off between probabilities of false alarms to probabilities of misdetections. Under the DX approach, Rossi [46] developed a technique that was able to quantify these probabilities and select a fault detection threshold that could minimize them. Another method of controlling false alarms to misdetections ratio was proposed by Kolcio and Fesq [48]. Under the latter approach, for every observed parameter, a rule is defined that the fault threshold should be exceeded at least "x" times at "y" consecutive time slices, in order for a fault to be detected.

2.4.2.2 Fault isolation challenges

At the fault isolation step, based on the functional interconnections among the components, all possible combinations of components that can theoretically be

faulty are identified. The number of the identified sets grows exponentially in the number of components. In cases of complex systems with many components, as reported by De Kleer and Kurien [49] and Stern et al. [50] the exhaustive search algorithm for identifying possibly faulty components, leads to algorithms with high computational time. Stochastic algorithms, as proposed by Feldman et al. [51] and machine learning algorithms, as proposed by Keren et al. [52] have been used to solve the problem more efficiently.

One of the main techniques used for fault isolation is the probabilistic reasoning approach. Under this technique, a probability is assigned to each set of possibly faulty components, based on the existing observations (available sensor measurements). The assigned probabilities are based on Bayes rule and are updated every time a new sensor observation becomes available. As reported by De Kleer and Kurien [49], a-priori probabilities that are used in Bayes rules are usually calculated from statistical data describing component faults. Stern et al. [50] proposed another methodology of assigning probabilities to components being faulty. At this methodology, each component is assigned a probability of being faulty, not based on the available sensor measurements, but based on the number of possibly faulty sets it is contained in. It was proved that the latter approach can produce accurate fault isolation results without considering all possible fault combinations of faulty components, thus the computational time of the method was reduced.

Constraint suspension introduced by Davis [42] is an alternative fault isolation technique. Under this approach, components are serially excluded from the system model and physical parameter values are not propagated through their equations. Every time a component is excluded, values of system's physical parameters are propagated through the remaining model components. If inconsistencies continue to be present between the estimated and the observed values, then the suspended component is not considered to be faulty. However, if after excluding a component, estimated and observed values are consistent, this component is suspected to be faulty.

As reported by Fesq [44] and Kolcio and Fesq [48], a limitation this technique faces is that there may be cases where the suspension of a component may result in insufficient number of parameter values to conduct consistency check for all remaining components. In such cases, ambiguity groups are created. A component *"comp_1"* belongs to the ambiguity group of component *"comp_2"* if by excluding component *"comp_2"* from the model, consistency check cannot be conducted to the input and output values of component *"comp_1".* In the study that is conducted by Kolcio et al. [53], it is concluded that the formation of ambiguity groups depends on the existing sensor suite, the equations used for modelling components and the connection types. A case study on the NASA rover's power system was conducted by [53] comparing the ambiguity groups formatted depending on the different sensor suites installed. The selection of the appropriate sensor suite depends on the specific application in order the algorithm to be able to identify faults and usually it targets the most critical components.

2.4.2.3 Bond graphs technique

Another fault diagnostic approach has been developed by Mosterman et al. [54], [55], Daigle et al. [56] and Narasimhan and Biswas [57], and is based on system modelling using bond graphs. Using a bond graph model, cause-effect relationships can be developed among the system's physical parameters. For example, fluid pressure (cause) in a tank can generate fluid flow (effect) in a pipe. When faults occur, positive or negative deviations (inconsistencies) are captured between the observed and the modelled values of the system's causes or effects. Based on the deviation of its nominal value (increase or decrease) cause-effect relationships can detect possible qualitative deviations of component characteristics (decrease in the effectiveness of mechanical components). In most applications, there exist more than one faulty candidate components. In such cases, each candidate fault generates a different rate of change of the model's physical values (causes and effects). Comparing each fault's cause-effect deviation signature, with measured system's values, the faulty component can be isolated.

2.5 Data-driven methods

Diagnostic analysis conducted by data-driven methods is based on machine learning algorithms and statistical algorithms. Data-driven algorithms correlate system observed measurements with a health state (healthy or faulty) and classification problems (machine learning) or assign a probability of a system or a component being healthy or faulty (statistical). These techniques have been proved to be successful in isolating both component and sensor faults.

It is noted that the methods that will be presented in the next sections are some representative techniques applied in diagnostics. There exist many different variations of data-driven algorithms. For example, there have been developed different types of Artificial Neural Networks (Probabilistic, Dynamic, etc.) or different dimensionality reduction algorithms (Principal Component Analysis, Non-Linear Principal Component Analysis, Partial Least Squares, etc.) that are not explicitly discussed in this paper. However, their fundamental characteristics and their main objectives fall into the methods described in the following sections.

2.5.1 Machine Learning (ML)

Machine learning is a field of computer science also called soft computing. Machine learning targets in estimating the output of a mathematical problem for any given input, by developing a set of rules derived from discrete solutions of the problem under examination. There have been developed various algorithms that propose different ways for developing the estimation rules (Artificial Neural Networks, Support Vector Machines, etc.). Machine learning is currently one of the most rapidly developing field in computer science with application on fields such as; image recognition [58] and economics [59], since it has been proved to provide accurate solutions in complex problems that analytical methods fail. At this section, the most popular techniques applied on diagnostic problems will be discussed.

2.5.1.1 Artificial Neural Networks (ANN)

The basic principle of neural networks is the mapping of a set of inputs to a set of outputs under the influence of weights and thresholds. Every input vector

corresponds to a desired output vector and the goal is to adjust the weights and the thresholds of the neural network to create an output vector as close as possible to the desired vector. As reported by Vapnik [60], the appropriate adjustments of the neural network weights and thresholds permit an optimal mapping (empirical risk minimization). The assignment of the appropriate weights and thresholds of the neural network is conducted by solving an optimization problem (training of the network) and as reported by Simon Haykin [61], the computational time for training a neural network is linear in terms of the depth of the network.

As reported by Winston [62], the underlying dangers of using ANN are:

- Divergence of the algorithm.
- Trapping in local extrema.
- Overfitting.

Divergence and trapping of the algorithm on local extrema are consequences of using deterministic optimization algorithms in the training stage. Techniques that can mitigate the risk of divergence and trapping of the algorithm in local extrema due to deterministic optimization algorithms have been proposed by Nocedal and Wright [63]. Winston [62] defines as overfitting of a neural network the situation where the network over-conforms to the training examples and cannot produce reliable outputs for new examples. A major reason for the overfitting of a neural network is the use of too many training examples. A rule of thumb to avoid overfitting, suggested by Winston [62] is that the number of trainable weights must be smaller than the number of samples. Also, Winston [62] explains that ANN can model physical systems with respect to non-linearity and have been used in diagnostic applications.

Component fault detection and isolation is approached using ANN by two different techniques. Under the first technique, as discussed by Muhammad et al. [64], Kanelopoulos et al. [65], and Sina Tayarani-Bathaie et al. [66], a neural network is trained in such a way that using the operating conditions as inputs, it produces the estimated system's output values. The estimated values are compared with the real system measurements and when appropriate thresholds

are exceeded, faults are detected. Under the second technique, a neural network gets as inputs the system measurements and estimates the system physical parameters. This approach can detect a fault and link the abnormal physical parameter to its corresponding component as reported by Pascoal et al. [67], Volponi et al. [33] and Zedda and Singh [68].

An architecture of ANN called Auto Associative Neural Networks (AANN) that map an input vector to itself was proposed by Kramer [69]. In cases where the input vector represents sensor measurements, AANN have been proved successful in noise filtering. Applications of pre-processing sensor measurements for noise filtering on gas turbines using AANN have been discussed by Uluyola et al. [70], Guo et al. [71], Zedda and Singh [72] and Sadough Vanini et al. [73].

2.5.1.2 Support Vector Machine (SVM)

Support vector machines were initially introduced by Vapnik [74]. The target of SVM is to separate data points with distinct characteristics in an optimal way. An optimization problem is solved using Laplace multipliers and KKT (Karush-Kuhn-Tucker) conditions. SVM selects a linear function to separate the data points in two-dimension space. If the data cannot be linearly separated into two dimensions, they are projected into higher dimensions using kernel functions (polynomial, radial-basis, sigmoidal) where can be linearly separated. A shortfall of SVM classification is their slow response and as a mitigation action, optimization techniques that can select the appropriate parameters used into the method's mathematical equation have been proposed by Zhao et al. [75].

SVM have been used widely in gas turbine diagnostic problems by utilizing their optimal classifier feature. SVM can be trained on a dataset of engine measurements, containing both healthy and faulty engine states. Therefore, when engine measurements enter a SVM, they can be classified as either healthy or faulty, as discussed by Vieira and Bizarria [76] or linked to specific faults, as discussed by Zhou et al. [77], and Hou and Wang [78].

A technique that combined ANN and SVM applied on a vehicle, was proposed by Nieto Gonzalez [79]. At the first stage, an ANN is used to detect faults by comparing the residual between the input and the output to a nominal threshold. The fault isolation is conducted by a multiclass SVM.

2.5.1.3 Fuzzy Logic (FL)

Fuzzy logic is a mathematical technique derived from set theory that has been applied to fault diagnostic problems. Frank and Köppen-Seliger [80] used fuzzy logic both for fault detection and for threshold adaptation. Under the proposed approach, initially, a residual was created between a system's observed values and its mathematical model. Fault detection using fuzzy logic is conducted in three stages:

i. Fuzzification
ii. Inference
iii. Defuzzification

The principle of operation of FL to the diagnostic problem has been discussed by Ross [81] and is based on the following logic. During the fuzzification step, membership functions for various residual groups are defined. Each data point of the residual space is assigned a degree of membership at each residual group. The next step is the inference, where each fault is corresponded with one or more residual groups. Finally, in the defuzzification step, each fault case is associated with a crisp value under predefined rules.

The most current trend is the combination of fuzzy logic with classification algorithms (ANN, SVM). Fuzzy logic is used in the initial stage in order to cluster the observed parameter into fuzzy sets (fault modes) and a classification algorithm is trained to classify system parameters to its corresponding health state. Allen et al. [82] conducted a diagnostic analysis on a Heat Ventilation and Air Condition system (HVAC) using fuzzy logic and neural networks. At the fuzzy logic stage, degrees of membership to five fuzzy sets (healthy, temperature sensor error, valve position sensor error, valve stuck open, valve stuck closed) were assigned at three system parameters (temperature, valve position, air flow).

A neural network was trained to classify the system parameters to its corresponding set. The proposed methodology was applied to simulated and experimental data and could accurately detect and isolate the system's faults. Hang et al. [83] developed a fault diagnosis algorithm for a wind turbine. The proposed algorithm uses a kernel fuzzy c-means clustering algorithm to cluster vibration signals into fuzzy sets (fault modes). The fuzzy sets are used for training a multiclass SVM that classifies input parameters to their corresponding fault modes. The proposed methodology was compared to a multiclass classic SVM and an ANN, without using the fuzzy logic stage, and demonstrated higher accuracy. Wang et al. [84] use a fuzzy c-means clustering algorithm to cluster exhaust gas temperature data from an industrial gas turbine. The fuzzy dataset is used to train and test a multiclass SVM on the failure modes that had been identified in the clustering step. A neural network was also tested for the data classification but the SVM demonstrated higher accuracy.

2.5.1.4 Genetic Algorithms (GA)

Genetic algorithms are stochastic optimization algorithms. The advantage they have compared to deterministic optimization methods is that they do not require the computation of the gradient of a function, so the objective function is not necessary to be differentiable. As discussed by Sivanandam and Deepa [85], their disadvantage is that the computational time required is much longer compared to the deterministic methods.

Zedda and Singh [86] and Kobayashi and Simon [87] used genetic algorithms to diagnose sensor faults in gas turbine engines and Zedda and Singh [86], Sampath and Singh [88], Ogaji et al. [89] and Kong et al. [90] used genetic algorithms to diagnose component faults in gas turbine engines. The genetics algorithms are able to solve diagnostic problems by defining an objective function that incorporates the residual between a system's simulated measurements and the real sensor observations. The variables of the objective function are the components physical parameters, which are estimated by the GA. Observing the residual between a parameter's estimated values compared to its nominal values, faults can be detected at the corresponding components. In gas turbine

applications genetic algorithms demonstrated better diagnostic results when compared to the Gas Path Analysis (GPA) method as reported by Sampath and Singh [88], and Kong et al. [90] as well as with neural networks and fuzzy logic as reported by Sampath and Singh [91].

A serious drawback of using GA is their slow response. Techniques have been proposed to decrease the high computational time of GA. Zedda and Singh [86], propose a technique in which only specific parameters of the objective function are allowed to deviate. These parameters are selected based on engineering judgment of each specific application. Also, Ogaji et al. [89] proposed a strategy that allows the algorithm to make bigger steps at the initial stages, so the search is accelerated. Finally, Sampath and Singh [91] introduce the response surface method, which allows the algorithm to discard members of the population that are not in the region of the global minimum at the initial stages.

2.5.2 Statistical methods

Techniques derived from statistics and probability theory can also be used in a diagnostic analysis. Statistical methods can be used to detect outliers in datasets which can either be a pre-processing part of the analysis or can suggest faulty cases. Principal Component Analysis (PCA) has been mostly used for this kind of applications. Also, Bayesian probability analysis and Dempster-Shafer theory can offer results associated with the probability of occurrence of a fault mode.

2.5.2.1 Principal Component Analysis (PCA)

PCA is a statistical technique that maps high dimension datasets into lower dimensional space. As discussed by Johnson and Wichern [92], the lower dimensional data are called principal components of the initial dataset and are selected to maintain the variability existing in the original data. In fault diagnostic applications, especially in cases where the data size is large and many data point have almost identical variances, it is beneficial to conduct a PCA on the initial data set in order to reduce the size of the data to be processed.

PCA technique for fault diagnosis can either be used as a pre-processor so that reduced dimension data can be analysed from another algorithm. Muhammad et

al. [64] used PCA on data from a rotating machinery and the principal components were used to train a neural network. Also, Zhou et al. [93] conducted a diagnostic analysis on an electronic device that is used to monitor human pulmonary functions. In the study that is conducted by Zhou et al. [93], initially, PCA is conducted on healthy data. A k-means clustering algorithm is applied on the reduced dimension principal components to identify the various patterns existing for the various operational modes. The Q test (Q test is a mathematical technique used to identify outliers out of a sample of measurements) was used to define the appropriate threshold for each cluster. The fault isolation step is conducted using a neural network. When a fault is detected, a neural network, that has been trained to predict sensor values, is used. Data collected a few sampling points before the fault occurrence are introduced to the neural network and if the predicted values are different from the observed values, the sensor is declared faulty. The proposed methodology was applied on real system's data and could accurately identify the injected sensor fault.

Misra et al. [94] introduced a technique called Multi Scale Principal Component Analysis (MSPCA). The proposed methodology, applied at a chemical plant, leverages both the advantage of the wavelet transform that considers the correlations within sensors and PCA that captures the correlations among the sensor measurements. The system data are decomposed on various levels from the wavelet transform and at the next step are analysed using PCA. Using the Q test appropriate thresholds for fault detection can be established. The proposed methodology was tested on real system data and demonstrated better diagnostic results compared to the conventional PCA without pre-processing the data using the wavelet transformation. Li and Wen [95] developed a diagnostic methodology that incorporates wavelet transformation and PCA for a building's air handling unit. The data are pre-processed by the wavelet transformation and the low frequency features are excluded from the analysis because they are due to weather or load variations and not due to component faults. PCA was applied on data from the real system in the fault free case before and after the wavelet pre-processing. The results demonstrated that when the data are not pre-processed false alarms are flagged. The corresponding thresholds were defined using Q

test. The proposed methodology was tested on faulty cases and could accurately identify the existing faults.

2.5.2.2 Bayesian network

Bayesian network architecture is a way to represent the joint probability of various events by means of capturing the effects each one of them has upon the others. The three main characteristics of a Bayesian network are:

- That each problem variable is represented by a single node.
- The nodes are connected by directed edges formatting a directed acyclic graph.
- Each node is assigned a conditional probability distribution (with the parent nodes as parameters).

As discussed by Jensen [96], an important prerequisite of constructing a diagnostic Bayesian network is the estimation of the a priori probability of the system's variables that are used in Bayes rule. The determination of the a-priori probability can be based either on historical data or on expert knowledge. Bayesian networks have been used successfully on diagnostic applications, since, as discussed by Sedighi et al. [97], they have the advantage of using probability assignment on the fault detection and isolation task that are useful in the design procedure of the diagnostic algorithms, as well as in decision making.

Jun and Kim [98] propose a Bayesian network methodology for fault diagnosis. The architecture of the network considers three levels (causes, symptoms, faults). The faults are categorized in catastrophic or degraded. Depending on the way the causes, symptoms and faults are interconnected, they are categorized in multiple or common causes/symptoms and cascading faults. Appropriate probability thresholds are assigned for the algorithm to classify each case. Using the node interconnections, sensitivity analysis is conducted to investigate which of the causes or symptoms contributes more to the faults. The proposed methodology was applied on a power plant's centrifugal compressor and the results demonstrated that the proposed metrics could accurately capture the causes or symptoms that affected the faults under investigation.

Zhao et al. [99], [100] applied diagnostic Bayesian networks on a building's AHU. There are three kinds of nodes in the network (evidence nodes, fault nodes, additional information nodes). The evidence nodes observe sensor readings or a component's mode of operation and direct to fault nodes. The additional information nodes capture data derived from visual inspections, historic logs and other heuristic sources of information and enhance the diagnostic accuracy of the algorithm or point out meaningful inspections to the technical personnel. The proposed method was tested on experimental data and could successfully detect and isolate component faults. The advantage of this method is that it was developed without considering fault data, thus, it can be implemented in cases were historic fault data are unavailable.

2.5.2.3 Dempster-Shafer (D-S) theory

Another technique derived from the probability theory and has been applied to fault diagnosis is Dempster-Shafer (D-S) theory. Under the D-S framework, degrees of belief are assigned to individual members or subsets of a set of events based on the existing evidence. As discussed by Shafer [101], the main difference compared to Bayesian network approach is that the belief value of a fact and its corresponding negation are not necessarily complementary.

Guralnik et al. [102] developed a diagnostic methodology using D-S theory, that was applied to an aircraft's Auxiliary Power Unit (APU). The aim of the proposed methodology was to calculate the probability of multiple faults existing in the system. Different diagnostic algorithms are used to detect faults in the various subsystems existing in the APU (i.e. gas generator subsystem, fuel subsystem, etc.). Calculation of belief values for each algorithm under the D-S framework are based on various evidence (sensors, features and method each algorithm uses). Diagnostic algorithms are classified as highly dependent, weakly dependent or independent based on the overlap of the evidence they use. Using D-S fusion rule on the results of highly dependent, weakly dependent and independent algorithms, belief values of the existence of various fault modes are created. The step forward of the proposed approach is that multiple faults can be detected (with a belief value) and a list of the most probable faults is created. The

shortfall of this approach is that the rules used at the D-S fusion step must be defined by the designer and require expert knowledge of the application under examination.

2.6 Hybrid methods

Data driven techniques have been used in combination to produce more accurate results or achieve a faster response. Fuzzy logic has been used in combination with ANN and SVM (Section 1.5.1). PCA has been used in combination with ANN and wavelet transformation (Section 1.5.2). Also, representative example of combining data-driven methods is proposed by Lo et al. [103]. Under this approach, there has been developed a diagnostic algorithm that combines genetic algorithms with fuzzy logic and is applied at an HVAC system. In the discussed study, diagnostic rules, expressed by threshold values, for various system faults are generated by a fuzzy logic algorithm. Following that, an objective function having as variables the rules (thresholds) is created and a genetic algorithm is used to calculate the threshold values that optimize the objective function.

Algorithms created by combining more than one data driven technique remain a data driven approach. This section focuses on algorithms that combine model-based and data-driven techniques (hybrid methods). As discussed by Eker [104], hybrid methods aim to enhance the diagnostic results by leveraging the advantages and avoiding the limitations of their consisting techniques.

Luo et al. [105] apply a diagnostic methodology that combines the FDI method and the SVM technique on a vehicle's antilock braking system. A physical model of the system is created, and four component faults and one sensor fault are considered into the analysis. The parity space technique (FDI), which has the advantage of faster response, is used to isolate the sensor faults and one component fault. The observer based (FDI) technique, which can construct residuals more robust to noise, is used to isolate the rest component faults. Finally, the SVM technique is used to isolate the two remaining component faults, which could not be distinguished using FDI approaches.

Ghimire et al. [106] propose a methodology that uses model-based techniques for fault detection and data-driven techniques for fault isolation. The proposed methodology is applied on a vehicle's electronic power system, observing six system values and considering four system component faults. The CUSUM algorithm (residual evaluation from the FDI technique) was used to detect faults in the system by comparing the cumulative sum of the squared residuals of the observed measurements to a predefined threshold. The fault isolation step consisted of three stages: dimensionality reduction, fault classification, severity estimation. Partial Least Square (PLS) algorithm was used to reduce the dimensionality of the dataset. The reduced dimensionality data was used to train machine learning algorithms (Support Vector Machine, Probabilistic Neural Network, and Nearest Neighbour) to classify different faults. Finally, SVM regression is used to estimate the fault severity. The proposed methodology was tested on data collected by a simulation model. The results demonstrated high classification rate and fault severity estimation accuracy improved as the fault severity increased.

Liang and Du [107] developed a hybrid fault diagnosis algorithm for fault detection and isolation. The proposed methodology was applied to an HVAC system. Simulations were conducted considering healthy conditions and three component faults under various severity degrees. At the fault detection stage, the moving average method (residual evaluation from the FDI technique) is used to detect a fault by evaluating the residual between healthy and faulty simulation cases. An SVM was trained to classify the faults under examination. This methodology was tested on simulation data and could accurately detect the injected faults.

2.7 System-level diagnostics

An emerging topic among the diagnostic community during the last decade is the system-level diagnostic approach. System-level diagnostics targets in accurately assessing the system's health state and when a fault is detected, identifying the system's faulty component. The system's components considered in the analysis are defined by the designer and are the Line Replaceable Units (LRU) of each application. System level diagnostics is an approach that targets in informing the

maintainer which LRU should be replaced when a system is not performing properly. A standard definition for system level diagnostics is still missing from the literature, but there are two major features that can be identified under this approach:

- Both structural and functional interconnection of the system components is being considered.
- When a faulty component has been identified, the diagnostic analysis is not continued in more detail to identify the root cause of the faulty component.

Saha and Vachtsevanos [11] developed a system level diagnostic algorithm using a model based methodology applied on a helicopter's gearbox. Initially, a database is created that contains the system's building components, their possible fault modes and physical parameters (Condition Indicators - CI) that can capture these fault modes. Based on the system structure, a functional model that describes the functionality of each component is created. Each element of the functional model is correlated with one or more fault modes and each fault mode is associated to one or more condition indicators. Based on the relationship between the fault modes and the condition indicators, a fault-symptom matrix is created. Using this matrix, the faulty components can be uniquely identified. After the fault identification, using the system's structure, a fault propagation tree is created. This tree points out components that are probable of developing a fault, due to their adjacency to a faulty component. The proposed technique was applied on a helicopter's intermediate gearbox considering as condition indicators different frequency bands captured by two accelerometers at the input and at the output of the gearbox. The diagnostic analysis could isolate all component faults.

Wang et al. [108] applied a system level diagnostic methodology on a Heat Ventilation and Air Condition (HVAC) system. The proposed algorithm consists of two modules, a sensor fault detection module and a component fault detection module. As regards the sensor fault detection module, Principal Component Analysis (PCA) was used to reduce the dimensionality of the data and the Q test was used to detect sensor faults. For the component diagnosis module,

subsystems of the same type of components, e.g. a Heat Exchanger subsystem (consisting of all the Heat Exchangers of the system), were considered to break the system down to a subsystem level. Appropriate physical parameters for each subsystem were selected (Performance Indicators - PIs). The PIs reflect the system's health state and can detect faults in the corresponding subsystem group. This methodology could accurately detect sensor faults or high severity component faults when examined separately. Limitation of this methodology were that its accuracy in detecting faults was decreased in cases of low severity component faults and in cases were sensor and component faults were combined.

Gao et al. [109], developed a system level diagnostic method to detect HVAC component faults that lead to delta-T syndrome. Delta-T syndrome is a phenomenon where water temperature difference produced from an Air Handling Unit (AHU) is lower than the design value. In this application the subsystems considered are an Air Handling Unit and Heat Exchangers since these are the systems that can cause delta-T syndrome. For each one of them, appropriate physical variables PI, that can effectively capture each component's degradation, are selected. PI baselines are created offline based on healthy historic data. Residual between observed PI and baseline PI is compared to adaptive threshold that captures the variations due to operating conditions. When the residual exceeds a PI threshold a fault is isolated to the corresponding component. The proposed method was tested and could accurately detect and isolate faults into systems under examination when a low delta-T syndrome occurs.

Ozkurt et al. [110] developed a methodology of estimating the health state of a battery of an electric vehicle. Batteries for electric vehicles consist of many cells and the techniques that focus on the cell level diagnostics cannot guarantee accurate system level diagnostics. In this study, the battery cells can be connected either to the "main" output, which is used to supply the electric vehicle with power or to the "test" output, which is used for the diagnostic analysis. The diagnostic analysis conducted on the cells connected to the "test" output can use any component (cell) - level technique. Data collected from a simulation model

under healthy and faulty conditions were used to conduct the diagnostic analysis. An experimental rig was used to validate the simulation model. A parameter estimation technique (from the FDI method) was used to assess each cell's health state (component level). It is concluded that as the number of cells connected to the test output increased, the accuracy of the diagnostic results increases as well. An important contribution of this methodology is that the cells used for diagnostics are randomly selected, thus the analysis is conducted at a system level.

Wang et al. [111] developed a method of assessing the health state of a building's power consumption subsystems (HVAC, lighting, lift, etc.). The system's data were classified into working days and non-working days. Furthermore, depending on weather conditions and operating modes of the subsystems, data were separated into cooling or heating categories. A building's power consumption system was divided into four major subsystems and a diagnostic analysis based on different time periods (hourly, weekly, daily) was conducted. By combining physical parameters for every component, appropriate metrics (Energy Performance Indices – EPI) that describe its corresponding performance are created. Based on historic data, regression models create the baseline for each Energy Performance Index. Conducting a statistical analysis on the data, thresholds that can detect faults and suggest their severity can be defined. Weekly diagnosis could accurately detect the total building's power consumption faults. However, there were cases were various system faults oversubscribed with each other and the weekly diagnosis could not accurately isolate a specific fault. Daily and hourly diagnosis could identify subsystems that operated under faulty conditions. The specific component and the root cause of the failure could not be identified by the algorithm and physical inspection was required.

Hare et al. [112], applied a system level diagnostic methodology at an aircraft's Environmental Control System (ECS). The proposed method breaks the ECS down into two major subsystems and each subsystem into two major components and one sensor module. Initially, a sensor dependency matrix (D-Matrix) is created that identifies the sensors that can capture deviations in each component's health state. The fault detection strategy used traverses the

system's pyramid top-down. Thus, at the first step, a subsystem that contains a fault is identified and at the second step, the specific faulty component or sensor module is isolated. The diagnostic analysis is based on neural networks. For training of each neural network for every subsystem and every component, there was considered a dataset for a healthy case and a dataset for a faulty case. The healthy case considered the subsystem or the component under examination to be healthy while one of the remaining components, in another subsystem, is faulty. The faulty case considered the component under examination to be faulty while all other components are healthy. The proposed methodology was tested and could accurately detect faults in all components under examination. Compared to an alternative training method which considered that at the healthy case every component was healthy and at the faulty case the component under examination being faulty and every other component healthy, the proposed training method demonstrated more accurate results. This proves that capturing the component's interconnections increases the diagnostic accuracy.

Lin et al. [113] developed a methodology that can detect and isolate faults in an aircraft's fuel system, using a Bayesian network. The proposed method could accurately estimate the degree of degradation of the component under examination. The novelty introduced in this work is that the calculation of a component's degradation level considered other system components suffering from various degrees of degradation. A Bayesian network was constructed considering the probability of multiple components being degraded at the same time. The results demonstrated that following this technique the various components degradation levels could be accurately identified. Compared to a Bayesian network that did not consider the probability of various components being simultaneously degraded, the proposed methodology demonstrated higher accuracy.

Verbert et al. [114] developed a system level diagnostic approach applied on a HVAC system. The proposed method considers the system components interdependencies. At the first step, physical analysis of the system under examination is conducted and the most representative features that can

accurately detect and isolate the components' failure modes are selected. The selected features are used to create a Bayesian network that connects features (symptoms) to the corresponding fault modes with their respective probabilities. The system faults under examination, as well as their respective a priori probabilities, are estimated using historic data. Optimal estimation techniques were used to capture variables necessary for the mass and energy balance in cases were physical sensors were missing. The proposed method was tested in two different case studies. In the first one a fault was considered only in one subsystem and in the second, faults could be present in two subsystems simultaneously. This study highlights that if the diagnostic analysis cannot capture the components interconnection in different hierarchical levels or the supplementary role various components have in the same level, the accuracy of the diagnostic results decreases. The case studies considered, demonstrated that when the components interconnections (mass and energy balance) are captured in the Bayesian network, the diagnostic results were more accurate.

2.8 Summary and Discussion

This section consists of two parts, the first part summarizes the various diagnostic methods and highlights the advantages and shortfalls of each one. The second part analyses more thoroughly the system level diagnostic concept, aiming to emphasize capability for specific applications as well as this concept's strengths and weaknesses.

2.8.1 Diagnostic methods summary

Each of the diagnostic methods elaborated in the previous sections offers specific advantages and disadvantages and demand compliance with particular prerequisites for their successful implementation. Major considerations include:

- Installed sensors or hardware
- Online or offline application

Discussion of advantages, disadvantages of each method as well as requirements for their successful application, was carried out at each respective

section. This section offers a comprehensive summary of the pros and cons of each method and the availability of their application.

Model based methods define thresholds and rules for fault detection and isolation based on physics-based simulation models. Analysis under this approach is highly dependent on modelling accuracy. This means that these methods are very useful for OEMs that have an accurate understanding of the system's behaviour (e.g. thermodynamic design analysis, structural design analysis). Accurate engineering understanding allows development of high fidelity models which can produce more precise diagnostics. System operators that are able to develop lower fidelity models require implementation of more complex fault diagnostic algorithms (e.g. adaptive thresholds, consecutive occurrence of faults) in order to achieve acceptable fault detection rates.

A design challenge faced by all diagnostic methods is false alarms to misdetections ratio. This problem usually arises due to noise or unmodelled parameters that exist in a system's operation. The advantage of model-based methods is that this ratio can be controlled. A proposed technique controlling this ratio is by selecting appropriate fault detection thresholds. These thresholds can either be selected by the designer of the diagnostic algorithm (subjectively) or can be quantified and selected objectively [46]. The great advantage of model-based analysis is that algorithms can be developed based on engineering knowledge of the system without the requirement of fault history of the system or component under examination. On the other hand, a disadvantage of this method is that complex systems cannot be easily modelled.

Data driven methods are based on machine learning and probability theory algorithms. Supervised or unsupervised learning algorithms are used to solve classification problems (classify systems or components healthy or faulty), probabilistic and stochastic algorithms are used to assign probabilities to systems or components associated with their health condition. Data driven algorithms are used in combination in many applications in order to combine high accuracy features (SVM, GA) with fast response features (neural networks). Results produced by data driven methods are based both on the quality of the data used

for training the algorithm as well as the training strategy used. Good quality training datasets should contain a wide representation of the system and component failure modes with the corresponding physical parameter values. Lower quality datasets require more complex training strategies that may need to combine more than one algorithm. A disadvantage of the data driven methods is that they cannot be easily adjusted in order to optimize the rate of false alarms to misdetections and are referred to as “black box” methods. Data driven methods are useful in cases where complex systems are under examination and limited engineering understanding is available for their performance.

Table 2-1 Advantages & Shortfalls of Diagnostic Methods

Method	Advantages	Shortfalls
Model Based	• Do not require historic knowledge of the system in operation • The rate of false alarms to misdetections can be adjusted	• Require knowledge of the engineering of the system or component under examination
Data Driven	• Can be used without knowledge of the performance of the system or components • Various algorithms can be easily combined to enhance the results	• The results depend on the quality of the training datasets • Algorithms are difficult to adjust for false alarms to misdetection rate “black box methods”
Rule & Case Based Reasoning	• A diagnostic analysis can be developed without engineering knowledge of the system	• Historic or expert knowledge of the system is hard to acquire and transform in an algorithm in many applications

Section 3 illustrated that diagnostic methods based on expert systems require historic knowledge of the system faults as well as the corresponding maintenance actions. Even in cases where this information is available, it is challenging to interpret databases containing historic information and develop rules that can be used by computer algorithms. Also, the developed rules will be associated with

systems working within a specific operational envelop and under common environmental conditions. However, diagnostic expert systems are valuable in cases where there are not sufficient sensors installed on the system under examination (legacy systems) and there is limited engineering knowledge for their performance.

Table 2-1 gives of tabulated representation of the pros and cons of each category of methods described above. Understanding the advantages, disadvantages and the necessary requirements for successful implementation for each one of them, allows the diagnostic engineer to select the most appropriate methods for the application under examination.

2.8.2 Discussion on system-level diagnostic techniques

System level diagnostics targets in accurately detecting faults in a system and identifying faulty LRUs. In industrial applications where unscheduled maintenance is expensive, prompt detection of faulty components that should be replaced is of great value.

A great strength of this approach is that it captures interconnections among system components. The analysis aims to identify fault symptoms that characterize each component's health state as well as cases where different components have identical fault symptoms.

Fundamental steps followed by system level diagnostics are:

- Identification of fault symptoms for all component
- Identification of cases in which a failure mode has unique fault symptoms
- Identification of cases in which a component's fault symptom can be confused with other components fault symptoms
- Identification of ambiguity groups created

Table 2-2 Applications of system level diagnostic approach

Application	Method	Key Advantage	Key Shortfall
Helicopter gearbox	Physics based (Condition Indicators)	Monitoring one physical parameter, all component faults can be identified.	Single physics system. No sensor faults considered.
Heat Ventilation and Air Condition	1st stage: PCA 2nd stage: Physics based (Performance Indicators)	Both components and sensor faults could be identified.	Single physics system. When both sensor and component faults were considered, sensor fault detection accuracy was decreased.
Environmental Control System	Artificial Neural Networks	Faults could be detected on major subsystems and sensors.	Single physics system. Limited ECS subsystems were considered.
HVAC	Physics based (Performance Indicators)	Accurate fault isolation on the subsystems under examination.	Single physics system. Limited HVAC subsystems were considered.
HVAC	Bayesian network	Multiple faults could be captured accurately.	Single physics system. No sensor faults considered.
Electrical vehicle battery	Accelerating aging test (component level) Separation of “main” output cells and “test” output cells (system level)	All battery cells can be tested.	Single physics system. Accuracy depends on the number of the tested cells.
Wind power plant	Unsupervised learning algorithms (DBSCAN, spectral clustering, PCA)	Fault detection capability for the overall power plant.	Single physics system. The faulty components could not be isolated.

Building power system	Energy Performance Indices	Fault on the major energy consumption subsystems were accurately identified.	Single physics system. The exact faulty components could not be accurately identified.
Fuel system	Bayesian network	Multicomponent degradation.	Single physics system. No sensor fault considered.

Table 2-2 summarizes reviewed publications of system level diagnostics presented in section 7, highlighting their main advantages and shortfalls. Most applications use a methodology of defining metrics or indicators that can be sensitive to a component's fault, but insensitive to all other components' faults (physics based). Designing metrics or indicators that are sensitive to specific faults and insensitive to all other faults is similar to the idea of generating residuals that correspond to specific faults at FDI methods. The difference is that development of FDI residuals was based on intelligent matrix manipulation. In system level diagnostics, health metrics are based on engineering judgement and are selected by the designer. Defined metrics can be either individual physical parameters or a function of system's physical parameters. Health state of modelled components is associated with the defined metrics. These components may either represent an LRU or a group of LRUs.

Data driven approaches such as neural networks, as discussed by Hare et al. [112], and Bayesian networks, as discussed by Lin et al. [113], have also been used for system level diagnostics. The key element that allows data driven algorithms to capture components interconnections is the training strategy used. As an example, is presented the methodology used by Hare et al. [112], to train a neural network (The healthy case considered the subsystem or the component under examination to be healthy while one of the remaining components, in another subsystem, is faulty. The faulty case considered the component under examination to be faulty while all other components are healthy.

However, there are still challenges in this area. System level diagnostic applications in the literature either consider a single sensor system, as in the case

study discussed by Saha and Vachtsevanos [11] or a system operating under a single physical environment, as in the case studies discussed by Gao et al. [109], Wang et al. [108], Lin et al. [113] and Ozkurt et al. [110]). Analysis of multiphysical systems has not been widely discussed.

Also, in cases where sensor and component faults were combined, diagnostic accuracy was lower compared to cases where each one of them was considered independently as in the study conducted by Wang et al. [108]. Methodologies more robust to combined sensor and component faults should be further developed.

An increasing trend among the diagnostic community is the integration of model based and data driven techniques (hybrid methods). In section 6, publications of hybrid methods were presented. These hybrid algorithms produce more accurate results and require less computational time compared to model based or data driven methods individually. This area should be further developed and applied more widely to system level diagnostics.

Concluding, areas of further research that could enhance the performance of system level diagnostics and expand its applications are:

- Application of system level diagnostic approach on multiphysical systems
- Integration of sensor and component faults
- Further development of hybrid techniques and application on system level diagnostics

2.9 Conclusion

This work presents a review of system diagnostics. The necessity of this approach in optimizing maintenance tasks in high value assets is highlighted and examples of its applications have been given. The key features of this approach and techniques employed for their implementation have been presented. Strengths and limitations of this approach are presented, and a discussion is conducted analysing the main reasons of the observed limitations and areas of further research were proposed.

Also, a literature review of the most recent diagnostic methodologies and diagnostic reasoning tools identified in the literature is conducted and a taxonomy is proposed. The wide spectrum of available diagnostic techniques is presented, and their strengths and weaknesses are highlighted. This aims in informing the reader about the existing diagnostic methods and based on them introduce system level diagnostics. This is also important for the diagnostic engineer, since by understanding the main features, the advantages and disadvantages of diagnostic methods, the most appropriate technique(s) can be used to develop system level diagnostic algorithms on each application.

As a synopsis, the potential accuracy of the diagnostic results can be significantly improved in any given application by identifying the special features and by deploying the most compatible or a combination of most suitable diagnostic techniques. In addition, the proposed taxonomy can be regarded as an enabler to down select the most appropriate diagnostics technique, method, and any combination of methods best suited to diagnose a hardware system efficiently.

2.10 References

[1] Jennions I. K., Ed., *Integrated Vehicle Health Management - Perspectives on an Emerging Field*. SAE International, 2011.

[2] Mobley R. K., “An introduction to predictive maintenance.” Elsevier, Wonburn, MA, p. 458, 2002.

[3] Evans P. C. and Annunziata M., “Industrial Internet: Pushing the boundries of Minds and Machines.” GE, 2012, [Online]. Available: http://www.ge.com/docs/chapters/Industrial_Internet.pdf.

[4] Esperon-Miguez M., John P., and Jennions I. K., “A review of Integrated Vehicle Health Management tools for legacy platforms: Challenges and opportunities,” *Prog. Aerosp. Sci.*, vol. 56, pp. 19–34, 2013, doi: 10.1016/j.paerosci.2012.04.003.

[5] Pelham J. G., Fan I.-S., Jennions I., and McFeat J., “Application of an AIS to the problem of through life health management of remotely piloted

aircraft," *AIAA Infotech at Aerospace*. Kissimmee, USA, 2015, doi: 10.2514/6.2015-1797.

[6] Piel Eric, Gonzalez-Sanchez A., Gross H., and Van Gemund A. J. C., "Online Fault Localization and Health Monitoring for Software Systems," *Situation Awareness with Systems of Systems*. Springer Science and Business Media, New York, pp. 229–245, 2013, doi: 10.1007/978-1-4614-6230-9.

[7] Ogaji S. O. T., Sampath S., Singh R., and Probert S. D., "Parameter selection for diagnosing a gas-turbine's performance-deterioration," *Appl. Energy*, vol. 73, no. 1, pp. 25–46, 2002, doi: 10.1016/S0306-2619(02)00042-9.

[8] Staszewski W. J., Boller W. J., and Tomlinson G. R., Eds., "Health monitoring of aerospace structures." John Wiley & Sons, Ltd, Chichester, p. 266, 2004.

[9] Ben-Daya M., Duffuaa S. O., Raouf A., Knezevic J., and Daoud A.-K., "Handbook of Maintenance Management and Engineering." Springer, London, pp. 223–235, 2009, doi: 10.1007/978-1-84882-472-0.

[10] Mehdi G., Naderi D., Ceschini G., and Roshchin M., "Model-based Reasoning Approach for Automated Failure Analysis : An Industrial Gas Turbine Application," *Annual Conference of the Prognostics and Health Management Society*. PHM Society, San Diego, CA, 2015.

[11] Saha B. and Vachtsevanos G., "A Model-based Reasoning Approach to System Fault Diagnosis," *Proceedings of the 10th WSEAS International Conference on Systems*. Athens, 2006.

[12] Bartlett L. M., Hurdle E. E., and Kelly E. M., "Integrated system fault diagnostics utilising digraph and fault tree-based approaches," *Reliab. Eng. Syst. Saf.*, vol. 94, no. 6, pp. 1107–1115, 2009, doi: 10.1016/j.ress.2008.12.005.

[13] Papadopoulos Y., "Model-based system monitoring and diagnosis of

failures using statecharts and fault trees," *Reliab. Eng. Syst. Saf.*, vol. 81, no. 3, pp. 325–341, 2003, doi: 10.1016/S0951-8320(03)00095-4.

[14] Singh S., Holland S. W., and Bandyopadhyay P., "Trends in the development of system-level fault dependency matrices," *IEEE Aerospace Conference Proceedings*. Big Sky, MT, 2010, doi: 10.1109/AERO.2010.5446825.

[15] Durkin J., "Expert systems: Design and development." Macmillan Publishing Company, New York, 1994.

[16] Dubrova E., "Fault-tolerant design." Springer, New York, p. 185, 2013, doi: 10.1007/978-1-4614-2113-9.

[17] Ferrara L. A., "Summary description of the AAP Apollo telescope mount." Technical Report: TM-68-1022-3 National Aeronautics and Space Administration (NASA), 1968.

[18] Shi N.-Z. and Tao J., "Statistical hypothesis testing." World Scientific Publishing Co. Pte. Ltd., Toh Tuck Link, Singapore, 2008.

[19] Siegmund D., "Sequential Analysis." Springer, New York, 1985, doi: 10.1007/978-1-4757-1862-1.

[20] Mohanty S. R., Pradhan A. K., and Routray A., "A cumulative sum-based fault detector for power system relaying application," *IEEE Trans. Power Deliv.*, vol. 23, no. 1, pp. 79–86, 2008, doi: 10.1109/TPWRD.2007.911160.

[21] Basseville M. and Nikiforov I., "Fault Isolation for Diagnosis: Nuisance Rejection and Multiple Hypotheses Testing," *Annu. Rev. Control*, vol. 25, no. 1, pp. 83–94, 2002, doi: 10.1016/S1367-5788(02)00027-5.

[22] Patton J. and Chen J., "Review of parity space approaches to fault diagnosis for aerospace systems," *J. Guid. Control Dyn.*, vol. 17, no. 2, 1994.

[23] Höfling T. and Isermann R., "Fault detection based on adaptive parity equations and single-parameter tracking," *Control Eng. Pract.*, vol. 4, no.

10, pp. 1361–1369, 1996, doi: 10.1016/0967-0661(96)00146-3.

[24] Patton R. J. and Chen J., “Robust fault detection using eigenstructure assignement: a tutortial considerations and some new results,” in *Proceedings of the 30th conference on decision and control*, 1991, vol. 94.

[25] White J. and Speyer J., “Detection filter design: Spectral theory and algorithms,” *IEEE Trans. Automat. Contr.*, vol. 32, no. 7, pp. 593–603, 1987, doi: 10.1109/TAC.1987.1104682.

[26] Frank P. M., “Analytical and Qualitative Model-based Fault Diagnosis – A Survey and Some New Results,” *European Journal of Control*, vol. 2, no. 1. pp. 6–28, 1996, doi: 10.1016/S0947-3580(96)70024-9.

[27] Frank P. M., “Fault diagnosis in dynamic systems using analytical knowledge-based redundancy – A survey and some new results,” *Automatica*, vol. 26, no. 3, pp. 459–474, 1990, doi: 10.1109/ROBIO.2011.6181275.

[28] Hwang I., Kim S., Kim Y., and Seahv C. E., “A survey of fault detection, isolation, and reconfiguration methods,” *IEEE Trans. Control Syst. Technol.*, vol. 18, no. 3, pp. 636–653, 2010, doi: 10.1109/TCST.2009.2026285.

[29] Patton R. J., Frank P. M., and Clarke R. N., “Fault diagnosis in dynamic systems: theory and application.” Prentice-Hall, Inc., Upper Saddle River, NJ, USA, 1989.

[30] Isermann R., “Fault diagnosis of machines via parameter estimation and knowledge processing-Tutorial paper,” *Automatica*, vol. 29, no. 4, pp. 815–835, 1993, doi: 10.1016/0005-1098(93)90088-B.

[31] Isermann R., “Process Fault Detection Based on Modeling and Estimation Methods-A Survey,” *Automatica*, vol. 20, no. 4, pp. 387–404, 1984, doi: 10.1016/0005-1098(84)90098-0.

[32] Volponi A. J., “Foundations of Gas Path Analysis I,” in *Gas turbine condition*

monitoring and fault diagnosis - Lecture series 2003-01, von Karman Institute for Fluid Dynamics, 2003.

[33] Volponi A. J., “Foundation of Gas Path Analysis II,” in *Gas turbine condition monitoring and fault diagnosis - Lecture series 2003-01*, von Karman Institute for Fluid Dynamics.

[34] Doel D. L., “An Assessment of Weighted-Least-Squares Based Gas Path,” *International gas turbinbe and aeroengine congress and exposition*. ASME, Cincinati, Ohio, 1993, doi: 10.1115/93-GT-119.

[35] Moseler O. and Isermann R., “Application of model-based fault detection to a brushless DC motor,” *IEEE Trans. Ind. Electron.*, vol. 47, no. 5, pp. 1015–1020, 2000, doi: 10.1109/41.873209.

[36] Urban L. A., “Gas path analysis applied to turbine engine condition monitoring,” *J. Aircr.*, vol. 10, no. 7, pp. 400–406, 1973, doi: 10.2514/6.1972-1082.

[37] Doel D. L., “A weighted-least-squares gas path analysis method for test cel or on-wing data,” in *Gas Turbine Condition Monitoring and Fault Diagnosis*, von Karman Institute for Fluid Dynamics, 2003.

[38] Doel D. L., “TEMPER—A Gas-Path Analysis Tool for Commercial Jet Engines,” *International gas turbinbe and aeroengine congress and exposition*. ASME, Cologne, Germany, 1992, doi: 10.1115/1.2906813.

[39] Stamatis A. G., “Optimum Use of Existing Sensor Information for Gas Turbine Diagnostics,” 2008, doi: 10.1115/GT2008-50296.

[40] Stamatis A., Mathioudakis K., Berrios G., “Jet engine fault detection with discrete operating points gas path analysis,” *J. Propuls. Power*, vol. 7, no. 6, 1991.

[41] Volponi A. J., “Gas Turbine Engine Health Management: Past, Present, and Future Trends,” *J. Eng. Gas Turbines Power*, vol. 136, no. 5, p. 051201, 2014, doi: 10.1115/1.4026126.

[42] Davis R., “Diagnostic reasoning based on structure and behavior,” *Artif. Intell.*, vol. 24, no. 1–3, pp. 347–410, 1984, doi: 10.1016/0004-3702(84)90042-0.

[43] Kolcio K., Hanson M., and Fesq L., “Validation of Autonomous Fault Diagnostic Software,” *IEEE Aerospace Conference Proceedings*. IEEE, Snowmass at Aspen, CO, USA, 1998, doi: 10.1109/AERO.1998.682197.

[44] Fesq L., “Marple: An autonomous diagnostician for isolationg system hardware failures.” PhD Dissertation, University of California, Los Angeles, CA, 1993.

[45] Kolcio K., Breger L., and Zetocha P., “Model-based fault management for spacecraft autonomy,” *IEEE Aerospace Conference Proceedings*. IEEE, Big Sky, MT, 2014, doi: 10.1109/AERO.2014.6836174.

[46] Rossi C., “Vehicle Health Monitoring Using Stochastic Constraint Suspension,” *AIAA Guidance, Nagivation, and Control Conference*. Minneapolis, Minnesota, 2012, doi: 10.2514/6.2012-4611.

[47] Rossi C., Benson D., Sargent R., and Breger L., “Model-Based Design for Vehicle Health Monitoring,” *Infotech@Aerospace 2012*. AIAA, Garden Grove, California, 2012, doi: 10.2514/6.2012-2577.

[48] Kolcio K. and Fesq L., “Model-based off-nominal state isolation and detection system for autonomous fault management,” *IEEE Aerospace Conference Proceedings*. Big Sky, MT, 2016, doi: 10.1109/AERO.2016.7500793.

[49] De Kleer J. and Kurien J., “Fundamentals of model-based diagnosis,” *IFAC Proc. Vol.*, vol. 36, no. 5, pp. 25–36, 2003, doi: 10.1016/S1474-6670(17)36467-4.

[50] Stern R., Kalech M., Rogov S., and Feldman A., “How many diagnoses do we need ?,” *Artif. Intell.*, vol. 248, pp. 26–45, 2017, doi: 10.1016/j.artint.2017.03.002.

[51] Feldman A., Provan G., and Van Gemund A., “Approximate model-based diagnosis using greedy stochastic search,” *J. Artif. Intell. Res.*, vol. 38, pp. 371–413, 2010, doi: 10.1613/jair.3025.

[52] Keren B., Kalech M., and Rokach L., “Model-Based Diagnosis with Multi-Label Classification,” *22nd International Workshop on Principles of Diagnosis, DX*. Murnau, Germany, 2011.

[53] Kolcio K., Fesq L., and Mackey R., “Model-Based Approach to Rover Health Assessment for Increased Productivity.” IEEE, Big Sky, MT, 2017, doi: 10.1109/AERO.2017.7943835.

[54] Mosterman P. J., Kapadia R., and Biswas G., “Using Bond Graphs for Diagnosis of Dynamic Physical Systems.” Sixth International Workshop Principles of Diagnosis, Goslar, Germany, 1995.

[55] Mosterman P. J. and Biswas G., “Diagnosis of continuous valued systems in transient operating regions,” *IEEE Trans. Syst. Man, Cybern. Part ASystems Humans.*, vol. 29, no. 6, pp. 554–565, 1999, doi: 10.1109/3468.798059.

[56] Daigle M., Field M., and Foygel M., “Model-based Diagnostics for Propellant Loading Systems.” IEEE, Big Sky, MT, 2011, doi: 10.1109/AERO.2011.5747596.

[57] Narasimhan S. and Biswas G., “Model-Based Diagnosis of Hybrid Systems,” *Syst. Man Cybern. Part A Syst. Humans, IEEE Trans.*, vol. 37, no. 3, pp. 348–361, 2007, doi: 10.1109/TSMCA.2007.893487.

[58] Chen B., Li J., Wei G., and Ma B., “A novel localized and second order feature coding network for image recognition,” *Pattern Recognit.*, vol. 76, pp. 339–348, 2018, doi: 10.1016/j.patcog.2017.10.039.

[59] Wang S., Li G., and Bao Y., “A novel improved fuzzy support vector machine based stock price trend forecast model.” International Conference on Innovations in Economic Management and Social Science (IEMSS 2017), Hangzhou, China, 2018, [Online]. Available:

http://arxiv.org/abs/1801.00681.

[60] Vapnik V., “The nature of statistical learning theory.” Springer, New Jersey, 1995, doi: 10.1109/TNN.1997.641482.

[61] Simon Haykin, “Neural networks: a comprehensive foundation.” Pearson Educational Limited, Delhi, India, 1999, doi: 10.1017/S0269888998214044.

[62] Winston P. H., “Artificial Intelligence.” Pearson Educational Limited, 1993.

[63] Nocedal J. and Wright S., “Numerical Optimization.” Springer, New York, 1999.

[64] Muhammad M. B., Sarwar U., Tahan M. R., and Karim Z. A. A., “Fault Diagnostic Model for Rotating Machinery Based on Principal Component Analysis and Neural Network,” *ARPN J. Eng. Appl. Sci.*, vol. 11, no. 24, pp. 14327–14331, 2016.

[65] Kanelopoulos K., Stamatis A., and Mathioudakis- K., “Incorporating Neural Networks into Gas Turbine Performance Diagnostics,” *ASME 1997 International Gas Turbine and Aeroengine Congress and Exhibition*. Orlando, Florida, USA, 1997, doi: 10.1115/97-GT-035.

[66] Sina Tayarani-Bathaie S., Sadough Vanini Z. N., and Khorasani K., “Dynamic neural network-based fault diagnosis of gas turbine engines,” *Neurocomputing*, vol. 125, pp. 153–165, 2014, doi: 10.1016/j.neucom.2012.06.050.

[67] Pascoal R. M., Vianna W. O. L., Gomes J. P. P., and Galvão R. K. H., “Estimation of APU failure parameters employing linear regression and neural networks,” *PHM 2013 - Proc. Annu. Conf. Progn. Heal. Manag. Soc. 2013*, pp. 664–670, 2013.

[68] Zedda M. and Singh R., “Fault diagnosis of a turbofan engine using neural networks - A quantitative approach,” *34th AIAA/ASME/SAE/ASEE Joint Propulsion Conference and Exhibit*. Cincinati, Ohio, 1998, doi:

10.2514/6.1998-3602.

[69] Kramer M. A., “Autoassociative neural networks,” *Comput. Chem. Eng.*, vol. 16, no. 4, pp. 313–328, 1992, doi: 10.1016/0098-1354(92)80051-A.

[70] Uluyola O., Buczaka A., and Nwadiogbub E., “Neural networks based sensor validation and recovery methodology for advanced aircraft engines,” in *Component and System Diagnostics, Prognosis, and Health Management*, 2001, vol. 4389, pp. 102–109.

[71] Guo T.-H., Saus J., Lin C.-F., and Ge J.-H., “Sensor validation for turbofan engines using an autoassociative neural network,” *Guid. Navig. Control Conf.*, no. July, 1996, doi: 10.2514/6.1996-3926.

[72] Zedda M. and Singh R., “Neural-network-based sensor validation for gas turbine,” *J. Syst. Control Eng.*, vol. 215, pp. 47–56, 2001, doi: 10.1243/0959651011539196.

[73] Sadough Vanini Z. N., Meskin N., and Khorasani K., “Multiple-Model Sensor and Components Fault Diagnosis in Gas Turbine Engines Using Autoassociative Neural Networks,” *J. Eng. Gas Turbines Power*, vol. 136, no. 9, p. 091603, 2014, doi: 10.1115/1.4027215.

[74] Vapnik V., “Support Vector Networks,” *Mach. Learn.*, vol. 20, no. 3, pp. 273–297, 1995, doi: 10.1007/BF00994018.

[75] Zhao Q. *et al.*, “An Improved Fault Diagnosis Approach Based on Support Vector Machine,” *2016 IEEE International Conference on Prognostics and Health Management (ICPHM)*. IEEE, Ottawa, ON, Canada, 2016, doi: 10.1109/ICPHM.2016.7542827.

[76] Vieira F. M. and Bizarria C. D. O., “Health monitoring using support vector classification on an auxiliary power unit,” *IEEE Aerospace Conference Proceedings*. Big Sky, MT, 2009, doi: 10.1109/AERO.2009.4839655.

[77] Zhou D., Zhang H., and Weng S., “A New Gas Path Fault Diagnostic Method of Gas Turbine Based on Support Vector Machine,” *J. Eng. Gas*

Turbines Power, vol. 137, no. 10, p. 6 p., 2015, doi: 10.1115/1.4030277.

[78] Hou C. and Wang Q., “Diagnosis of Aircraft Engine Performance Deterioration Based on Support Vector Machines.” IEEE International Conference on Reliability, Maintainability and Safety (ICRMS), Guangzhou, China, 2014, doi: 10.1109/ICRMS.2014.7107133.

[79] Nieto Gonzalez J. P., “Vehicle fault detection and diagnosis combining an AANN and multiclass SVM,” *Int. J. Interact. Des. Manuf.*, vol. 12, pp. 273–279, 2017, doi: 10.1007/s12008-017-0378-z.

[80] Frank P. M. and Köppen-Seliger B., “Fuzzy logic and neural network applications to fault diagnosis,” *Int. J. Approx. Reason.*, vol. 16, no. 1, pp. 67–88, 1997, doi: 10.1016/S0888-613X(96)00116-8.

[81] Ross T. J., “Fuzzy logic with engineering applications.” John Wiley & Sons, Ltd, West Sussex, England, 2004.

[82] Allen W. H., Rubaai A., and Chawla R., “Fuzzy Neural Network-Based Health Monitoring for HVAC System Variable-Air-Volume Unit,” *IEEE Trans. Ind. Appl.*, vol. 52, no. 3, pp. 2513–2524, 2016, doi: 10.1109/TIA.2015.2511160.

[83] Hang J., Zhang J., and Cheng M., “Application of multi-class fuzzy support vector machine classifier for fault diagnosis of wind turbine,” *Fuzzy Sets Syst.*, vol. 297, pp. 128–140, 2016, doi: 10.1016/j.fss.2015.07.005.

[84] Wang Z., Zhao N., Wang W., Tang R., and Li S., “A Fault Diagnosis Approach for Gas Turbine Exhaust Gas Temperature Based on Fuzzy C-Means Clustering and Support Vector Machine,” *Math. Probl. Eng.*, vol. 2015, pp. 1–11, 2015, doi: 10.1155/2015/240267.

[85] Sivanandam S.N. and Deepa S.N., *Introduction to Genetic Algorithms*. Springer, 2008.

[86] Zedda M. and Singh R., “Gas turbine engine and sensor fault diagnosis using optimization techniques,” *J. Propuls. Power*, vol. 18, no. 5, pp. 1019–

1025, 2002, doi: 10.2514/2.6050.

[87] Kobayashi T. and Simon D. L., “A hybrid neural network - genetic algorithm technique for aircraft engine performance diagnostics,” *J. Propuls. Power*, vol. 21, no. 4, pp. 751–758, 2005.

[88] Sampath S. and Singh R., “An integrated fault diagnostics model using genetic algorithm and neural networks,” *J. Eng. Gas Turbines Power*, vol. 128, no. 1, pp. 49–56, 2006, doi: 10.1115/1.1995771.

[89] Ogaji S. O. T., Sampath S., Marinai L., Singh R., and Probert S. D., “Evolution strategy for gas-turbine fault-diagnoses,” *Appl. Energy*, vol. 81, no. 2, pp. 222–230, 2005, doi: 10.1016/j.apenergy.2004.07.003.

[90] Kong C., Kang M., and Park G., “Study on Condition Monitoring of 2-Spool Turbofan Engine Using Non-Linear Gas Path Analysis Method and Genetic Algorithms,” *Int. J. Mater. Mech. Manuf.*, vol. 1, no. 2, pp. 214–220, 2013, doi: 10.7763/IJMMM.2013.V1.46.

[91] Sampath S. and Singh R., “An Integrated Fault Diagnostics Model Using Genetic Algorithm and Neural Networks,” *J. Eng. Gas Turbines Power*, vol. 128, no. January 2006, p. 49, 2006, doi: 10.1115/1.1995771.

[92] Johnson R. A. and Wichern D. W., “Applied Multivariate Statistical Analysis,” *Pearson Education International*. Pearson Educational Limited, p. 773, 2008, doi: 10.1198/tech.2005.s319.

[93] Zhou J., Guo A., Celler B., and Su S., “Fault detection and identification spanning multiple processes by integrating PCA with neural network,” *Appl. Soft Comput. J.*, vol. 14, pp. 4–11, 2014, doi: 10.1016/j.asoc.2013.09.024.

[94] Misra M., Yue H. H., Qin S. J., and Ling C., “Multivariate Process Monitoring and fault Diagnosis by Multi Scale PCA,” *Comput. Chem. Eng.*, vol. 26, pp. 1281–1293, 2002.

[95] Li S. and Wen J., “A model-based fault detection and diagnostic methodology based on PCA method and wavelet transform,” *Energy Build.*,

vol. 68, no. PARTA, pp. 63–71, 2014, doi: 10.1016/j.enbuild.2013.08.044.

[96] Jensen F. V, “An introduction to Bayesian networks.” vol.210 UCL press, London, 1996.

[97] Sedighi T., Phillips P., and Foote P. D., “Model-based intermittent fault detection,” *Procedia CIRP*, vol. 11, pp. 68–73, 2013, doi: 10.1016/j.procir.2013.07.065.

[98] Jun H. B. and Kim D., “A Bayesian network-based approach for fault analysis,” *Expert Syst. Appl.*, vol. 81, pp. 332–348, 2017, doi: 10.1016/j.eswa.2017.03.056.

[99] Zhao Y., Wen J., Xiao F., Yang X., and Wang S., “Diagnostic Bayesian networks for diagnosing air handling units faults – part I: Faults in dampers, fans, filters and sensors,” *Appl. Therm. Eng.*, vol. 111, pp. 1272–1286, 2017, doi: 10.1016/j.applthermaleng.2015.09.121.

[100] Zhao Y., Wen J., and Wang S., “Diagnostic Bayesian networks for diagnosing air handling units faults - Part II: Faults in coils and sensors,” *Appl. Therm. Eng.*, vol. 90, pp. 145–157, 2015, doi: 10.1016/j.applthermaleng.2015.07.001.

[101] Shafer G., “A Mathematical Theory of Evidence.” Princeton University Press, 1976.

[102] Guralnik V., Mylaraswamy D., and Voges H., “On Handling Dependent Evidence and Multiple Faults in Knowledge Fusion for Engine Health Management,” *2006 IEEE Aerospace Conference*. IEEE, Big Sky, MT, 2006, doi: 10.1109/AERO.2006.1656100.

[103] Lo C. H., Chan P. T., Wong Y. K., Rad A. B., and Cheung K. L., “Fuzzy-genetic algorithm for automatic fault detection in HVAC systems,” *Appl. Soft Comput. J.*, vol. 7, no. 2, pp. 554–560, 2007, doi: 10.1016/j.asoc.2006.06.003.

[104] Eker Ö. F., “A Hybrid Prognostic Methodology and its Application to Well-

Controlled Engineering," *Cranfield University*. PhD Dissertation, Cranfield University, Cranfield, UK, 2013.

[105] Luo J., Namburu M., Pattipati K. R., Qiao L., and Chigusa S., "Integrated model-based and data-driven diagnosis of automotive antilock braking systems," *IEEE Trans. Syst. Man, Cybern. Part ASystems Humans*, vol. 40, no. 2, pp. 321–336, 2010, doi: 10.1109/TSMCA.2009.2034481.

[106] Ghimire R. *et al.*, "Integrated model-based and data-driven fault detection and diagnosis approach for an automotive electric power steering system," *AUTOTESTCON (Proceedings)*. IEEE, Baltimore, MD, USA, 2011, doi: 10.1109/AUTEST.2011.6058760.

[107] Liang J. and Du R., "Model-based Fault Detection and Diagnosis of HVAC systems using Support Vector Machine method," *Int. J. Refrig.*, vol. 30, no. 6, pp. 1104–1114, 2007, doi: 10.1016/j.ijrefrig.2006.12.012.

[108] Wang S., Zhou Q., and Xiao F., "A system-level fault detection and diagnosis strategy for HVAC systems involving sensor faults," *Energy Build.*, vol. 42, no. 4, pp. 477–490, 2010, doi: 10.1016/j.enbuild.2009.10.017.

[109] Gao D., Wang S., Shan K., and Yan C., "A system-level fault detection and diagnosis method for low delta-T syndrome in the complex HVAC systems," *Appl. Energy*, vol. 164, pp. 1028–1038, 2016, doi: 10.1016/j.apenergy.2015.02.025.

[110] Ozkurt C., Camci F., Atamuradov V., and Odorry C., "Integration of sampling based battery state of health estimation method in electric vehicles," *Appl. Energy*, vol. 175, pp. 356–367, 2016, doi: 10.1016/j.apenergy.2016.05.037.

[111] Wang H., Xu P., Lu X., and Yuan D., "Methodology of comprehensive building energy performance diagnosis for large commercial buildings at multiple levels," *Appl. Energy*, vol. 169, pp. 14–27, 2016, doi: 10.1016/j.apenergy.2016.01.054.

[112] Hare J., Gupta S., Najjar N., Orlando P. D., and Walthall R., “System-Level Fault Diagnosis with Application to the Environmental Control System of an Aircraft.” SAE Technical Paper 2015-01-2583, 2015, 2015, doi: 10.4271/2015-01-2583.

[113] Lin Y., Zakwan S., and Jennions I., “A Bayesian Approach to Fault Identification in the Presence of Multi-component Degradation,” *Int. J. Progn. Heal. Manag.*, vol. 8, no. March, 2017.

[114] Verbert K., Babuška R., and De Schutter B., “Combining knowledge and historical data for system-level fault diagnosis of HVAC systems,” *Eng. Appl. Artif. Intell.*, vol. 59, no. April 2016, pp. 260–273, 2017, doi: 10.1016/j.engappai.2016.12.021.

3 EXPERIMENTAL INVESTIGATION AND SIMULATION OF A BOEING 747 AUXILIARY POWER UNIT

Auxiliary Power Units (APUs) are a major driver of maintenance on civil aircraft. However, experimental data and performance simulations are rarely seen in public domain literature. While there is recourse to aircraft engine experience, this does not address the loading and the failure modes of an APU. This work aims to add to the literature, by experimentally investigating a Boeing 747 APU, collecting data under various power settings and ambient conditions, and using this data to calibrate a simple simulation model. This simulation model will subsequently be used to explore failure modes in the APU and hence what sensors may be needed for health monitoring purposes in future work. In this paper, a Boeing 747 APU rig development process and the testing strategy are presented. The rig is validated through a process that includes uncertainty analysis, repeatability tests, consistency tests, and comparison of the collected data with the calibrated simulation model. The results from the rig's validation indicate that the data collected from the APU is independent of its running time or the order of loading cycles imposed on it, i.e. the results are path independent. Changes in pneumatic and electrical power result in small changes in the rotational speed despite the fact that the rotational speed should remain constant. The rotational speed shows a slightly increasing trend when the extracted power rises, and this affects the APU thermodynamic characteristics. This work has resulted in a calibrated simulation model that will be further used in examining fault mode scenarios, as injecting these directly into the rig is seen as high risk.

3.1 Introduction

Reducing operating cost and maximising profit are two important goals for any airline. Operating costs are dominated by fuel consumption, expenses related to cockpit crew and maintenance as reported by Saxon and Weber [1]. The overall fuel consumption is driven by the efficiency of engines, as reported by Peeters et al. [2]. The same study reports that, since 1960, aircraft fuel consumption has reduced by 69% due to continuous improvement in engine design. Maintenance represents 9.5% of an airline's total costs with an estimated 5.1% increase per

year. As with fuel consumption, engines and APUs are the most expensive parts of the aircraft to maintain, and a major driver of maintenance reported by IATA [3].

OEMs rarely reveal critical engine performance information, claiming intellectual property rights, Gorinevsky et al. [4]. Due to the fact that the engine and APU systems contribute disproportionally to maintenance costs, aircraft manufacturers, airliners and academics have a profound interest in developing an in-depth understanding of these systems, aiming for performance optimisation and health monitoring to aid in maintenance and operation.

In this paper, an experimental investigation and simulation of a Boeing 747 Auxiliary Power Unit (APU) is conducted. An APU is a powerplant system installed in all commercial aircraft and, as its name suggests, it serves as an alternate power source for the aircraft. Normally it is operated when the aircraft is at the gate and provides compressed air to the Environmental Control System and electrical power to the aircraft's electrical system. For this reason, airport management and government are interested in monitoring APU exhaust emissions and noise levels [5]–[8]. Furthermore, an APU serves as an emergency system in flight, in case an engine shuts down. The most famous example of an APU operated as an emergency system is US Airways flight 1549 in 2009, where an A320 aircraft landed on the Hudson River in New York [9]. In this incident, both engines stopped operating due to bird strikes and the APU was used to provide the necessary electrical power to control the aircraft.

3.2 Literature review

Collection of experimental data from engine and APU systems is a very challenging process, and for this reason, experimental data are rarely available in public domain literature. Real systems' data provides valuable insight into the system's performance and is necessary for validating simulation models. This section presents the most important experimental studies conducted on engines and APUs as well as examples of simulation studies that are validated against real systems' data.

The most relevant research efforts, to the purposes of this paper, have been conducted at the German Aerospace Center (DLR). Two APU test rigs (APS3200 and GTCP36-28) have been developed by Siebel et al. [10] and Zanger et al. [11] respectively. In both works, APU thermodynamic data, exhaust emissions and noise emissions were collected and discussed under various pneumatic and electrical loads. In these referenced studies, insights are provided for the efficiency and control characteristics of the APU systems. One of the findings suggests that APUs that have a single compressor for bleed air and power generation are less efficient than APUs that have a compressor for each function. The most relevant work that is related with the aim of this paper, which was published before the APU tests in DLR was conducted by Der Wiesche [12] who developed a mobile test rig for a micro gas turbine (SPM5). The thermodynamic parameters of the micro gas turbine were collected under various shaft loads.

The remaining experimental studies of APU systems investigate methods to reduce NO_X emissions. The effect that water injection has on NO_X emissions of an Artouste APU were analysed by Alexandro et al. [13]. The results suggest that water injection decreases emissions by up to 25% which is attributed to the cooling of the combustor and the compressor. Furthermore, Li et al. [14] measured the effects that six different alternative fuels have on the exhaust emissions of an Artouste APU. The main finding was that, compared to Jet A-1, all alternative fuels had a similar level in NO_X and CO emissions but presented a major decrease in Unburnt Hydrocarbons (UHB).

Due to the difficulty in conducting experimental studies on engine systems, analysis of these systems has been mainly accomplished through simulation models. A model that can accurately simulate the system's performance can provide data corresponding to healthy or degraded conditions. Simulation models have been used in engine optimization studies, diagnostic applications and in adaptation of component design maps. In order to validate the developed models, researchers compare their results with real systems' data. Depending on the available information and the scope of the research, various approaches exist. Representative examples of this approach [15]–[18] investigate engine

performance characteristics through simulation models validated on experimental data. Also, other studies [19]–[21] used experimental data in order to adapt component maps.

The literature survey indicates that the validity and accuracy of a simulation model is highly dependent on the experimental data used in calibration. This finding reveals the importance of real systems' data in performance and diagnostic analyses of engines and APUs. Quantifying the uncertainties in the experimental data provides boundaries for the accuracy of the simulation model, and the analysis that follows.

3.3 Boeing 747 APU description

Boeing 747-100/200/300 aircraft are equipped with a GTCP660-4 APU manufactured by Honeywell International Inc. The APU is made up of a number of different systems and a brief description of some of them is given below.

Table 3-1 GTCP660-4 Performance characteristics

GTCP 660-4 Performance Characteristics at Standard Day Conditions	Value
Rotational speed [rpm]	20,000
Bleed mass flow [kg/s]	3.82
Maximum fuel power [kW]	5,681.33
Maximum electrical power [kVA]	40
Maximum exhaust gas temperature [°C]	620

An APU converts the fuel's chemical energy to compressed air and electrical energy. This is achieved by a gas turbine that generates compressed air and transmits mechanical power through its shaft to electrical generators. The high level GTCP660-4 APU performance characteristics are provided in Table 3-1 and a cross section of the gas turbine is presented in Figure 3-1. This gas turbine consists of a four-stage axial compressor, a Load Control Valve (LCV), a Surge

Control Valve (SCV), an annular combustor, which contains sixteen fuel nozzles and one spark plug, followed by an axial two-stage turbine.

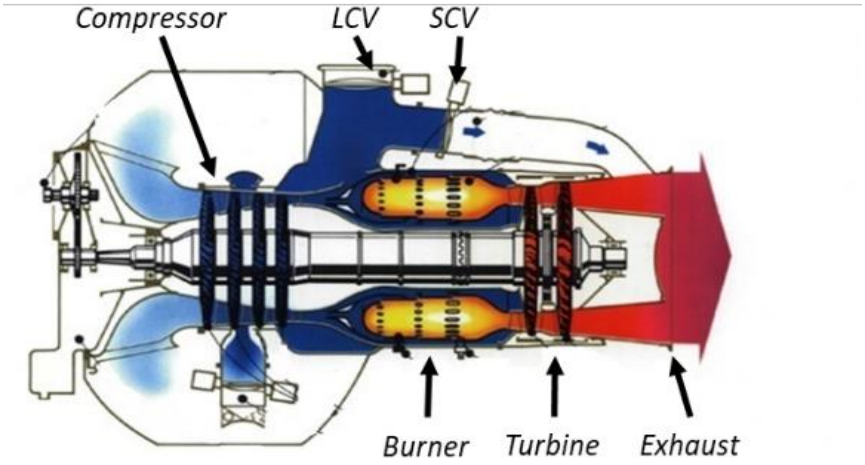

Figure 3-1 GTCP660-4 cross section

APUs are designed to spill a minimum amount of airflow from the compressor outlet in order to prevent compressor surge. For this reason, the compressed air splits into two streams. The first stream enters the combustor and then expands through the turbine. The second stream exits the gas turbine either through the SCV or through the LCV. The airflow through the SCV is directed to the APU exhaust and is mixed with the turbine outlet flow. Mixing of the two airstreams affects the APU performance because it changes the turbine's backpressure, an effect discussed in Section 6. The airflow through the LCV is directed to the aircraft's bleed air system, which distributes it to various systems such as the Environmental Control System, the wing de-icing, or used for the main engine starting.

Continuous supply of pressurised fuel to the gas turbine is provided from the aircraft's fuel system through a geared pump mounted on the gearbox. Fuel flow is regulated by an electromechanical valve controlled by the Electronic Turbine Controller (ETC). The gas turbine is protected from foreign objects in the fuel by a filter installed downstream of the fuel pump.

The APU bearings are lubricated and protected from overheating by the lubrication and cooling system. A geared pump, mounted on the gearbox, provides a continuous flow of lubricant to all parts of the system. The heat transferred from the bearings to the lubricant is dissipated in an air-oil heat exchanger. Cooling air is provided to the air-oil heat exchanger by the APU's cooling system. A fan mounted on the gearbox provides continuous ambient airflow to the air-oil heat exchanger, the generators, and the ETC. Cooling air is directed to these components through flexible ducts, and then is dispatched to the environment.

Starting of the APU is initiated by an electric motor mounted on the gearbox which provides rotation to the gas turbine's shaft. At 7% of the design speed, the ETC energises the ignition system and allows fuel flow. Until 50% of the design speed, both the starter motor and the combustion gases expanded at the turbine contribute to APU acceleration. At 50% of the design speed, the ETC stops the starter motor, and the gas turbine is driven only by the combustion gases. During the starting stage, the ETC regulates the fuel flow based on the acceleration schedule. Once rotation above 95% of the design speed is reached, steady-state operation is assumed. During steady state, the control logic aims to maintain a steady rotational speed despite any changes in the imposed load and ambient conditions by adjusting the fuel flow appropriately. The ETC also shuts down the APU in case any of its critical parameters exceed their safe limit.

3.4 Test rig development

A Boeing 747 APU test rig has been developed in Cranfield University's Gas Turbine Engineering Laboratories and it is presented in Figure 3-2a. The rig is used to collect air and fuel flow parameters through the gas turbine for APU steady-state operation under a wide range of operating conditions. To achieve this, various sensors were installed in the rig, and some modification to its structure and components were carried out. The installed sensor locations are shown in Figure 3-2b; their characteristics are presented in Table 3-2 and will be discussed in the rest of this section. The airflow parameters are measured at five different stations across the gas turbine as indicated in Figure 3-2b and the

symbols T, p and M represent the temperature, pressure, and mass flow measurements respectively, measured at the gas turbine stations. Also, the fuel flow is measured by a flowmeter at the engine inlet, which is symbolised by F and the sensor that measures the shaft's rotational speed is represented by the symbol S.

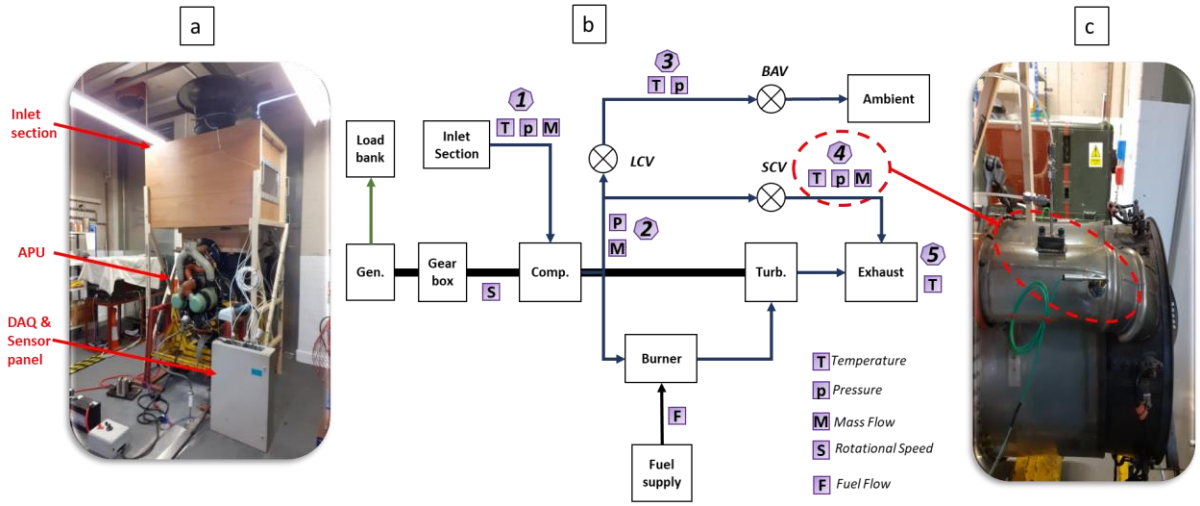

Figure 3-2 APU rig and sensors - a. APU rig - b. Instrumentation schematic - c. Pitot tube and thermocouple installation at the surge flow duct

The APU is oriented in the rig as it would be in the Boeing 747 aircraft. The airflow enters a plenum chamber vertically from above the rig and undergoes a vertical to horizontal transition to proceed through the gas turbine (proceeding away from the viewer in Figure 3-2a). The exhaust gases are directed outside of the test cell by the turbine outlet section, which acts as a free jet.

Measurement of the inlet airflow is complicated due to the APU plenum chamber's geometry. For this reason, an air inlet section was designed and installed on top of the APU air inlet plenum. Figure 3-3a presents a cross-section of the inlet section installed on the APU. The air inlet section consists of three parts: a circular duct which has a bellmouth type inlet, a plenum section, and an APU transition section. The inlet airflow is straightened through the circular duct, and its velocity is measured by installing three Pitot tubes. In order to select the location of the Pitot tubes, three notional sections with equal areas (A_1, A_2 and A_3) are considered, as shown in Figure 3-3b, and the velocities measured by

each Pitot probe are considered to be characteristic of the area in which they were placed. The Pitot tube that corresponds to A_1 is located at the centreline, the Pitot tube that corresponds to A_2 is located 0.188m away from the centreline and the Pitot tube that corresponds to A_3 is located 0.245m away from the centreline. The calculations of the total circular area and the individual areas (A_1, A_2 and A_3), as indicated in Figure 3-3b, are calculated by rounding up to the 3rd significant digit. The Pitot tube pressures are captured by differential pressure transducers (Honeywell, 142PC01D). The reliability of the inlet mass flow measurements is discussed in Section 6. Another consideration for the inlet mass flow measurement is related to the cooling air system arrangement. When the APU is installed in the aircraft, a flexible rubber hose directs a small part of the air inlet flow to the cooling fan. In order to avoid airflow escaping from the inlet section, the rubber hose was removed, and the blank in the air inlet plenum was covered by a piece of plywood.

Table 3-2 Sensors characteristics

Manufacturer, P/N	Type	Measurement range	Accuracy	Reference
Honeywell, 142PC01D	Differential pressure	0 to 6.89 kPa	0.5% (BFSL)	[22]
Omega, PX119-030AI	Absolute pressure	0 to 206.84 kPa	0.5% (BFSL)	[23]
Omega, PX119-100AI	Absolute pressure	0 to 689.47 kPa	0.5% (BFSL)	[23]
RS PRO, K-type thermocouple	Temperature	0 to 1100 °C	0.4% -0.75% (Depending on operating temperature)	[24]
Omega, FTB1313	Flowmeter	3.4 to 34 litre/min	1% (Compared to the reading)	[25]

As has been described in the previous section, the largest portion of the compressed air enters the combustion chamber and finally expands through the turbine. A smaller portion of the flow exits the gas turbine either through the SCV or the LCV. Bleed flow variation is achieved through the Bleed Air Valve (BAV) (fitted as a rig modification to the APU), which is a modulating butterfly valve. Its position can be adjusted between fully closed and fully open by an electric

actuator, through a 4 to 20 mA input signal. The input signal to the valve is provided by a signal generator via a manual knob located in the control room. The bleed air is directed, through a series of ducts, outside of the test cell.

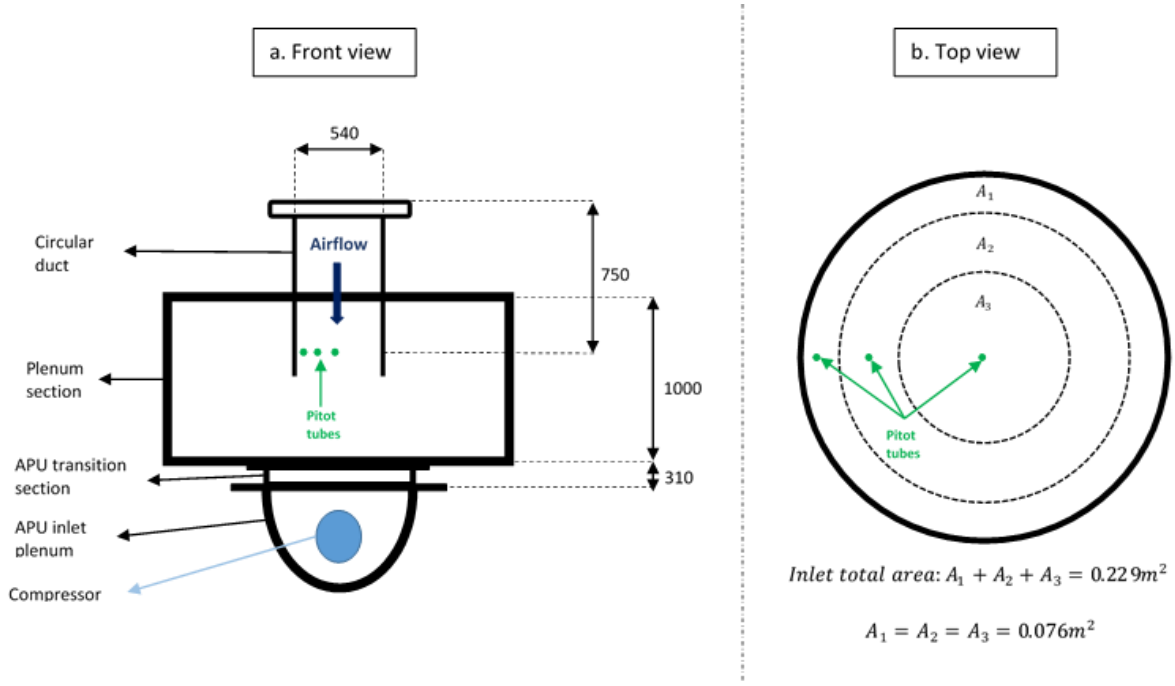

Figure 3-3 Inlet section schematic

The flow exiting the compressor is measured by a flow sensor located before the surge and bleed air are extracted (Station 2 in Figure 3-2b). This sensor is a part of the APU, and its original purpose is to allow control of the SCV during start up. The flow at compressor exit is calculated using an effective area of 51.09 cm2, a number provided in the maintenance manual. Pitot probes, installed in the ducts, measure flow downstream of the SCV and LCV respectively, in a similar way to the compressor exit flow. The effective area of the surge flow duct is 50.93 cm2 and that of the bleed duct is 182 cm2. The Pitot tubes are positioned at the centre of both the surge and bleed ducts. In order to ensure that the probe remains parallel to the flow, the probe is welded to a boss and the boss is secured to the duct by two bolts, as shown in Figure 3-2c.

After analysing the uncertainty of the collected data, it was observed that the uncertainty error propagated to the mass flow measured at the bleed air duct is excessive and for this reason, mass flow readings from Station 3 in Figure 3-2b

are considered unreliable and are ignored for the analysis in this paper. The excessive uncertainty in this measurement is caused from the pressure transducers' accuracy error. As regards the mass flow measurements at Station 2 and 4 of Figure 3-2b, their calculated uncertainties are acceptable for the purposes of this work, and they will be used in the rest of this paper. This issue is further discussed in Section 5.1 where the uncertainty analysis for the collected measurements is presented.

APU pressure readings, at positions shown in Figure 3-2b, are measured by pressure transducers (Omega, PX119-030AI and PX119-100AI). The pressure transducers are installed at a panel near the rig (Figure 3-2a), and the relevant pressure is transferred to them through polyethylene tubes. The polyethylene tubes allow the pressurised air to decrease in temperature by radiating heat to the environment and this results in the pressurised air reaching the transducers at almost ambient temperature. This phenomenon ensures that the high temperatures developed by the APU do not affect the pressure transducer readings.

Measurement of compressor outlet temperature is achieved by installing K-type thermocouples in the surge and bleed air ducts. The Exhaust Gas Temperature (EGT) is measured by twelve K-type thermocouples equally distributed at a radial arrangement at the turbine outlet. These thermocouples are an original part of the APU and transfer the EGT measurement to the ETC. The EGT value is extracted from the ETC through a DC signal varying from 0 to 1 mA that corresponds to temperatures from 0 to 900°C.

Electrical power is extracted from the generators by an electric load bank, constructed as part of previous research projects conducted in the gas turbine engineering laboratory. The load bank comprises a circuit of resistive elements. The load bank's resistance can be increased or decreased by adding or removing resistive elements to the circuit by switches located in the control room. The load bank is able to extract 10.38 kW, 15.57 kW, 20.76 kW or 25.95 kW of electric power and a fan is used to protect its heating elements from overheating. For the purposes of the test, the 15.57 kW and 25.95 kW settings were used. The

electrical power extracted during testing is lower than the maximum load that can be extracted from the APU, which is 40 kVA. During airborne APU operation, an Automatic Voltage Regulator (AVR) is used to adjust the excitation voltage in order to maintain a steady output voltage regardless of the load. The AVR was not available during test rig development, so a suitable replacement was designed, and the excitation voltage was manually adjusted to provide the necessary DC excitation voltage. The excitation voltage for various loads was established during the rig commission run.

Starting and stopping the rig is achieved through a control panel that communicates with the ETC through a circuit of switches and relays. Input power for the control panel and the ETC is provided by three independent power supplies rated at 24 VDC, 10 amps. The starter motor is powered by two heavy-duty batteries rated at 12 V, 1000 amps, connected in series. The rotational speed is measured by an inductive type speed sensor installed in the APU gearbox. The rotational speed signal is transferred from the sensor to the ETC and is extracted from the ETC through a DC signal that varies from 0 to 1 mA and corresponds to rotational speed from 0 to 22,000 rpm. Jet A-1 fuel is provided by an external fuel system which consists of a fuel tank, a fuel filter, a boost pump, an electric shut-off valve, and a manual shut-off valve. The fuel flow is measured by a turbine-type flow meter (Omega, FTB1313) which is installed in the fuel line before the engine inlet.

Sensor data is collected at a frequency of 1 Hz by a National Instruments data acquisition (DAQ) module. The DAQ, along with the pressure transducers and their power supplies, is installed in a panel near the rig, shown in Figure 3-2a. During testing, the panel door is kept open in order to maintain sufficient ventilation and ensure that there will not be an excessive increase in temperature. The measurements are displayed in real-time in the control room using LabVIEW software. During every APU run, fuel, oil and air leak checks were conducted in order to verify safe operation and reliable data acquisition.

3.5 Test rig operational envelope and validation process

In this section, the method followed to analyse the measurements' uncertainty is explained, the rig's operational envelope is defined, and its validation presented. The operational envelope is dictated by the regions of APU steady-state operation and by the rig's safety limits. The rig's validation process consists of repeatability test, consistency test, and then comparison of the experimental data with a simulation model. These topics are presented and discussed in this order below.

3.5.1 Uncertainty analysis

An essential feature that must be considered when analysing experimental data is the uncertainty error. Uncertainty consists of two elements, the accuracy (bias) error, which is the measurement's deviation from the real value, and the precision error, which measures how far away the measured values are to each other. The total uncertainty error is the Root Mean Square Error (RMSE) of the accuracy and precision errors and is calculated as follows:

$$MSE = \sqrt{(accuracy\ error)^2 + (precision\ error)^2} \quad \textbf{(3-1)}$$

The sensors used on the rig are pressure transducers, thermocouples (K-type), and a turbine type flow meter. The accuracy error as quoted by their manufacturer is presented in Table 3-2. The accuracy error is based on the sensors' design characteristics as well as their operating temperature. Based on the relevant datasheets, the pressure readings did not require temperature calibration under the operating conditions that data were collected. As regards the thermocouples, their accuracy depends on their operating temperature and this information is given by National Instruments [24]. Finally, the fuel entering the APU is at almost ambient temperature and, based on the flowmeter's specifications, the fuel flow readings did not require calibration for the ambient conditions that data were collected.

The value of the sensors' accuracy quoted by their manufacturers is based on a worst-case scenario hypothesis. However, based on the worst-case accuracy, a typical accuracy for each sensor can be calculated as reported by Beyer [26].

Assuming that the accuracy error follows a Gaussian distribution, the worst-case accuracy equals three standard deviations of this distribution and the typical accuracy equals one standard deviation. At the end of this section, a numeric example will be given, by calculating the uncertainty error assuming both the worst case and typical scenarios.

The precision error depends on external factors associated with the rig's operation and the operating environment. Sources of precision error considered are:

- The APU components operation. The APU being a turbomachine, creates unsteady conditions to the airflow and the fuel flow which contribute partially to measurement uncertainty.
- The environmental conditions. Due to the nature of the rig's operating environment, the ambient conditions under which data are collected cannot be controlled and change during testing. The effects of the environmental conditions on the APU operation are discussed in Section 5.3.2.
- The APU control system. Small variations to the positions of the APU valves either related with their control, or with their degradation, are also sources of uncertainty.
- The data acquisition system. Apart from the sensor errors, the DAQ module is also a source of uncertainty which can be associated either with the hardware module or with the signal transformation from analogue to a digital signal. However, based on the DAQ specifications, the DAQ contributions to uncertainty are very minor and for this application can be considered negligible.

The accuracy error for pressure, temperature and fuel flow is given by the sensor manufacturer. The precision error corresponds to the standard deviation of the collected measurements at each station in Figure 3-2b. The uncertainty of the inlet and extracted mass flows depend on the pressure and temperature readings since mass flow rate is defined by:

$$\dot{m} = \rho * v * A \tag{3-2}$$

and air density is given by:

$$\rho = \frac{p_t}{R_{gas} * T} \tag{3-3}$$

Velocity can be found from:

$$v = \sqrt{\frac{2 * \Delta p}{\rho}} \tag{3-4}$$

and with $R_{gas} = 287.05\ \frac{J}{kg*K}$, by considering eq. (3-3) and eq. (3-4), eq. (3-2) can be transformed to:

$$\dot{m} = \sqrt{\frac{p_t * \Delta p}{T}} * 0.08347 * A \tag{3-5}$$

The differential pressure Δp, for the inlet mass flow, is calculated by three differential pressure transducers. Based on the description of the inlet section provided in Section 4, it is calculated by:

$$\dot{m}_{in} = \dot{m}_{in,1} + \dot{m}_{in,2} + \dot{m}_{in,3} \tag{3-6}$$

Where, from eq. (3-5):

$$\dot{m}_{in,i} = \sqrt{\frac{p_t * \Delta p_i}{T}} * 0.08347 * A_i \tag{3-7}$$

The uncertainty associated with the $\dot{m}_{in,i}$ can be calculated based on rules provided by Kirkup and Frenkel [27]. This calculation is shown below, with the uncertainty of a general parameter *X* being denoted by δX.

$$\delta\dot{m}_{in,i} = \dot{m}_{in,i} * \frac{1}{2} * \frac{\delta\left(\frac{p_t * \Delta p_i}{T}\right)}{\frac{p_t * \Delta p_i}{T}} \tag{3-8}$$

Finally, considering eq. (3-6), the uncertainty of the inlet mass flow $\delta\dot{m}_{in}$ is:

$$\delta\dot{m}_{in} = \sqrt{(\delta\dot{m}_{in,1})^2 + (\delta\dot{m}_{in,2})^2 + (\delta\dot{m}_{in,3})^2} \quad \textbf{(3-9)}$$

For the extracted mass flow, the differential pressure element Δp used in eq. (3-5) is calculated by two pressure transducers that measure the total and static pressure. Thus, in order to calculate the uncertainty of the extracted mass flow, eq. (3-5) is written as:

$$\dot{m}_{ext} = \sqrt{\frac{p_t * (p_t - p_s)}{T}} * 0.08347 * A \quad \textbf{(3-10)}$$

By using the same rules for calculating the uncertainty for the inlet mass flow, the extracted mass flow uncertainty is given derived as:

$$\delta\dot{m}_{ext} = \dot{m}_{ext} * \frac{1}{2} * \frac{\delta(\frac{p_t * (p_t - p_s)}{T})}{\frac{p_t * (p_t - p_s)}{T}} \quad \textbf{(3-11)}$$

Tables 3-3 and 3-4 present a numeric example for the compressor inlet and outlet pressure, temperature, and mass flow uncertainty calculations, from data collected for the maximum power imposed on the rig (case 15, Table 3-6) considering worst case and typical scenarios for the accuracy error, respectively.

Table 3-3 Example of uncertainty error (worst case scenario)

Parameter	Mean Value	Accuracy Error	Precision Error	RMSE	Comparison with mean value (%)
Inlet Pressure [Pa]	101013	±1034.21	±100.38	±1039.07	1.02
Inlet Temperature [C]	20	±0.15	±0.02421	±0.1519	0.75
Inlet Mass Flow [kg/s]	10.84	N/A	N/A	±0.119	1.09
Compressor Outlet Total Pressure [Pa]	348580	±3447.38	±867.5	±3554.73	1.01
Compressor Outlet Temperature [C]	193.42	±1.522	±0.196	±1.5345	0.79
Extracted Mass Flow [kg/s]	3.06	N/A	N/A	±0.092	3

Table 3-4 Example of uncertainty error (typical scenario)

Parameter	Mean Value	Accuracy Error	Precision Error	RMSE	Comparison with mean value (%)
Inlet Pressure [Pa]	101013	±344.73	±100.38	±358.34	0.35
Inlet Temperature [C]	20	±0.05	±0.02421	±0.0555	0.27
Inlet Mass Flow [kg/s]	10.84	N/A	N/A	±0.07	0.64
Compressor Outlet Total Pressure [Pa]	348580	±1149.12	±867.5	±1439.8	0.41
Compressor Outlet Temperature [C]	193.42	±0.507	±0.196	±0.5435	0.28
Extracted Mass Flow [kg/s]	3.06	N/A	N/A	±0.045	1.4

In order to understand the propagation of the pressure and temperature uncertainty to the mass flow error, the results in Table 3-3 will be used as a working example. The RMSE values calculated for the inlet pressure and temperature, compared to their mean values, are 1.02% and 0.75% respectively, and the calculated inlet mass flow uncertainty error is 1.09%. This means that the uncertainty propagated to the inlet mass flow has a very minor increase compared to the inlet temperature and pressure uncertainties. As regards the compressor outlet total pressure and temperature, even though their uncertainties are 1.01% and 0.79% respectively, the uncertainty propagated to the extracted mass flow is 3%. In contrary to the inlet mass flow, the uncertainty propagated to the extracted mass flow increases significantly. This phenomenon is attributed to the fact that the differential pressure (Δp) in eq. (3-5), for the inlet mass flow is measured by a single differential pressure transducer, while for the extracted mass flow there are used two independent pressure transducers to measure the total (p_t) and static (p_s) pressure (eq. (3-10)). The contribution of an additional pressure transducer to the uncertainty calculations results in an increase of the extracted mass flow uncertainty error.

Table 3-5 presents the uncertainty error, expressed as a percentage of the mean value, for the inlet and extracted mass flow, calculated based on the worst case

and typical scenarios. As expected, the values that correspond to the typical scenario accuracy calculations are significantly lower than the worst case. The decision regarding the acceptable level of the accuracy error and the approach used to calculate the uncertainty error depends on the scope of the work conducted. Also, it is observed that the changes in the inlet mass flow uncertainty error are negligible while the BAV settings increase. As regards the extracted mass flow, for BAV settings 50% - 80%, as the BAV settings increase, the uncertainty error reduces, however, the uncertainty for BAV settings 0% do not follow this trend. This occurs because the mass flow for BAV settings 50% - 80% is measured at Station 2 in Figure 3-2b, while the mass flow for BAV settings 0% is measured at Station 4 in Figure 3-2b. The pressure transducers used in Station 2 (Omega, PX119-100AI) have a higher accuracy error than the transducers used in Station 4 (Omega, PX119-030AI), hence the lower error for these cases. The observed changes of the extracted mass flow error while the BAV settings increase, are attributed to the fact that extracted mass flow depends on the differential pressure ($p_t - p_s$) and this is calculated by two independent pressure transducers.

By concluding this section, it is observed that the uncertainty error is dominated by the accuracy error which is significantly higher compared to the precision error (for steady-state operation). Thus, a way to reduce the uncertainty errors is by using sensors with lower accuracy error. This, however, depends on the scope of each application, since the lower the sensor's accuracy error the more expensive it becomes.

Table 3-5 Inlet and extracted mass flow uncertainty errors compared to their mean value

		Uncertainty error compared to mean value (%)			
		Worst case scenario		Typical case scenario	
		Inlet mass flow	Extracted mass flow	Inlet mass flow	Extracted mass flow
	0	±1.8	±3.3	±0.6	±2.7

BAV open (%)	**50**	±1.8	±7	±0.6	±4.7
	60	±1.8	±6.3	±0.6	±4.9
	70	±1.8	±3.8	±0.6	±2.5
	80	±1.8	±3	±0.6	±1.5

It is noted that the error bars included in the graphs in the rest of this paper represent the RMSE uncertainty which is calculated based on the worst-case scenario described in this section.

3.5.2 Definition of the operational envelope

The definition of the operational envelope considers regions of APU steady-state operation with respect to safety limitations. The regions of steady operation are affected by the SCV's operation. This occurs because, as in every gas turbine engine, the APU has embedded mechanisms that ensure that the compressor operates away from the surge region. In the GTCP660-4, a minimum air mass flow is always extracted from the compressor outlet and directed to the exhaust, even when no bleed air is required from the aircraft. This is achieved by the SCV, which is a pneumatic valve that has been designed to automatically adjust its position so that the mass flow rate extracted from the compressor is always higher than the minimum mass flow rate ($\dot{m}_{min}$) required to avoid compressor surge. For operating conditions under which no bleed air is extracted (i.e. the LCV is closed), $\dot{m}_{min}$ is extracted entirely through the SCV (i.e. $\dot{m}_{min} = \dot{m}_{surge}$). When the bleed flow demand increases, the SCV changes its position so the total surge and bleed flow equals $\dot{m}_{min}$ (i.e. $\dot{m}_{surge} + \dot{m}_{bleed} = \dot{m}_{min}$). In this case, the SCV constantly readjusts its position resulting in unstable flow characteristics for both $\dot{m}_{surge}$ and $\dot{m}_{bleed}$. The SCV is fully closed only when $\dot{m}_{bleed} > \dot{m}_{min}$. The LCV can be selected to be either fully open or fully closed based on the operator's command. Bleed flow demand depends on the aircraft systems to which bleed air is an input (e.g. Environmental Control System).

The instability caused to $\dot{m}_{surge}$ and $\dot{m}_{bleed}$ by the SCV's operation was observed during the BAV commission test. The collected data of the extracted mass flow readings corresponding to four different BAV settings, as measured at Stations 2 and 4 in Figure 3-2b, are plotted in Figure 3-4. The mass flow measurements through the surge duct are indicated with a blue line and the mass flow readings that correspond to the airflow sensor are illustrated with a red line. Also, the value of $\dot{m}_{min}$ is marked on the vertical axis and the observed unsteady region is highlighted. For the commission test, the rig was operated at four different pneumatic loads. In order to identify the unsteady conditions that develop when mass flow is extracted simultaneously through the SCV and the LCV, the error bars in Figure 3-4 represent the Root Mean Square Error (RMSE) of the measurements' uncertainties.

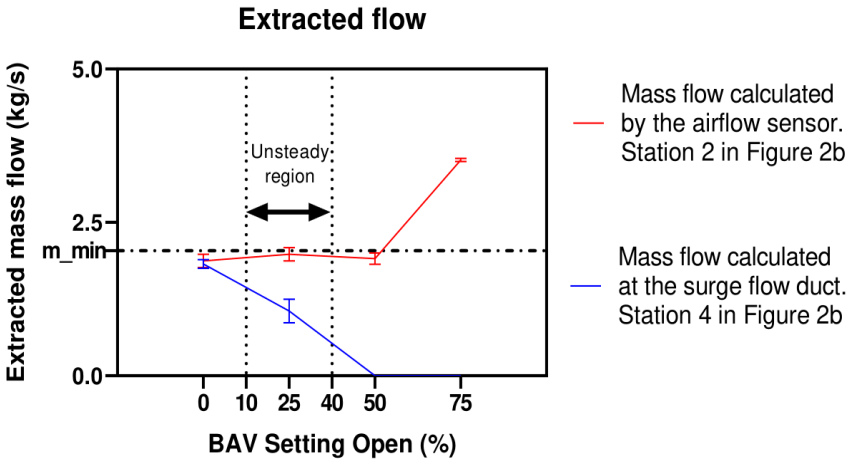

Figure 3-4 Extracted flow characteristics

The adjustment of the BAV corresponded to these four different loads: 0% open, 25% open, 50% open, and 75% open. When the BAV is fully closed, the extracted airflow ($\dot{m}_{ext}$) is directed to the exhaust duct through the SCV. Also, when the BAV was selected to be 50% or 75% open, $\dot{m}_{ext}$ is flowed to the environment through the BAV, and the SCV is fully closed. When the BAV was adjusted to be 25% open, $\dot{m}_{ext}$ was split between the SCV and BAV. During this case, increased uncertainty is observed for the flow through the surge duct. As it can be observed in Figure 3-4, during 25% BAV settings the uncertainty error corresponding to the

surge flow increases by approximately three times, as compared to the uncertainty of the surge flow at 0% BAV settings. The observed increase in the surge mass flow uncertainty is caused mainly due to the increase in the precision error of the pressure readings associated with its calculation. As it has been discussed in Section 5.1, the precision error is related with the machine's operation. Thus, this phenomenon occurs because the SCV's control system constantly readjusts its position based on the bleed airflow demand and is responsible for the observed unsteady behaviour of surge airflow. The APU behaviour is expected to be similar in all cases where the flow can be directed simultaneously through the SCV and the BAV. APU operation in such situations is deemed as unsteady and, therefore, all these cases were excluded from the final testing plan.

Table 3-6 Final testing plan

		Electrical Power (kW)		
		0	**15.57**	**25.95**
BAV Open (%)	**0**	*Case 1*	*Case 2*	*Case 3*
	50	*Case 4*	*Case 5*	*Case 6*
	60	*Case 7*	*Case 8*	*Case 9*
	70	*Case 10*	*Case 11*	*Case 12*
	80	*Case 13*	*Case 14*	*Case 15*

By considering 10% increments of the BAV settings, the excluded cases correspond to BAV 10%-40% open. It is noted that based on the range of the extracted airflow during airborne operation, given in the relevant technical manuals, the APU operation will never fall into the unsteady region while the aircraft is in flight. Furthermore, it was noticed that when the APU operates above the 80% BAV settings, the EGT value was approaching, without exceeding, the recommended maximum safe limit. Due to the fact that this is a machine with unknown history, it was decided to avoid exercising the APU at its extreme BAV settings. Therefore, for the purposes of this study, the upper limit of the experimental plan was set at 80% BAV opening.

Having considered the above points, the operating envelope was defined as shown in Table 3-6. It includes all the combinations of the BAV being 0%, 50%, 60%, 70% and 80% open, and electrical load being extracted at 0 kW, 15.57 kW and 25.95 kW. These electrical loads are chosen because of the limits of the load bank available in the test cell. The process followed during data collection, in order to explore all the cases in the operational envelope, was to keep the bleed flow steady while changing the electical power output. The numbering of each cell in Table 3-6 corresponds to its sequence in the the experimental process. The data corresponding to the operational envelope in Table 3-6 is used for the simulation model calibration which is described in Section 5.4, with the trends discussed in Section 6.

3.5.3 Test rig validation

In order to verify that the rig produces reliable data, repeatability and consistency tests were conducted. The repeatability test investigates if the rig requires a “warm-up” period before data can be reliably collected and if the data collected under the same loading conditions is repeatable. The consistency test compares data collected under the same power settings for different ambient conditions in order to verify that they present consistent trends based on the ambient temperature.

3.5.3.1 Repeatability test

The difficulty of conducting repeatability testing is the fact that the environmental conditions cannot be controlled. In order to minimize the effect of the ambient conditions, data is collected during one single run, by loading and unloading the APU with electric and pneumatic power through its operating envelope and collecting data for test cases under pneumatic and electric load. This run is then extended by repeating the sequence two more times and repeatable datasets are collected. The target cases for repeatability testing correspond to 0%, 50%, 60%, 70% and 80% BAV settings under 0 kW and 15.57 kW of electric power in order to ensure repeatability for both pneumatic and electric power settings. The process followed in order to collect repeatable data for these test cases is described below.

Table 3-7 Sequence of test cases at repeatability test

Electric Power (kW)		0			15.57			25.95		
Loading Dataset		1st	2nd	3rd	1st	2nd	3rd	1st	2nd	3rd
BAV Open (%)	0	1	21	35	2	22	24	3	23	
	50	4	20	25	5	26	28	6	27	
	60	7	19	29	8	30	32	9	31	
	70	10	18	33	11			12		
	80	13	17	34	14	16		15		

Table 3-7 presents the power settings at which the APU was imposed during the repeatability test and the numbering represents their sequence. Initially, the load increases by increasing the electric power for each BAV setting (Cases 1-15). After reaching the maximum power setting (Case 15), the load decreases, by removing the electrical power (Cases 16 and 17) and then the pneumatic power (Cases 18-21). Following that, for 0% BAV settings, the electrical load increases (Cases 22 and 23) and then decreases (Case 24). The latter is repeated for BAV

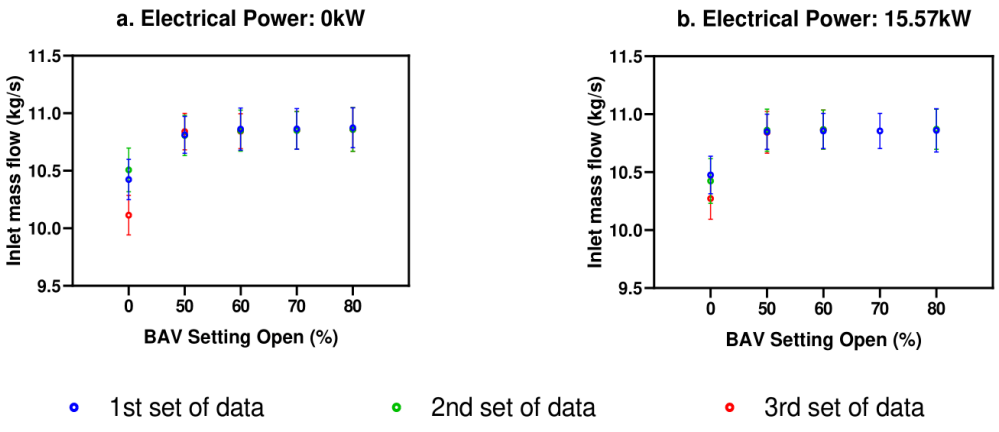

Figure 3-5 Inlet mass flow repeatability test

settings 50% and 60% (Cases 25-33). At this point of the test sequence, a circuit breaker in the load bank tripped and for this reason, at the rest of the test cases

electric power was not applied. Test case 34 corresponds to 80% BAV settings without electrical load and test case 35 corresponds to APU operation without pneumatic or electric load. Data for the selected power settings was collected when the values of the measured parameters stabilized to steady state, in order to exclude transients.

The repeatable measurements for the inlet mass flow are presented, since this parameter presented the highest difference compared to the other performance parameters. The inlet mass flow repeatable measurements for 0%, 50%, 60%, 70% and 80% BAV settings under 0 kW of electric power are presented in Figure 3-5a and under 15.57 kW in Figure 3-5b. By comparing the mean value of the measurements corresponding to the different loading cycles with the individual measured values under the same power settings, it is observed that the maximum deviation appears at the inlet airflow without electric loading and is 2.5% (Figure 3-5a, BAV 0%). As regards the other parameters, the maximum variation between the mean value and the measured values for the compressor outlet pressure is 0.67%, the compressor outlet temperature is 0.3%, the extracted mass flow is 2.2%, the EGT is 0.49% and the fuel flow is 1.05%. It is observed that the values of all measured parameters for the same power settings change only slightly for the repeated datasets. These small discrepancies can be attributed to the slight changes that were observed at the ambient temperature during testing. In general, by taking into account the measurements' uncertainties, the APU produced repeatable data for the same power settings even though it had been imposed at repeated loading conditions and operated over one and half hours. Based on the APU's observed behaviour under this test, the data collected from the rig can be trusted to be reliable regardless of its power variations and the running time.

3.5.3.2 Consistency test

The second part of the rig's validation is associated with the consistency test. The aim of this test is to ensure that the data produced from the rig are consistent with the changes in imposed ambient temperature. For the purposes of this test, data that corresponds to different BAV settings, without electrical load (Cases 1, 4, 7,

10 and 13 of Table 3-6), are compared for three different runs with ambient temperature at 9 °C, 20 °C and 27 °C (Figure 3-6). It is highlighted that, apart from the ambient temperature, more factors change during data collection under different environmental conditions (e.g. relative wind and dust accumulation in the air), that can affect the gas turbine's performance. Especially changes in the air's humidity, as it has been reported by Bird and Grabe [28], can impose considerable changes to a gas turbine's performance. Therefore, the precise identification of the quantitative changes in the APU performance parameters under different environmental conditions is a challenging task, that needs to consider all environmental elements that contribute to APU performance. By taking into account these points, in this section, the observed changes of the collected data are discussed from a qualitative point of view.

A decrease in the ambient temperature, increases the air's density (assuming barometric pressure remains constant), and by considering a fixed control volume entering the compressor, the lower the ambient temperature the higher the mass flow that enters the compressor. The changes of the inlet mass flow due to variations in the ambient temperature are presented in Figure 3-6a. In this figure, the general observation is that the inlet mass flow measurements present an increasing trend as the ambient temperature decreases, consistent with expectations. At BAV settings 70% and 80%, data corresponding to 9 °C and 20 °C tests are close to each other, compared with the data corresponding to the 27 °C test which present a higher difference. This phenomenon is also reflected at the compressor outlet pressure and fuel consumption for these cases and the reasons that this occurs are discussed at the end of this section.

Furthermore, the increased mass flow rate under lower ambient temperature results in increased compressor outlet pressure (Figure 3-6c). This phenomenon occurs because the BAV settings remain constant and increased mass flow through the same effective area results in increased outlet pressure. The measurements for the three tests present clear trends that agree with the reasoning provided above. It is observed that under 70% and 80% BAV settings, the measurements for the 9 °C and 20 °C tests are very close to each other while

data from the 27 °C test present a higher difference. This is consistent with the behaviour of the inlet mass flow corresponding to 70% and 80% BAV settings.

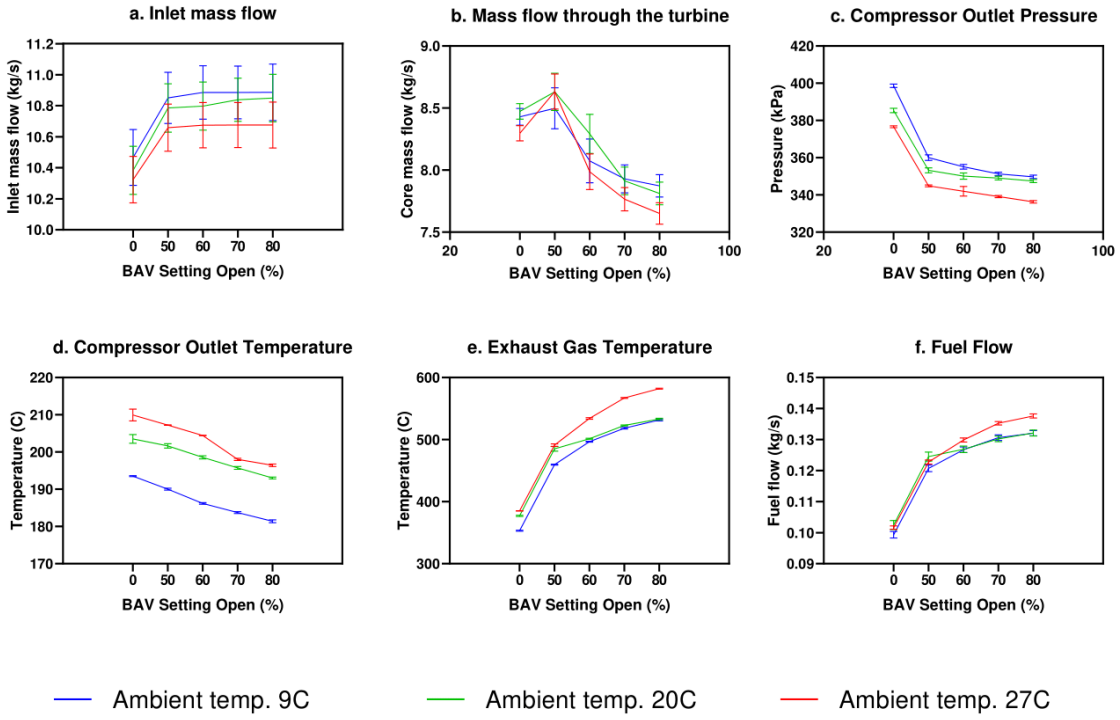

Figure 3-6 Consistency test

The change in the compressor outlet temperature presented in Figure 3-6d is the result of three competing factors. The compressor outlet temperature depends on the ambient temperature, the compressor pressure ratio, and the polytropic efficiency, as it is given by:

$$\frac{T_{out}}{T_{in}} = \left(\frac{p_{out}}{p_{in}}\right)^{\frac{1}{\eta_{com\_pol}}\left(\frac{\gamma-1}{\gamma}\right)} \quad \textbf{(3-12)}$$

The compressor polytropic efficiency, calculated by eq. (3-12), rises slightly as the pressure ratio increases. Also, the pressure ratio rises while the ambient temperature reduces. Thus, the changes in the inlet temperature and efficiency oppose the change in pressure ratio. Under the test cases that the data were collected, the change in pressure ratio is minor compared to the influence of the

inlet temperature and efficiency. For this reason, data collected under higher ambient temperatures correspond to higher compressor outlet temperatures.

Furthermore, the reduced mass flow due to increased ambient temperature results in a tendency of the APU to decrease its rotational speed because the turbine power reduces. The engine controller increases the fuel flow in order to maintain a constant rotational speed. The increased ambient temperature that enters the combustion chamber in combination with the rise in the fuel flow result in the EGT rise. Figure 3-6b presents the mass flow that enters the turbine, which is calculated from the inlet mass flow subtracting the bleed flow. Figures 3-6e and 6f present the EGT and fuel flow readings, respectively.

For BAV settings 0% and 50%, the mass flow through the turbine for the 9 °C, 20 °C, and 27 °C are very close to each other, with their differences, however, being small and falling into the measurements' uncertainties. This situation is reflected on the fuel flow measurements for these cases, which are also very close, since the mass flow through the turbine is a major driver of fuel consumption. Especially for the 50% BAV case, the core mass flow for the 20 °C and 27 °C tests are almost identical. This results in the fuel flow and EGT values, for the 20 °C and 27 °C tests, under the discussed power setting, to have almost the same value. This situation is mainly attributed to the fact that in these cases, other environmental conditions that are not considered in the analysis affect the APU performance. The EGT readings for the 27 °C test are higher compared to the 20 °C test due to the increased compressor outlet temperature corresponding to the 27 °C test. As regards the 9 °C test for the same BAV settings, the EGT readings are clearly lower than the 20 °C and 27 °C tests, which is something also related with the lower compressor outlet temperature existing at this test case.

For BAV settings 60%, 70% and 80%, the core mass flow measurements for the 27 °C test present a decreasing trend, which influences both the fuel flow and EGT measurements, that present a clear increasing trend. As regards the 9 °C and 20 °C cases, their core flow measurements are very close and fall into their uncertainty region. This phenomenon results in the differences of the fuel flow measurements, for the discussed cases to be very small. Finally, the EGT

measurements for the 20 °C test for BAV settings 60%, 70% and 80% are slightly higher compared to the 9 °C test cases and this is mainly associated with increased compressor outlet temperature for the 20 °C test.

One of the reasons that the inlet and core mass flows, EGT and fuel flow are very close for the 9 °C and 20 °C tests was described in the beginning of this section and is related with the fact the rig's operating environment cannot be totally controlled. The 20 °C and 27 °C tests were conducted during the summer, and the air's humidity during these days was lower compared to the 9 °C test which was conducted during the winter. Based on the results reported by Bird et al. [28], the increased air humidity leads to decreased inlet mass flow and increased fuel consumption. This is one of the reasons that, for the 9 °C and 20 °C tests, the differences for the inlet and core mass flows and fuel consumption are very small. Also, another factor that can impose changes in the APU performance, are the slight variations in the ambient temperature in the test cell that have been noticed even during the same run.

Concluding this section, it is observed that the differences among the 9 °C, 20 °C and 27 °C tests present distinct differences for the compressor outlet pressure and temperature, while the changes in the inlet and core mass flows, EGT and the fuel flow, in some test cases, might be masked from the measurements' uncertainties. The latter is mainly attributed to the differences in the air's humidity observed during the different tests. There were observed cases that the behaviour presented by the performance parameters cannot be clearly associated with the differences in the ambient temperature. Therefore, it is concluded that the precise understanding of the machine's behaviour under different environmental conditions requires the design of a set of experiments that are able to capture all environmental factors that contribute to the APU operation. The aim of this test is to validate the APU rig, by ensuring that the observed trends are reasonably consistent with the changes in the environmental conditions. Thus, based on the trends presented during the different tests and the discussion conducted, it can be stated that the data produced by the rig can be trusted to be consistent depending on the imposed ambient conditions.

3.5.4 Comparison of the test data with a calibrated simulation model

This section presents the process of calibrating and testing a simple gas turbine simulation model of the APU. The first objective of this task is to verify the rig testing by comparing experimental data against data calculated from a physics-based simulation model. The second objective of this task is to provide a model that can simulate the APU's performance and can be used as a baseline for future performance or diagnostic studies. The experimental data used to calibrate and test the simulation model are based on the tests conducted under varying pneumatic and electric loads and correspond to the experimentation plan presented in Table 3-6. The experimental data under no-load conditions (test case 1 of Table 3-6) were used to calibrate the components characteristics and the remaining cases (test cases 2-15 of Table 3-6) were used to test the simulation results.

The model that will be presented in this section has been built in Simulink by using the "Toolbox for the Modelling and Analysis of Thermodynamic Systems (T-MATS)". T-MATS is an open-source library developed by NASA Glenn Research Centre that provides a modelling capability for thermodynamic systems. Details regarding the equations used to model the gas turbine components, the fluid properties, and the numeric methods used to solve the equations are provided by Chapman et al. [29] and Zinnecker et al. [30]. In order to build the simulation model, an architecture of the appropriate components with defined component characteristics and boundary conditions is created. An iterative solver is used to solve the thermodynamic equations and calculates the thermodynamic parameters across the gas turbine while a Proportional – Integral (P-I) controller adjusts the fuel flow in order to maintain the rotational speed constant. More details regarding the mathematical equations used to model the APU components as well as the convergence process are included in Appendix A.

Before detailing the model's calibration process, a comment regarding the rotational speed needs to be made. All APUs are designed to operate at a constant rotational speed regardless of their operating conditions. However,

during experimental data collection, it was observed that load variations resulted in small changes in the engine's rotational speed. This phenomenon is illustrated in Figure 3-7, which presents the rise in rotational speed with an increase in extracted flow and electrical load. The maximum increase in rotational speed between the lowest and highest power setting is 0.4%. The variations in the rotational speed are attributed to the ETC design which permits certain tolerances regarding the machine's rotational speed. The effects caused to the performance parameters due to the unstable rotational speed are discussed in Section 6. Although experimental measurements indicate that the rotational speed changes during load variations, the simulation model is designed to maintain the rotational speed constant.

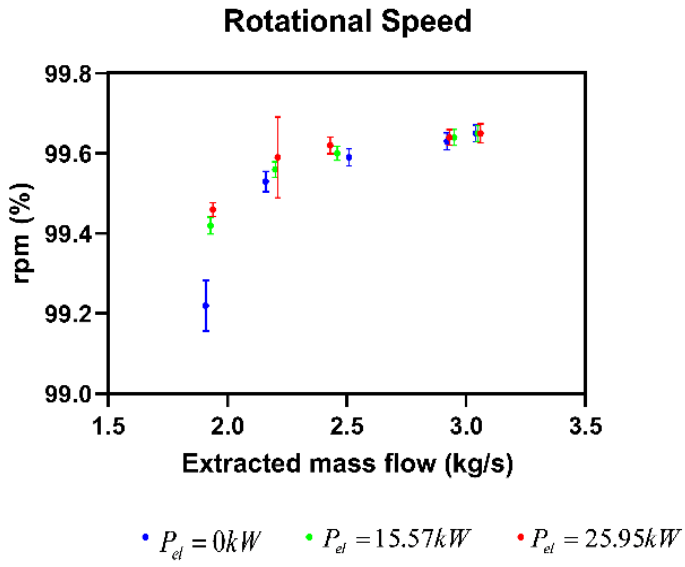

Figure 3-7 Rotational speed measurements for various power settings

The most challenging task in constructing the simulation model is the identification of the component characteristics. The characteristics that markedly affect the model's behaviour, and that will be discussed in this section, are: the compressor map that corresponds to a four-stage axial compressor, the turbine map that corresponds to a two-stage axial turbine, the burner efficiency for an annular combustion chamber, and the exhaust nozzle throat area. In order to set the compressor and turbine maps, an initial approximation for them is required.

Then these initial maps are calibrated by modifying their mass flow rate, pressure ratio, and isentropic efficiency using appropriate scaling factors.

Table 3-8 Compressor and turbine maps scaling factors

	Parameter	Scaling Factor
Compressor	Mass flow rate	$SF\_MF_{com} = \frac{MF_{com\_final}}{MF_{com\_initial}}$
	Pressure ratio	$SF\_PR_{com} = \frac{PR_{com\_final} - 1}{PR_{com\_initial} - 1}$
	Isentropic Efficiency	$SF\_EFF_{com} = \frac{EFF_{com\_final}}{EFF_{com\_initial}}$
Turbine	Mass flow rate	$SF\_MF_{tur} = \frac{MF_{tur\_final}}{MF_{\_tur\_initial}}$
	Pressure ratio	$SF\_PR_{tur} = \frac{PR_{tur\_final} - 1}{PR_{tur\_Initial} - 1}$
	Isentropic Efficiency	$SF\_EFF_{tur} = \frac{EFF_{tur\_final}}{EFF_{tur\_initial}}$

In order to identify informed estimates for the component characteristics, information from public domain literature was sought. As regards the compressor map, the rotational speed, the mass flow rate, and the pressure ratio for the original component map are given by Davenport [31] and Condon [32]. Figure 3-8 presents the original compressor map with representative operating points of the test cases in Table 3-6 superimposed. Region A on the compressor map corresponds to test cases 1-3 of Table 3-6 and Region B corresponds to test cases 4-15 of Table 3-6. The differences in APU performance between Region A and B are discussed in the next section. The only parameters missing from the compressor map are the values of isentropic efficiency. The isentropic efficiency values are estimated from the collected experimental data given by eq. (3-12), which correlates the compressor pressure and temperature ratio with its polytropic efficiency. Information for the turbine map was not available, so a notional map for the turbine was estimated. In the paper by Snyder et al. [33], a gas turbine engine for a large civil tilt rotor is characterised and its components' characteristics are estimated. This is achieved by developing notional maps for the compressor and turbine that fit the purposes of their application. One of the

results of their analysis is the identification of a notional turbine map which was derived from examples of gas turbine engines that were equipped with two-stage axial turbines. The turbine map identified by Snyder and Thurman [33] was used as the initial estimate for the turbine map in the current simulation of the GTCP660-4. Finally, the estimates for the burner's efficiency and the pressure drop across this component were based on the technology level of the period that this APU was designed. Typical values of burner's efficiency are given by Schlein [34] and range from 80% to 100%.

The process of selecting the appropriate scaling factors for the compressor and turbine maps, the value for the exhaust nozzle throat area, and the value of the burner efficiency, starts by selecting an operating point on each map and an initial guess for the burner's efficiency. The scaling factors for the compressor and turbine map, and the exhaust nozzle throat area are calculated in order to match the experimental with the simulated data for the calibration reference case. The calculation of the scaling factors follows a trial and error method until the

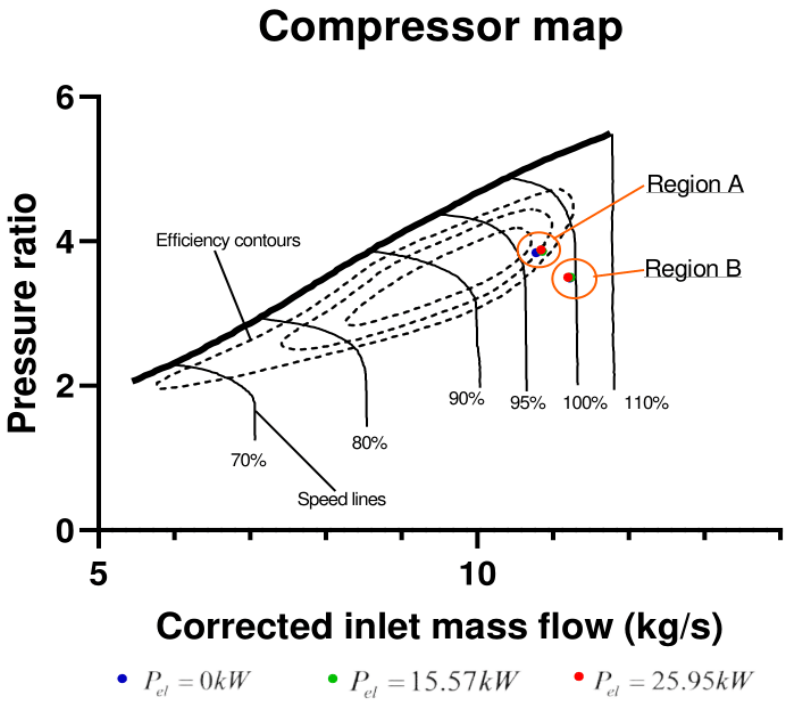

Figure 3-8 Original compressor map of GTCP660-4 with superimposed operating points

difference between the simulated and experimental data for the reference case are very small. Table 3-8 presents the formulas based on which the scaling factors for the compressor and turbine maps are calculated.

By using the modified maps and the selected values for the burner efficiency, and the throat area, the data corresponding to the other test cases are compared to the data calculated by the simulation model. If the differences between them are high, the operating points selected for scaling the maps and the value of the burner's efficiency are updated manually based on the comparison results and a new set of scaling factors, values for the burner efficiency and a value for the exhaust throat area are calculated. This process terminates when the differences between the experimental and simulated data are below an acceptable limit. After the calibration and testing process finished, the burner's efficiency is defined to be 88%, and the throat area is identified $858\ cm^2$. The pressure drop across the burner is defined to be 5%, apart from the test cases 1-3 in Table 3-6, that increases to 9.8%. The incease in the burner pressure drop, in the discussed cases, is a consequence of the increase of the turbine backpressure that reduces the velocity of the flow through the burner.

For the purposes of this work, the model's calibration process was terminated when the maximum difference for the inlet airflow was 0.61%, for the compressor outlet pressure 0.67%, for the compressor outlet temperature 0.87%, for the EGT 2.91%., and for the fuel flow 2.74%. Figure 3-11 presents the graphs that compare the experimental and simulation cases for the inlet airflow, the compressor outlet pressure, compressor outlet temperature, exhaust gas temperature, and fuel flow. By comparing the simulation results with the experimental data, it is observed that all parameters present the same trends and the difference between them is small. The differences between the experimental and simulation data can be mainly attributed to the fact that there was limited information available for the APU design characteristics and also to unmodelled effects (e.g. heat exchange between the APU and the surrounding environment). Since the model has now been calibrated and tested against experimental data,

and is based on physics, it can be trusted to simulate APU operation under degraded component conditions and can be used for future diagnostic studies.

3.6 Power variations results and discussion

In this section, the effects of loading the APU based on the test plan presented in Table 3-6 are investigated. The changes that the air and fuel flow parameters present under various loading conditions are investigated. Initially, the process of measuring the inlet mass flow is discussed. Following that, the effects that the flow extraction through the SCV has on the APU performance are examined. Finally, the variations of the performance parameters due to changes in bleed flow and electrical power are analysed.

3.6.1 Inlet mass flow measurements

The mass flow entering the compressor is measured at the inlet section of the circular duct using the equations provided in Section 5.1. Figure 3-9 presents the velocity profiles corresponding to test cases 3, 6, 9, 12 and 15 of Table 3-6. Based on the velocity measurements and the circular duct's diameter, the Reynolds number of the airflow entering the compressor is given by:

$$Re = \frac{\rho * v * D}{\mu} \quad \textbf{(3-13)}$$

and for $D = 0.54\,m$ and $\mu = 18.13 * 10^{-6}\,Pa * s$, the Reynolds number is between $13.86 * 10^5$ and $14.22 * 10^5$ which means that the flow through the inlet section is turbulent. The entrance length required for a fully developed turbulent flow as reported by Munson et al. [35] is given by:

$$L_E = D * Re^{1/6} \quad \textbf{(3-14)}$$

and it is approximately $L_E \approx 5.7m$ .The Pitot tubes in the circular duct are positioned $0.75m$ from the duct's inlet, hence the velocity profile measured in the inlet section corresponds at a flow that has not reached its fully developed state.

Based on the analysis conducted by Richman and Azad [36], for developing turbulent flows in circular ducts, an example of the velocity profile of a turbulent flow as it develops in a smooth pipe is given in Figure 3-10. The vertical axis in Figure 3-10 represents the relative radial position from the centre to the wall of the circular duct and the horizontal axis represents the ratio of the velocity at each radial point compared with the flow's velocity at the pipe's inlet. Based on the dimensions of the circular duct in the inlet section and the position of the Pitot tubes, the velocity profile is expected to have a shape similar to the line associated with $^{x}/_{D} = 2$ in Figure 3-10. Also, on Figure 3-10 there are marked the three notional areas A1, A2 and A3 of the circular duct in the inlet section as defined in Section 4, and there are superimposed the velocity measurements from the three Pitot tubes that correspond to test case 15 of Table 3-6. The expected velocity profile of the airflow through the APU inlet section explains the reason why the velocity measured by Pitot tube 2 is almost the same as the velocity measured by Pitot tube 3, which is on the centreline. Furthermore, the velocity measured by Pitot tube 1, which is closer to the wall, is lower than the

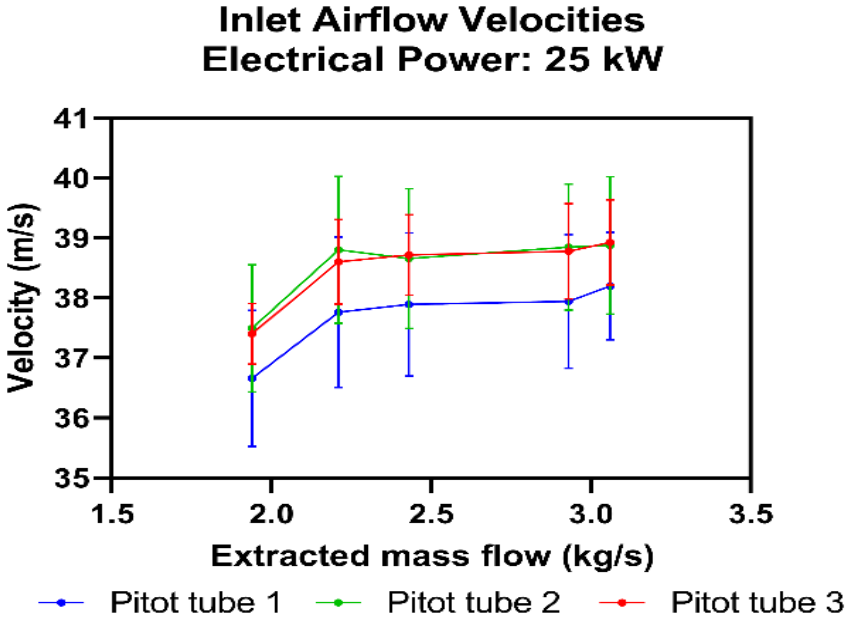

Figure 3-9 Air inlet velocity measurements for electrical load 25.95kW

velocities measured by the other Pitot tubes, which agrees with the shape of the velocity profile presented in Figure 3-10.

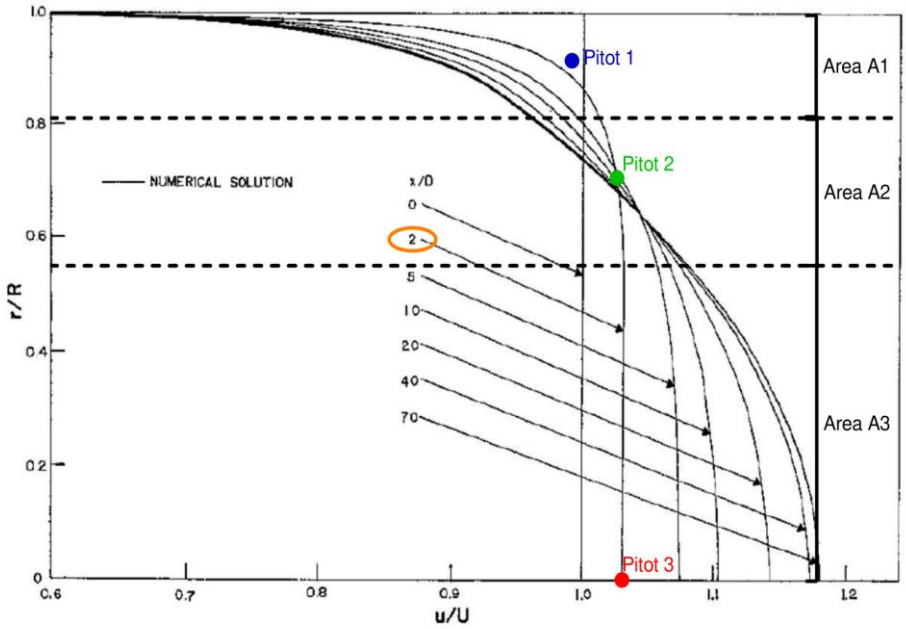

Figure 3-10 Velocity profile for developing turbulent flow reported by Richman and Azad [36]

The inlet mass flow is found from eq. (3-6). The calculation of the total inlet mass flow is the sum of the mass flows through the notional areas A1, A2 and A3 in the circular duct. Based on the positioning of the Pitot tubes 1-3, the measured velocities from each one of them are considered to be representative of the areas A1-A3. Since the mass flow through the duct remains constant, regardless of the flow development state, the integral of the relative velocity function across the relative radial position equals to the relative mass flow and is equal to one.

$$\dot{m}_{rel} = \int_0^1 \frac{v}{V}\left(\frac{r}{R}\right) d\left(\frac{r}{R}\right) \qquad \textbf{(3-15)}$$

Considering the discrete velocity measurements collected by the Pitot tubes 1-3, the above integral for the test case 15 of Table 3-6 is calculated $\dot{m}_{rel} = 1.011$. The measured mass flow is 1.1% higher than the theoretical mass flow, which means that the inlet section with the described arrangement of Pitot tubes provides reliable mass flow measurements.

3.6.2 Performance at no bleed load conditions

Figure 3-11 presents the inlet mass flow, the compressor outlet pressure, the compressor outlet temperature, the exhaust gas temperature, and the fuel flow for various cases of extracted airflow and electrical load as defined in Table 3-6. A feature observed in all parameters, apart from the compressor outlet temperature, is the significant change in the measurements for the cases corresponding to extracted flow below $2\frac{kg}{s}$ (i.e. test cases 1-3 of Table 3-6) compared to the rest of the test cases. During these test cases, as has been explained in Section 3, the airflow at the compressor outlet is extracted through the SCV and mixed with the turbine outlet flow before it exits the exhaust section. Mixing of the two streams results in an increase in the turbine's backpressure. This changes the turbine's boundary conditions and has a strong influence on the gas turbine's performance.

The increase in the turbine's backpressure results in a decrease in the mass flow rate through the gas turbine and this can be observed in Figure 3-11a. Since ambient conditions remain constant and the APU is designed to maintain its rotational speed, the compressor's operating point remains approximately on a constant speed line. Therefore, the reduced mass flow rate, caused by the increase in the turbine's back pressure, will drive the compressor to a higher pressure ratio. This phenomenon is presented in Figure 3-11b, where the compressor outlet pressure is significantly higher for the discussed cases. This also correlates with the change of the operating point on the compressor map observed between Regions A and B in Figure 3-8.

The inlet mass flow decrease leads to reduced power demand from the compressor, and for this reason, the power provided by the turbine also reduces. The reduced turbine power results in a drop in the fuel flow as it is presented in Figure 3-11e. Furthermore, the reduced fuel flow results in a decrease in the EGT, which further decreases since the turbine outlet flow is mixed with the extracted flow which has a lower temperature (Figure 3-11d).

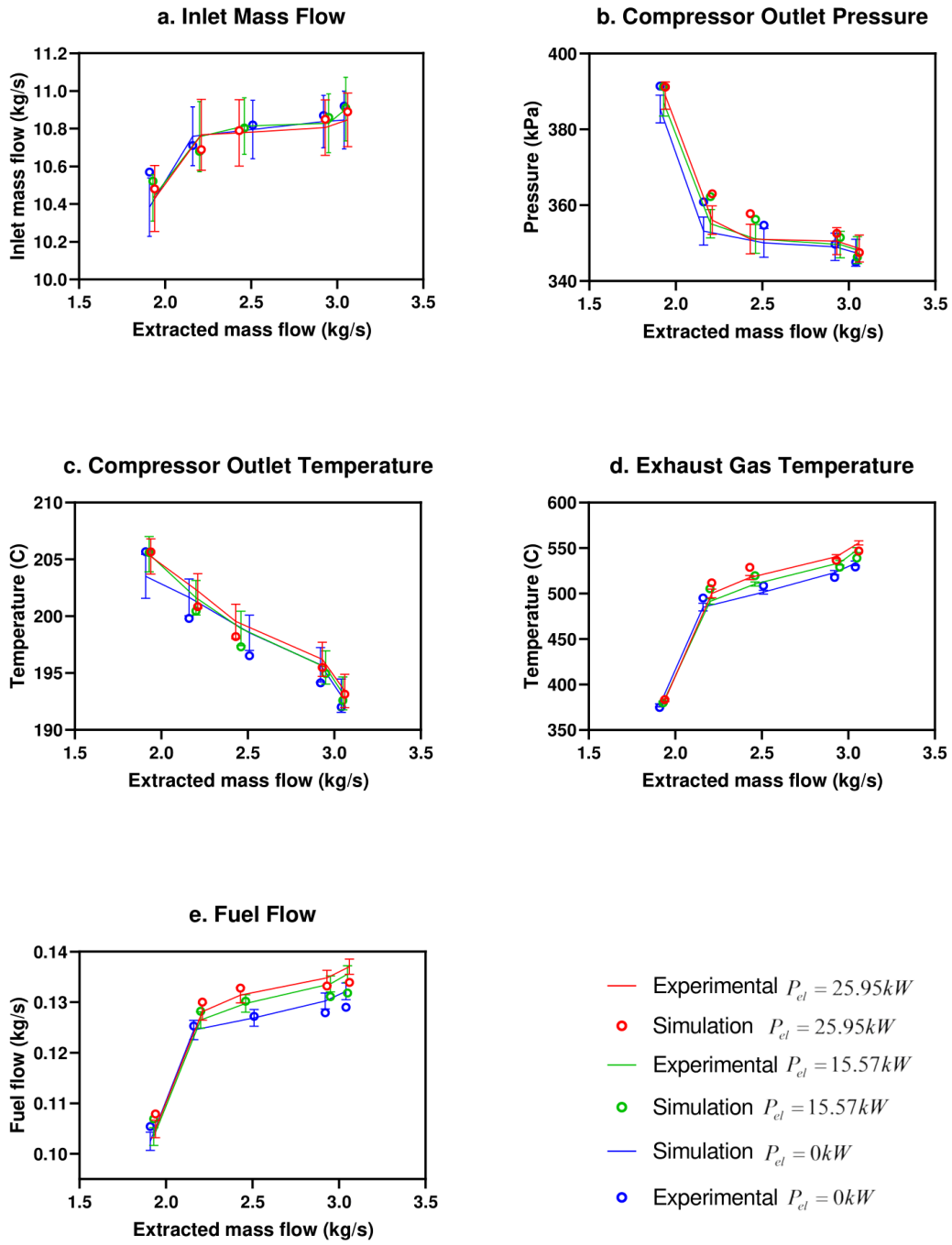

Figure 3-11 Performance parameters for power variations

Finally, as it is illustrated in Figure 3-11c, the mixing of the extracted flow with the SCV does not have a strong influence on the compressor outlet temperature. Since the ambient temperature is constant, the compressor outlet temperature depends on the compressor outlet pressure and the compressor's polytropic efficiency based on eq. (3-12). During the cases where flow is extracted through

the SCV, the compressor operates at a region with higher polytropic efficiency as it can be observed in regions A and B in Figure 3-8. Thus, the increased compressor polytropic efficiency opposes the strong increase in the outlet temperature caused by the increased pressure. This explains that, even though the increase in the turbine's backpressure has a strong influence on the outlet pressure, the effect in the outlet temperature is milder.

3.6.3 Power variation performance

As regards the test cases with both bleed flow and electric power (i.e. cases 4-15 of Table 3-6), the bleed air is not mixing with the turbine outlet flow, thus the turbine expands to ambient pressure. In these cases, while the bleed flow increases, the mass flow rate available to the turbine drops and this results in a reduction in the power generated by the turbine. Due to the reduction in the turbine's power, the rotational speed tends to decrease. Since the APU is designed to be a constant speed engine, the ETC increases the fuel flow in order to maintain the rotational speed. This phenomenon is presented in Figure 3-11e, which illustrates the changes in the fuel flow while the bleed flow increases. The direct effect from the rise in fuel flow is the increase in the EGT, which is presented in Figure 3-11d.

Furthermore, the increase in fuel flow causes a slight increase in the rotational speed due to the controller's imperfections as is shown in Figure 3-7. The rise in the rotational speed leads to an increase of the inlet mass flow. The changes in the mass flow rate for different power settings are presented in Figure 3-11a. It is noted that the rise in the mass flow rate for increasing bleed flow settings is small and can be masked from the measurement uncertainty, since these changes are generated from the rotational speed variations which are also very small.

Figure 3-11b and 3-11c present the decreasing trends of the compressor outlet pressure and temperature when the bleed flow increases. The increase in bleed flow is achieved by increasing the effective area of the bleed flow duct, which results in the decrease of the compressor outlet pressure. The pressure drop is slightly reduced by the mass flow increase, but the increased mass flow is not

enough to maintain the outlet pressure. The outlet temperature follows the same trend as the outlet pressure since they are related by eq. (3-12).

Electrical power extraction creates a reverse torque on the generator's rotor reported by Wildi [37]. The reverse torque increases the gas turbine shaft's resistance, and this tends to decrease the gas turbine's rotational speed. The ETC senses this drop in rotational speed and increases the fuel flow in order to maintain a steady rotational speed. The increase of both fuel flow and EGT is illustrated in Figures 3-11e and 3-11d, respectively.

The increase in the fuel flow due to increased electrical load causes a slight increase in the rotational speed (Figure 3-7). However, the increase in the rotational speed in these cases is so small that their effects on the inlet mass flow are masked from the measurement uncertainty (Figure 3-11a), hence no clear trends can be identified. Due to the fact that the increased electric load has a negligible effect on the inlet mass flow, no distinct trends can be identified in the compressor outlet pressure and temperature either (Figures 3-10b and 3-10c respectively). The reason that changes in the electrical power do not cause large changes in the performance parameters can be understood by considering the relation between the electrical power extracted compared with the fuel's inlet chemical power. As will be discussed more analytically in Section 6.4, the electrical power is very small compared to the fuel chemical power.

Comparing the changes in the performance parameters with the results of the most relevant study in the public domain literature, Zanger et al. [11], the following observations are made. The major difference between the two APUs under investigation is that the GTCP660-4 tends to increase its rotational speed with increasing power settings but the APU in Zanger et al. [11] presents the opposite tendency. Therefore, the effects described throughout this section related to the slight increase in rotational speed present an opposite effect in the work of Zanger et al. [11]. Also, the operation of the SCV is a characteristic of the GTCP660-4, thus its effects are unique for this APU. Finally, there are observed similarities between the machines' behaviour. These are related to the increase in the fuel

flow and the EGT in both studies caused by increasing bleed flow and electrical load, since both APUs are designed to maintain constant rotational speed.

3.6.4 APU efficiency

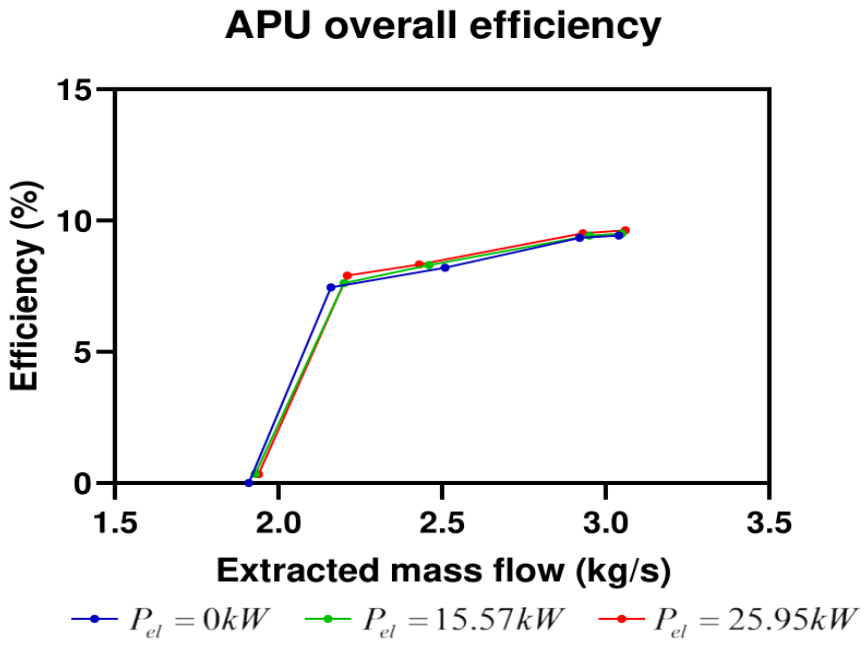

Figure 3-12 APU overall efficiency for various power settings

Following the definition provided by Zanger et al. [11], the APU overall efficiency can be defined as the ratio between the sum of bleed air and electric power to the fuel's chemical power.

$$\eta = \frac{P_{bl} + P_{el}}{P_{chemical}} \tag{3-16}$$

By this definition, the useful work that the APU delivers to the aircraft is compared with the inlet energy provided. For this reason, it is expected that the APU efficiency calculated based on eq. (3-16) will be low since it ignores the energy consumed by the compressor and the other ancillary components, which are necessary to operate the APU. P_{bleed} and $P_{chemical}$ are defined as:

$$P_{bl} = \dot{m}_{bleed} C_{p,air} (T_{out} - T_{in}) \tag{3-17}$$

$$P_{chemical} = H_f \dot{m}_f \quad \textbf{(3-18)}$$

where $C_{p,air}$ is the air specific heat at constant pressure and H_f is the kerosene's lower heating value.

Figure 3-12 presents the overall efficiency against the compressor extracted flow for three different electrical loads. The overall efficiency rises when the extracted mass flow increases. The efficiencies corresponding to no-bleed flow conditions are substantially lower compared to bleed flow conditions. During no-bleed conditions only the electrical power contributes to the APU efficiency because the extracted flow is directed through the SCV to the exhaust and does not contribute to the overall efficiency calculations. The maximum value of the overall efficiency is 9.63% for bleed flow 3.06 kg/s and electrical load 25.95 kW. The electrical efficiency is much smaller than the overall APU efficiency. The trends observed at the APU efficiency agree with the observations presented by Zanger et al. [11]. This suggests that APUs that use a single compressor for load and power generation have lower overall efficiencies compared with APUs that have separate compressors for load and power generation, as reported by Siebel et al. [10].

3.7 Summary and Conclusion

This paper offers a comprehensive experimental investigation of a Boeing 747 APU. A number of different aspects involved in this process were explored. The development of the test rig describing the APU components and their functionality, as well as information regarding the installed instrumentation, is provided. Also, described are the methods used to apply pneumatic power by installing the BAV and electric power through a load bank, and properly adjusting the generator's excitation voltage. During the rig's commissioning, it was observed that the operation of the SCV results in a region of unsteady operation. Based on the steady operating regions and safety considerations, the operational envelope was identified. The uncertainty errors of the collected data are analysed by considering the accuracy and precision errors and it was found that the

propagation of uncertainty error to the extracted mass flow measurements increases if more sensors are used for the mass flow calculation.

As regards the rig's validation, the repeatability of the collected data was investigated by designing a repeatability test. For the purposes of this test, repeated datasets were collected for test cases corresponding to the same pneumatic and power settings and their differences were measured. The results indicate that the data produced by the rig are path independent and are not affected by the running time. Also, the variations of the APU performance parameters were explored under three different ambient temperatures in order to ensure that the data collected are consistent with the ambient conditions. The outcome of this test shows that, apart from the ambient temperature, the air's humidity has a considerable influence on APU performance. The results of the consistency test indicate that the data produced by the rig are in general consistent with the imposed ambient conditions. Also, a simple gas turbine simulation model was calibrated and tested against experimental data. The process used to select the initial estimates for the components' characteristics and the identification of the appropriate scaling factors used for calibration are described. The parameters calculated by the simulation model matched closely the experimental data.

At the final part of the paper, the behaviour of the APU performance parameters under power variations was investigated. During this process, the measurement of the inlet airflow velocity profile is verified against theoretically calculated velocity profiles for developing turbulent flow. Following that, discussed is the fact that the SCV operation increases the turbine's backpressure and this impacts the APU performance. Finally, analysed are the observed trends of the performance parameters and the overall efficiency due to changes in the pneumatic and electric load.

A validated APU test rig that can be trusted to produce reliable data, and a simulation model that is considered to be representative of the APU, are the major outcomes of this work. Due to the fact that the simulation model is based on physics, it can be expanded in order to incorporate more APU components. Also,

fault modes can be injected in the modelled components and the calculated data can be used for health monitoring purposes.

3.8 References

[1] Saxon, S., and Weber, M., 2017, “A Better Approach to Airline Costs,” McKinsey & Company Travel, Transport & Logistics, McKinsey&Company, ▪New York, USA, accessed 18 July 2020, https://www.mckinsey.com/industries/travel-transport-and-logistics/our-insights/a-better-approach-to-airline-costs

[2] Peeters, P., Middel, J., and Hoolhorts, A., 2005, “Fuel Efficiency of Commercial Aircraft: An Overview of Historical and Future Trends,” National Aerospace Laboratory NLR, Amsterdam, The Netherland, accessed 18 July 2020, http://www.transportenvironment.org/Publications/prep_hand_out/lid/398

[3] IATA's Maintenance Cost Technical Group, 2019, “Airline Maintenance Cost Executive Summary,” IATA, Montreal, Canada, accessed 18 July 2020, https://www.iata.org/contentassets/bf8ca67c8bcd4358b3d004b0d6d0916f/mctg-fy2018-report-public.pdf

[4] Gorinevsky, D., Dittmar, K., and Mylaraswamy, D., 2002, “Model-Based Diagnostics for an Aircraft Auxiliary Power Unit,” IEEE International Conference on Control Applications, E. Nwadiogbu, ed., Glasgow, Scotland, 18-20 Sept. 2002, ▪DOI: 10.1109/CCA.2002.1040188.

[5] Fleuti, E., and Hofman, P., 2005, “Aircraft APU Emissions at Zurich Airport,” Unique (Flughafen Zürich AG), Zurich, Switzerland, accessed ▪18 July 2020, https://www.zurich-airport.com/~/media/flughafenzh/dokumente/das_unternehmen/laerm_politik_und_umwelt/luft/2005_zrh_apu-emiscalcmeth.pdf

[6] Dellaert, S. N. C., Hulskotte, I. J. H. J., 2017, “Emissions of Air Pollutants From Civil Aviation in The Netherlands,” Earth, Life & Social Sciences, Utrecht, The Netherlands, TNO Report No. 2017 R10055.

[7] Kinsey, J. S., Timko, M. T., Herndon, S. C., Wood, E. C., Yu, Z., Miake-Lye, R. C., Lobo, P., Whitefield, P., Hagen, D., Wey, C., Anderson, B. E., Beyersdorf, A. J., Hudgins, C. H., Thornhill, K. L., Winstead, E., Howard, R., Bulzan, D. I., Tacina, K. B., and Knighton, W. B., 2012, "Determination of the Emissions From an Aircraft Auxiliary Power Unit (APU) During the Alternative Aviation Fuel Experiment (AAFEX)," J. Air Waste Manag. Assoc., 62(4), pp. 420–430.10.1080/10473289.2012.655884

[8] Walker, C., 2018, "Heathrow Airport 2017 Emission Inventory," Ricardo Energy and Environment, Cheshire, UK, Report No. ED11486.

[9] National Transport Safety Board, 2009, "Loss of Thrust in Both Engines After Encountering a Flock of Birds and Subsequent Ditching on the Hudson River," National Transport Safety Board, Washington, D.C., USA, Report No. NTSB/AAR-10/03 PB2010-910403.

[10] Siebel, T., Zanger, J., Huber, A., Aigner, M., Knobloch, K., and Bake, F., 2018, "Experimental Investigation of Cycle Properties, Noise, and Air Pollutant Emissions of an APS3200 Auxiliary Power Unit," ASME J. Eng. Gas Turbines Power, 140(6), pp. 1–9.10.1115/1.4038159

[11] Zanger, J., Krummrein, T., Siebel, T., and Roth, J., 2019, "Characterization of an Aircraft Auxiliary Power Unit Test Rig for Cycle Optimization Studies," ASME J. Eng. Gas Turbines Power, 141(1), pp. 1–9.10.1115/1.4041119

[12] Aus Der Wiesche, S., 2012, "A Mobile Test Rig for Micro Gas Turbines Based on a Thermal Power Measurement Approach," ASME J. Eng. Gas Turbines Power, 134(11), pp. 467–477, DOI: 10.1115/1.4007201.

[13] Alejandro, D., Novelo, B., Igie, U., Prakash, V., and Szyma, A., 2019, "Experimental Investigation of Gas Turbine Compressor Water Injection for NOx Emission Reductions," Energy, 176, pp. 235–248.10.1016/j.energy.2019.03.187

[14] Li, H., Altaher, M., Wilson, C., Blakey, S., 2013, "Influence of Fuel Composition, Engine Power and Operation Mode," ASME Paper No. GT2013-94854.10.1115/GT2013-94854

[15] Owen, A. K., Daugherty, A., Garrard, D., Reynolds, H. C., and Wright, R. D., 1999, “A Parametric Starting Study of an Axial-Centrifugal Gas Turbine Engine Using a One-Dimensional Dynamic Engine Model and Comparisons to Experimental Results: Part I—Model Development and Facility Description,” ASME J. Eng. Gas Turbines Power, 121(3), pp. 377–383.10.1115/1.2818484

[16] Owen, A. K., Daugherty, A., Garrard, D., Reynolds, H. C., and Wright, R. D., 1999, “A Parametric Starting Study of an Axial-Centrifugal Gas Turbine Engine Using a One-Dimensional Dynamic Engine Model and Comparisons to Experimental Results: Part II—Simulation Calibration and Trade-Off Study,” ASME J. Eng. Gas Turbine Power, 121(3), pp. 384–393.10.1115/1.2818485

[17] Henke, M., Klempp, N., Hohloch, M., Monz, T., 2015, “Validation of a T100 Micro Gas Turbine Steady-State Simulation Tool,” ASME Paper No. GT2015-42090.

[18] Plis, M., and Rusinowski, H., 2017, “Predictive, Adaptive Model of PG 9171E Gas Turbine Unit Including Control Algorithms,” Energy, 126, pp. 247–255.10.1016/j.energy.2017.03.027

[19] Roumeliotis, I., Aretakis, N., and Alexiou, A., 2017, “Industrial Gas Turbine Health and Performance Assessment With Field Data,” ASME J. Eng. Gas Turbines Power, 139(5), p. 051202.10.1115/1.4034986

[20] Pablo, J., Bootello, N., and Price, H., 2020, “Improved Method for Gas-Turbine Off- Design Performance Adaptation Based on Field Data,” ASME J. Eng. Gas Turbines Power, 142(4), pp. 1–15, DOI: 10.1115/1.4044470.

[21] Li, Y. G., Marinai, L., Gatto, E. L., Pachidis, V., and Philidis, P., 2009, “Multiple-Point Adaptive Performance Simulation Tuned to Aeroengine Test-Bed Data,” J. Propuls. Power, 25(3), pp. 635–641.10.2514/1.38823

[22] Honeywell, “Honeywell Differential Pressure Transducer P/N:142PC01D,” Honeywell International, North Carolina, USA, accessed June ▪18 July 2020, https://datasheet.octopart.com/142PC01D-Honeywell-datasheet-

11804713.pdf

[23] Omega, 2020, “Omega Pressure Transducers P/N: PX119,” ▪Omega Engineering, Connecticut, USA, accessed June 9, https://br.omega.com/omegaFiles/pressure/pdf/PX119.pdf

[24] National Instruments, 2020, “Thermocouple Accuracy Table by Type and Temperature,” National Instruments, Texas, USA, accessed June 9, https://knowledge.ni.com/KnowledgeArticleDetails?id=kA00Z000000P8kSSAS&l=en-GR

[25] Omega, 2020, “Omega Flow Meter, P/N: FTB1300,” ▪Omega Engineering, Connecticut, USA, accessed June 9, https://br.omega.com/omegaFiles/green/pdf/FTB1300_SERIES.pdf

[26] Beyer, M., 2008, “Do You Know the Accuracy of Your Pressure Sensor ?,” Sensor Magazine, pp. 54–56, WIKA Alexander Wiegand GmbH & Co. KG, Bavaria, Germany, accessed 18 July 2020, https://en.wika.com/upload/MS_TA_0408_en_co_56493.pdf

[27] Kirkup, L., and Frenkel, B., 2006, An Introduction to Unceratinty Measurement Using the GUM, Cambridge University Press, New York.

[28] Bird, J., and Grabe, W., 1991, “Humidity Effects on Gas Turbine Performance,” ASME Paper No. 91-GT-329. 10.1115/91-GT-329

[29] Chapman, J. W., Lavelle, T. M., Litt, J. S., and T. H., Guo, “A Process for the Creation of T-MATS Propulsion System Models From NPSS Data,” National Aeronautics and Space Administration, Cleveland, OH, Report No.NASA/TM-2014-218409.10.2514/6.2014-3931

[30] Zinnecker, A. M., Chapman, J. W., Lavelle, T. M., 2014, “Development of a Twin-Spool Turbofan Engine Simulation Using the Toolbox for the Modeling and Analysis of Thermodynamic Systems (T-MATS),” AIAA Paper No. 2014-3930. 10.2514/6.2014-3930

[31] Davenport, W. R., 1974, “Impact of Turbine Modulation on Variable-Cycle Engine Performance—Phase IV: Additional Design and Fabrication Engine

Modification, Engine Modification and Altitude Test Part IIIb," AiResearch Manufacturing Company of Arizona, Phoenix, Arizona, Report No. F33615-71-C-1625.

[32] Condon, P., 2007, Flying the Classic Learjet: A Pilot Training Manual for the Learjet 35A/36A Aircraft, Flying the Classic Learjet, ▪Publisher: Peter D Condon (Individual).

[33] Snyder, C. A., Thurman, D. R., 2010, "Gas Turbine Characteristics for a Large Civil Tilt-Rotor (LCTR)," National Aeronautics and Space Administartion, Ohio, USA, Report No. NASA/TM-2010-216089.

[34] Schlein, B., 1985, "Gas Turbine Combustion Efficiency," International Gas Turbine Symposium and Exposition, Beijing, China, 1-7 Septemb, 1985, Paper No: 85-IGT-121, V002T04A

[35] Munson, B. R., Okiishi, T. H., Huebsch, W. W., 2013, Fundamentals of Fluid Mechanics Seventh Edition, 7th ed., A. P. Rothmayer, ed., Wiley, New Jersey, USA.

[36] Richman, J. W., and Azad, R. S., 1973, "Developing Turbulent Flow in Smooth Pipes," Appl. Sci. Res., 28(1), pp. 419–441.10.1007/BF00413081

[37] Wildi, T., 2014, Electrical Machines, Drives, and Power Systems, 6th ed., Pearson Educational Limited, Essex, UK.

4 FAULT SIMULATIONS AND DIAGNOSTICS FOR A BOEING 747 AUXILIARY POWER UNIT

Health monitoring of aircraft systems is of great interest to aircraft manufacturers and operators because it minimises the aircraft downtime (due to avoiding unscheduled maintenance), which in turn reduces the operating costs. The work that is presented in this paper explores, for a Boeing 747 APU, fault simulation and diagnostics for single and multiple component faults. Data that corresponds to healthy and faulty conditions is generated by a calibrated simulation model, and a set of performance parameters (symptom vector) are selected to characterise the components health state. For each component under examination, a classification algorithm is used to identify its health state (healthy or faulty) and the training strategy that is used considers the existence of multiple faults in the system. The proposed diagnostic technique is tested against single and multiple fault cases and shows good results for the compressor, turbine, Load Control Valve (LCV) and Fuel Metering Valve (FMV), even though these faults present similar fault patterns. On the contrary, the classifiers for the Speed Sensor (SS) and the generator do not provide reliable predictions. As regards the SS, the sensitivity assessment for this component showed that the existence of faults in the other components can sometimes mask the SS fault. The reason that the generator diagnosis fails under the proposed diagnostic technique is attributed to the fact that it has only a very slight influence on the other symptom vector parameters. In both cases, additional diagnostic strategies are suggested.

4.1 Introduction

4.1.1 Auxiliary Power Unit – System Background

The Auxiliary Power Unit (APU) is a system installed in all commercial aircraft and its purpose is to provide bleed air and electrical power to the aircraft systems. The APU is mainly operated when the aircraft is at the airport gate, when the main engines have not started, or in case of an emergency during flight. The APU is one of the main drivers of maintenance as reported by Liu et al. [1], and APU maintenance costs significantly increase due to component faults that lead to

unscheduled maintenance, as reported by Yabsley et al. [2]. Hence this system is worthy of study.

The APU consists of a single spool gas turbine engine that transfers energy to an electrical generator through its shaft. Bleed air is extracted either from the gas turbine's compressor or from an independent compressor (load compressor) connected to the main shaft. Representative examples for these configurations are provided by Skliros et al. [3] and by Siebel et al. [4]. The gas turbine bearings are lubricated and protected from overheating by a lubrication and cooling system. An electric motor and an ignition system are used to start the APU. Fuel flow during starting and steady-state is regulated by the fuel system, which is controlled by the APU control unit, and in modern APUs, this is a Full Authority Digital Electronic Controller (FADEC).

Previously [3] an APU simulation has been developed, calibrated, and validated against Boeing 747 APU test data. This was previous work by the current authors, which explored electrical power and bleed air extraction across a number of healthy test cases. This paper aims to take this rich simulation and extend it into a simulation of fault modes, for which experimental testing cannot readily be performed, against which to test a diagnostic technique that is able to identify multiple component faults.

4.1.2 Literature review on APU health monitoring methods

The APU has been identified by aircraft operators as a major driver for maintenance as reported by Liu et al. [1]. The system's complexity and the fact that APU performance data is rarely available, make health monitoring of the APU a very challenging task. Based on the available information and the scope of the work conducted, researchers use either model-based or data-driven methods to investigate the system's health state.

In model-based methods, performance data generated by a simulation model is compared with real systems data and, based on this comparison, component faults can be identified. These methods require accurate information regarding the component design characteristics. However, this information belongs to the

system manufacturer and it is not generally available in public domain literature. For this reason, model-based methods are not used frequently. The two most important model-based health monitoring studies have been reported by Gorinevsky et al. [5] and Gorinevsky et al. [6]. Both studies follow a similar approach in which a physics-based simulation model calculates the values of the performance parameters for given boundary conditions under healthy and faulty states. The model differences between the healthy and degraded conditions are used as an input to a fault estimator module, which has been designed to identify component faults. The results reported demonstrate that the proposed methods can identify fault modes to an acceptable level, considering the uncertainties and noise that exist in real systems.

Since model-based methods are not easily produced, and detailed engineering knowledge is needed, most published research efforts use data-driven methods. These methods aim at identifying system faults by analysing data collected from real APU systems. The analysis is conducted by machine learning algorithms that can detect patterns in the data and correlate them with known fault modes, or by statistical methods that assign probabilities to a component being healthy or faulty. The bibliography for data-driven methods in general is vast, and a comprehensive review of these methods has been provided by Lei et al. [7].

Data-driven methods require the system's performance data under healthy and degraded conditions. This can be either real system's data taken from the aircraft data reporting systems or data generated from a simulation model. In the work conducted by Vianna et al. [8] a physics-based model is used to simulate the system's operation under eight fault modes and the diagnostic analysis that was conducted considered single faults. In this analysis, the differences in the performance parameters between the healthy and degraded conditions were used to train a Classification and Regression Tree. The results demonstrated that the healthy state could be detected in all cases, but some fault modes were misclassified due to insufficient modelling data. Also, Pascoal et al. [9], used a simulation model to generate APU data under three different component faults, and based on the Exhaust Gas Temperature (EGT), bleed air pressure and fuel

flow, a linear regression classifier and a neural network classifier were trained to classify healthy and faulty conditions under single fault cases. The results showed that the neural network classifier had higher diagnostic accuracy compared to the linear regression.

Data-driven methods have been used to predict the Remaining Useful Life (RUL) of the APU system or its components. Wang et al. [10] used data from the Aircraft Condition Monitoring System to train a random forest algorithm that predicts the EGT based on other APU performance parameters. The system's health state was baselined by the random forest model and the system's degradation over time is modelled by a Bayesian probabilistic framework which assumes that degradation evolves based on a Dynamic Linear Model (DLM). The DLM is used to predict the system's RUL. This method was tested against field data of APUs belonging to a small fleet of aircraft and presented satisfactory results. Liu et al. [1] also used aircraft data to develop an algorithm that predicts the APU's RUL. Gaussian Process Regression and Relevance Vector Machine are used to predict the RUL. The EGT is used as the major RUL prediction parameter, and the influence of the bleed mass flow and gearbox oil pressure and temperature on RUL predictions are investigated. The main conclusion of this analysis was that the RUL prediction accuracy increases when more prediction parameters were considered.

The common target of all health monitoring approaches is to accurately identify component faults, or predict their RUL, in order to advise prompt maintenance action that can minimize downtime. The health monitoring studies for APU systems, presented in this section, are the most representative examples. However, many diagnostic methods can be applied to an APU depending on the scope of the research and the components examined. In the work conducted by Skliros et al. [11], a review of the different diagnostic methods that can be applied to a complex system such as the APU is presented. The selection of the most appropriate method depends on the subsystems or components under examination, taking into account all the available information.

4.2 Failure modes selection and diagnostic methodology

4.2.1 Scope of the present chapter

From a system operator's point of view, a health monitoring analysis is most valuable if it can accurately assess the system's health state and identify the Line Replaceable Units (LRUs) that should be replaced to minimise the system's downtime and avoid unscheduled maintenance. In real systems almost all components have a degree of degradation and, many times, different failure modes have similar fault patterns. This phenomenon makes the identification of the degraded components a challenging task. The aim of this work is to assess the APU health state and develop a diagnostic technique that is able to identify degraded components for single or multiple fault conditions.

In order to achieve this, a fault mode for each component under investigation is selected and its effects on the system performance is explored by injecting it into the simulation model. The effects that single and multiple faults impose on the system performance are analysed by conducting various runs for single and multiple faults under different fault severity levels. This analysis reveals the different component faults that result in similar fault patterns, and aids in the definition of the component fault severity range that will be used in the diagnostic analysis.

Following that, various simulations for single and multiple component faults are conducted, and a rich database that includes many different fault combinations is produced. Using these datasets, for each component under examination, a classification algorithm is trained appropriately in order to recognise the component health state. The most critical part of the work that is presented in this paper is that the classifier training strategy considers the existence of multiple component faults. Thus, the classifiers are trained to recognise each component health state while other components can be either healthy or faulty. Datasets that include single and multiple component faults, and have been generated independently from the training datasets, are then used to test the diagnostic classifiers. The results of the various test cases reveal the strengths and

weaknesses of the proposed technique. In the final part of this paper, methods to enhance the overall diagnostic capability are proposed.

4.2.2 Failure mode selection methodology

The Boeing Company that supports and funds this project, has identified the most frequent component faults in APU systems. Investigation of these faults by injecting them into the APU rig would be unsafe, therefore an alternate approach is taken. In this work, the validated gas turbine model is modified in order to simulate component faults, for steady-state conditions. The aim of this paper is to explore the effect that different component faults impose on the APU performance and propose a diagnostic technique that can identify the component health state for single and multiple faults, based on the system's performance parameters. The investigation of all possible fault modes that can develop in APU components is not possible due to their excessive number. For this reason, the components that have been reported to fail more frequently were chosen, and for each component a single fault mode was selected based on the relevant studies in the literature.

At this point, it is important to note that the APU which is used as a case study in this paper has an unknown history, and its health state is assumed to be deteriorated compared to a refurbished unit. The component characteristics (e.g. compressor map, turbine map, combustor efficiency, and generator windings resistance) that are used in the simulation model were adjusted in order to match the experimental data as was described in Skliros et al. [3]. These characteristics, which are calibrated against the experimental data, are used as a "healthy" baseline for the analysis that follows.

Starting with the gas turbine subsystem, the components that have been reported to influence the APU performance are the compressor, turbine, and Load Control Valve (LCV). As reported by Kurz and Burn [12], the fault modes that develop in the combustor do not cause a major effect on the gas turbine system thermodynamic performance, and for this reason this component is not included in the analysis.

Faults in the compressor can develop due to a number of different reasons (e.g. fouling, erosion, corrosion, or increased tip clearance). Most of these conditions are generated from the accumulation of foreign objects on the compressor blades which can result in changes in the geometry of the blades, and finally affect the compressor characteristics. The effects that these faults impose on the compressor performance have been discussed by many researchers and various experimental and simulation studies exist [12]–[14]. The relevant literature suggests that the changes in the compressor performance characteristics (mass flow, pressure ratio and isentropic efficiency) depend on the nature of the fault. For instance, faults that are related with increased tip clearance have been reported to decrease all three compressor performance characteristics, as reported by Graf et al. [15] and Frith [16], while fouling or erosion faults have a much stronger influence on the isentropic efficiency compared to the mass flow and pressure ratio as reported by Mund and Pilidis [17] and Fouflias et al. [18]. The compressor fault that is considered in this paper assumes that the compressor isentropic efficiency has a small decrease (up to 1%) compared to the baseline efficiency, while the relationship between the mass flow and pressure ratio in the performance map remains unaffected compared to the baseline characteristic.

As regards the turbine, the high temperature of the gas flow that enters this component damages the turbine blades and this results in various fault modes (e.g. fouling, erosion, corrosion, increased tip clearance, or thermal distortion). The relevant literature studies report that turbine degradation has a much stronger influence on the isentropic efficiency, compared to the flow capacity, as reported by Boyle [19] and Diakunchak [20]. The turbine fault that is considered in this paper, emulates a condition in which the turbine isentropic efficiency has a small decrease (up to 1%), while the mass flow and pressure ratio characteristics in the performance map do not change compared to the baseline.

The LCV directs the mass flow that exits the compressor to the aircraft pneumatic system. The LCV is a pneumatically operated valve and it consists of many different parts. The part that typically fails is the valve’s actuator, and this is

usually caused by leakage between the piston chamber of the pneumatic actuator, degraded springs, or excessive piston friction, as reported by Shang and Liu [20], and by Daigle and Goebel [21]. These faults result in deviation of the valve's commanded position, and this affects the bleed flow extraction, which in turn affects the entire APU performance. The LCV fault that is considered in this paper, simulates a sticking valve that reduces the extracted bleed flow compared to the operator's settings. This fault results in operating conditions that correspond to APU operation under lower bleed flow settings.

As regards the control system, a fault mode in the Speed Sensor (SS) is investigated. The SS calculates the APU rotational speed based on the frequency of a gear in the gearbox. Measurement of the gear frequency is achieved by a monopole in the speed sensor that changes the generated magnetic flux based on the gear's rotation. The magnetic flux measurements are converted to electrical signals that correspond to the rotational speed, and these are transferred to the APU controller. Overheating or ageing of the SS electrical parts result in faults in the SS. These faults can be bias, drift, noise, or gain in the output signal, as has been reported by Balaban et al. [23] and Goebel and Yan [24]. The fault mode that is considered in this paper simulates a condition that the output signal has a positive bias compared to the input signal. This means that the rotational speed signal that is transferred to the controller is higher than the real APU rotational speed.

The effects in the APU performance due to a fault in the Fuel Metering Valve (FMV) are also considered. The FMV is a solenoid valve, which regulates the fuel flow to the gas turbine according to the controller commands, thus it can be subjected to both mechanical and electrical faults. As regards the electrical parts, overheating can result in an increase in the resistance of the solenoid windings or, in the worst case, can cause an open circuit in one of the windings. Degradation of the valve's mechanical components and seals can also result in jamming or locked rotating parts as reported by Balaban et al. [24], Xiao et al. [25] and Cao et al. [26]. Electrical and mechanical faults can result in the following conditions:

- Drift in the valve’s position.
- Offset in the valve’s position.
- A sticking valve at a constant position.
- An inoperative valve.

The fault mode that is considered in this work simulates a sticking valve condition. This fault results in a constant fuel flow that is increased compared to the healthy state.

Finally, the influence of a generator fault in the APU performance is also explored. The generator is a complex component and it can develop faults that belong to electrical or mechanical parts. The work that is presented in this paper considers only generator faults that belong to electrical parts. Electrical faults are mostly generated from overheating, which results in an increase in resistance of the generator windings. If the resistance increases excessively open circuits can be created in the generator's windings, as it is reported by Batzel et al. [28], Batzel and Swanson [29] and Tantawy et al. [30]. The generator fault that is simulated in this work considers the increase in the generator stator resistance. The increased stator resistance increases the power imposed on the gas turbine shaft, which in turn affects the gas turbine performance.

4.2.3 Diagnostic methodology

The proposed diagnostic technique is designed to identify component health state based on system performance parameters. In order to diagnose the component health state, it is necessary to run simulations for all possible fault combinations and identify appropriate fault characteristics. Classification algorithms, if trained appropriately, can identify fault characteristics for complex systems as reported by Bettocchi et al. [31] and Bettocchi et al. [32]. For this reason, under the proposed diagnostic method, for each system component a classification algorithm is trained to recognize its health state (healthy or faulty).

The training strategy that is adopted to train the classifiers considers the simultaneous existence of multiple faults in the system. The diagnostic technique that is proposed in this work is motivated by the work conducted by Hare et al.

[33], in which Neural Network (NN) classification algorithms were trained to recognize multiple faults in an aircraft Environmental Control System. The training strategy, that considered multiple component faults, provided more accurate diagnostic predictions compared to the training strategy that was based on the single fault hypothesis.

Table 4-1 System health state scenarios

	Scenario 1	Scenario 2	Scenario 3	Scenario 4
Healthy	All components are free from degradation.	One component (different from the component under examination) is degraded and all other components are free from degradation.	The component under examination is free of degradation and other components can be either healthy or faulty.	The component under examination is free of degradation but all other components are degraded.
Faulty	Component under examination is degraded but all other components are free from degradation.	The component under examination and one more component are degraded.	The component under examination is degraded and other components can be either healthy or faulty.	The component under examination is degraded and all other components are degraded.

The diagnostic technique that is discussed in this paper is applied to the APU which is an equally complicated system, by considering more components and expanding the training scenarios compared to those used by Hare et al. [33]. The classification algorithms are trained by considering four scenarios regarding the system's health state (Table 4-1). This training strategy aims to train each component's classifier to recognize the health state of the component under investigation, while multiple faults exist in the system. The simplest scenario is based on a single fault hypothesis. This scenario assumes that only one component is degraded while all other components are healthy. The second and third scenarios assume that some components in the system can be healthy while others can be degraded. These scenarios replicate realistic maintenance situations, where some components are replaced, while others remain in the system. Finally, the fourth scenario assumes that all components suffer from a degree of degradation due to the system's operation and the individual component ageing. The advantages and limitations of the proposed method are discussed in Section 5.

4.3 Fault simulations

4.3.1 Simulation model background

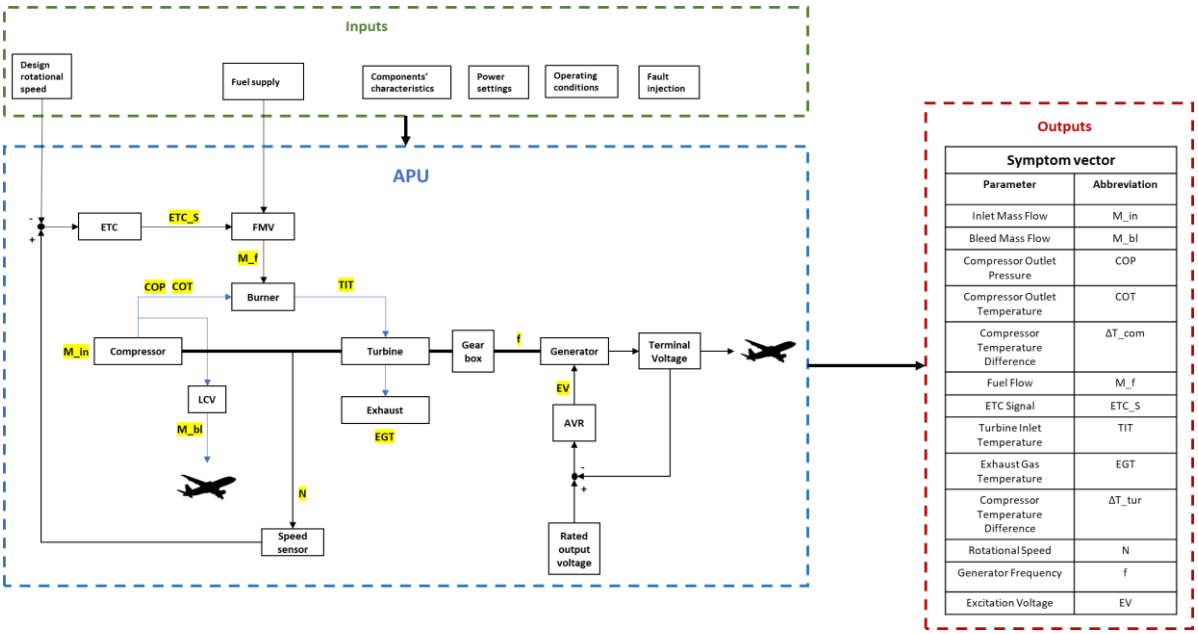

Figure 4-1 APU model schematic

Figure 4-1 presents the schematic diagram of the APU model. This model includes a 0-D simulation of the gas turbine, fuel control system and the electric generator. This model has been developed in Simulink by leveraging the Toolbox for Modelling and Analysis of Thermodynamic Systems (T-MATS) library and the characteristics of the components have been calibrated against experimental data from the GTCP660-4 APU. The inputs to the model are the fuel supply, the rated rotational speed, the operating conditions, the component characteristics, the power settings, and the component health state. The model's outputs are the APU performance parameters, from which the symptom vector values are extracted. The symptom vector characterises the system's health state and is created from virtual sensors located across the system (Figure 4-1). These virtual sensors capture the parameters that represent operation of the components and together form the symptom vector, which is the input to the diagnostic algorithm. More details related with the mathematical equations used to model the APU

components, the convergence process, and the methods used to inject faults in the gas turbine components are included in Appendix A.

Table 4-2 presents the failure modes that are considered in this analysis, as a result of the discussion given in Section 2.2. In the rest of this section, the fault injection mechanism of the respective component is presented, and the degradation range that will be considered for each one of them is be explained. The classification algorithm that is selected for each component is discussed in Section 5.

Table 4-2 Component faults that are considered into the diagnostic analysis

Subsystem	Symbol	Component	Simulated failure mode and degradation range	Classification algorithm
Gas turbine	N1	Compressor	Decreased efficiency up to 1%.	Logistic regression
	N2	Turbine	Decreased efficiency up to 1%.	Logistic regression
	N3	Load Control Valve	Bleed flow reduced up to 1%.	Support vector machine
Control	N4	Speed sensor	Output signal increased up to 0.5%.	Classification tree
Fuel	N5	Fuel Metering Valve	The valve is stuck in a position that is increased up to 1% compared to the healthy case.	Classification tree
Generator	N6	Generator	Generator's stator resistance increased up to 5%.	k-nearest neighbour

4.3.2 Gas turbine

The gas turbine's model schematic is presented in Figure 4-1 and the iterative solver that calculates the model's solution is presented in Figure 4-2. The iterative solver aims to drive E1-E3 to zero by changing the values of the Independent Variables. The gas turbine's performance parameters are based on the inlet mass flow, and the operating points on the compressor and turbine maps. They are calculated by thermodynamic equations included in T-MATS.

The literature that is cited in Section 2, and investigates faults in the compressor and turbine, reports various fault modes that result in changes in the mass flow, pressure ratio and isentropic efficiency of the compressor or turbine. In this work, a simplified approach for these component faults is taken by assuming that the compressor or turbine isentropic efficiency decreases, while the characteristics of the mass flow and the pressure ratio, as they are defined in the component design maps, remain unaffected. The compressor and turbine isentropic efficiencies are defined by the following equations:

$$\eta_{com,isen} = \frac{\Delta T_{com}}{\Delta T_{com,isen}} = \frac{COT - CIT}{COT_{(isen)} - CIT} \quad \textbf{(4-1)}$$

$$\eta_{tur,isen} = \frac{\Delta T_{tur}}{\Delta T_{tur,isen}} = \frac{TIT - EGT}{TIT - EGT_{(isen)}} \quad \textbf{(4-2)}$$

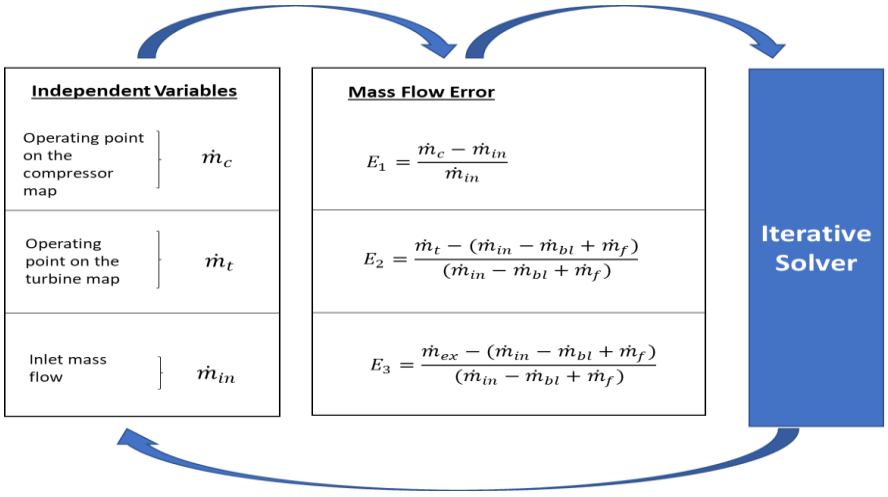

Figure 4-2 Gas turbine solver schematic

The reduced efficiency of the compressor and turbine change the component operating point, and this affects the entire system's performance. The effects that these faults impose on the symptom vector are discussed in Section 4.1.

The fault mode considered in the LCV simulates a condition that the valve is stuck, and it cannot provide the requested bleed flow. This fault mode is emulated by decreasing the bleed flow demand and the system's performance corresponds to healthy operation under lower power settings. The changes imposed on the symptom vector due to these faults are further elaborated in Section 4.1.

4.3.3 Control and Fuel System

The APU's control system monitors the machine's performance and ensures its safe operation. The part of the control system discussed in this paper is related to the adjustment of fuel flow to the gas turbine. The components that are involved with fuel control are illustrated in Figure 4-1.

The fuel flow to the gas turbine is adjusted in order to maintain constant rotational speed regardless of the changes in power settings, operating conditions, or the degradation of the components. The fuel flow is regulated by the FMV which is controlled by the APU Electronic Turbine Controller (ETC). The ETC is simulated by a PI controller that accepts as an input the difference between the sensed rotational speed and the rated rotational speed, regulating the FMV's position between fully open and fully closed.

The maximum fuel flow to the gas turbine (FMV fully open) is given by the APU maintenance manuals and based on this information the controller's signal is regulated accordingly.

The fault injected in the FMV assumes that the valve is stuck and the fuel flow to the gas turbine is constant regardless of the controller's command. The gas turbine's rotational speed is transferred to the controller by a speed sensor (SS). For the purposes of this work, the sensor's dynamic characteristics are ignored. The failure mode that is injected into the SS simulates a condition that the signal transferred to the ETC has a constant positive bias. The changes caused to the symptom vector due to the FMV and SS faults are discussed in Section 4.2.

4.3.4 Generator

The electric generator is a synchronous machine that consists of an excitation and a load circuit. Mechanical power is transmitted to the generator's shaft from the gas turbine through a gearbox (Figure 4-1). The generator provides constant output voltage regardless of the load, the changes in the rotational speed or the generator's health state. This is achieved via an Automatic Voltage Regulator (AVR) that adjusts the excitation voltage in order to regulate the armature's magnetic flux accordingly.

The generator model assumes steady-state operation and balanced load across its phases. The output Line-to-Line voltage is calculated by the following equations:

$$V_{out} = V_{arm} - I_{load} * \left(\sqrt{{X_{in}}^2 + {R_{stat}}^2}\right) \quad \textbf{(4-3)}$$

$$V_{arm} = \sqrt{2} * \pi * \varphi * \frac{N_{gen}}{20} \quad \textbf{(4-4)}$$

In eq. (4-3), V_{arm} is the armature's voltage, I_{load} is the current flow through the electric load, R_{stat} is the stator resistance and X_{in} is the sum of the stator and armature inductive reactance. The stator's resistance is $R_{stat} = 0.4\,\Omega$ and the value of the generator's total inductive reactance (X_{in}) was adjusted in order that the simulation results could match the experimental data. The excitation circuit and the AVR are simulated by a PI controller that compares the output voltage with the rated voltage and adjusts the armature's magnetic flux accordingly. However, as opposed to the excitation voltage, the magnetic flux cannot be measured in real systems. For this reason, an empirical relationship between the magnetic flux and the excitation voltage is created. Experimental data of the excitation voltage are correlated with the simulated armature's magnetic flux through a polynomial equation and the following empirical relationship is established:

$$V_{ex} = 5497.328 * \varphi^2 - 1235{,}807 * \varphi + 73.54 \quad \textbf{(4-5)}$$

The generator's operation creates a counter torque to the generator shaft, which is transmitted to the gas turbine's shaft. The power demand from the generator is calculated based on the following formula:

$$P_{gen} = \frac{V_{arm}^2}{R_{arm}} \quad \textbf{(4-6)}$$

In eq. (4-6), the armature's resistance is: $R_{arm} = 1.52\ \Omega$.

The generator fault mode considered in this work assumes that the stator resistance (R_{stat}) increases due to overheating. The changes imposed on the symptom vector under the generator fault, for various degradation levels, are presented in Section 4.3.

4.4 Sensitivity assessment of the APU model under the influence of faults

In this section, the component faults are injected into the simulation model, the changes in the APU performance are discussed and the model's sensitivity is assessed by simulating various levels of degradation for each component fault. The sensitivity assessment ensures that the simulation results are consistent with the APU performance under faulty conditions and contributes to the definition of the component degradation ranges that will be investigated in the diagnostic analysis.

The boundary conditions selected to conduct the fault simulations correspond to the maximum power settings imposed on the APU rig that was used to calibrate the model, these are:

- Bleed flow: 3kg/s
- Electric power: 25 kW
- Ambient temperature: 20 °C
- Altitude: Sea level
- Mach number: APU stationary

The influence of each component fault is investigated in isolation, following the methodology reported by Norton [34]. Also, representative examples of multiple

faults that create similar changes in the symptom vector and result in ambiguous fault conditions are discussed in this section. The influence that all fault combinations impose on the symptom vector cannot readily be analysed due to the large number of all possible fault combinations. The effects that multiple faults have on the APU performance are captured by classification algorithms that are used to identify each component's health state under single and multiple faults and are further discussed in the diagnostic analysis in Section 5.

The compressor operating point influences the APU performance under the various faults. For this reason, the operating points that correspond to the faults that are considered in this paper (for a single case) are illustrated in Figure 4-3. The points N1-N6 correspond to the component faults shown in Table 4-2. The change of the compressor operating point aids the understanding of the APU performance under faulty conditions and will be discussed throughout this section.

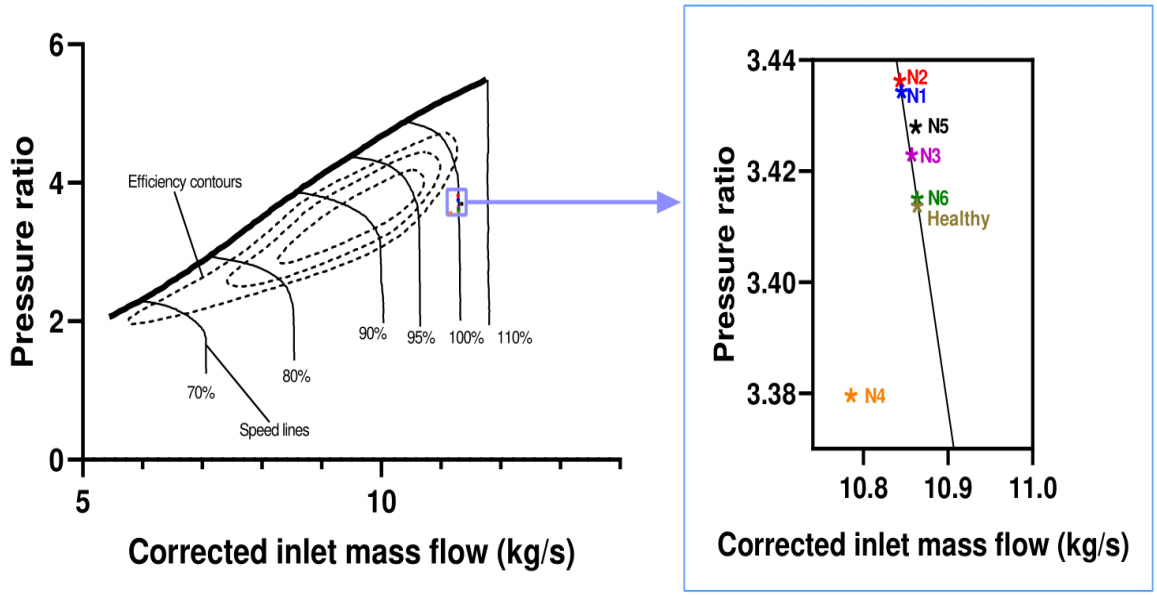

Figure 4-3 Compressor operating points

4.4.1 Gas turbine faults

In this section, the effects of the gas turbine component faults on the APU performance are analysed. Initially, each fault is discussed in isolation and then,

at the end of this section, representative examples of multiple faults are presented.

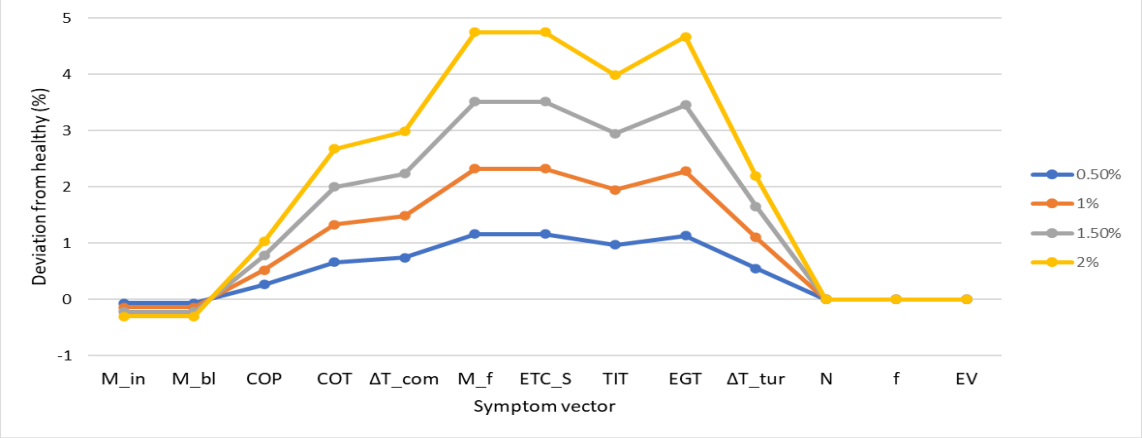

Figure 4-4 Sensitivity assessment for the compressor fault

Starting with the compressor, a fault in this component is simulated by reducing the component efficiency and the imposed changes on the symptom vector are presented in Figure 4-4. In this, and subsequent figures, the deviation of a variable from healthy (y-axis) is plotted for each variable (x-axis). The variables are shown in the table of Figure 4-1 and represent the main parameters governing the performance of the APU. Each individual deviation is connected with a solid line to give a visual representation of the symptom vector and conveys no other meaning. The change of the compressor's operating point that corresponds to decreased efficiency by 1% is illustrated in Figure 4-3 (N1). Due to the fact that the APU maintains constant rotational speed, the compressor operating point remains on the same speed line and the relationship between the inlet mass flow and the pressure ratio is dictated by the shape of the speed line on the compressor map.

Under the discussed compressor fault, the decreased compressor efficiency shifts the compressor operating point to reduced mass flow. As a consequence, based on the compressor's design characteristics (Figure 4-3), the pressure ratio and the compressor outlet temperature increase. The power consumed by the compressor can be calculated from:

$$P_{com} = \dot{m}_{in} * C_{p,air} * \Delta T_{com} \quad \textbf{(4-7)}$$

Assuming that the specific heat of air at constant pressure ($C_{p,air}$) remains almost constant, the compressor power depends on two opposing factors: the inlet mass flow and the temperature difference across the compressor. Since the temperature difference across the compressor presents a stronger change compared with the inlet mass flow (Figure 4-4), the compressor power consumption increases. As a consequence, since the controller keeps the rotational speed constant, the turbine needs to provide more power, which leads to a rise in the fuel flow.

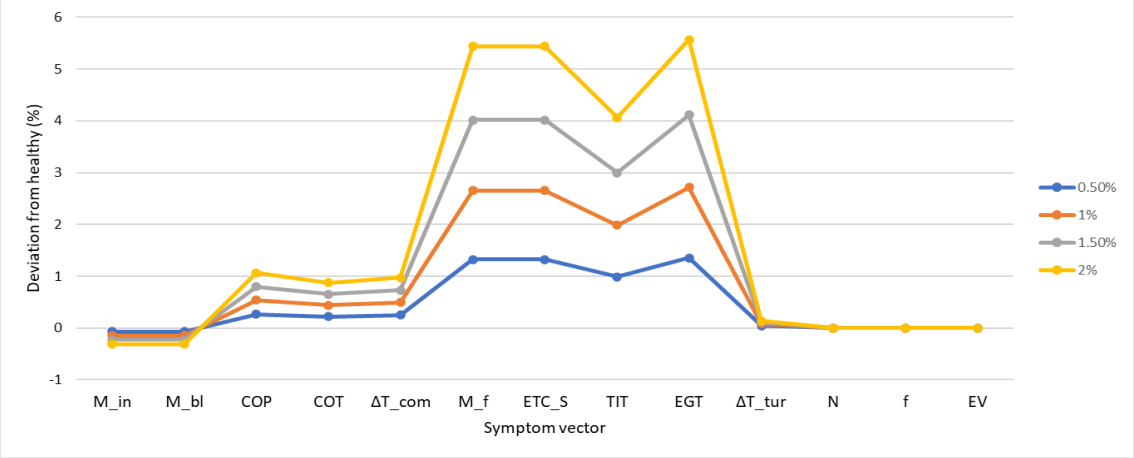

Figure 4-5 Sensitivity assessment for the turbine fault

The effects of a turbine fault on the APU performance are investigated next. The turbine fault is emulated by decreasing the turbine efficiency and Figure 4-5 illustrates the changes in the symptom vector due to this fault for 4 severity levels. Figure 4-3 (N2) presents the change in the compressor operating point due to a decrease in the turbine efficiency by 1%. The reduced turbine efficiency drives the compressor and turbine operating points to reduced mass flow. Thus, since the APU keeps its rotational speed constant, the COP and COT increase due to the shape of the compressor characteristic line (Figure 4-3).

The changes in the fuel flow are associated with the power balance between the compressor and the turbine. The power provided by the turbine is calculated by the following equation:

$$P_{tur} = (\dot{m}_{in} + \dot{m}_f - \dot{m}_{bleed}) * C_{p,gas} * \Delta T_{tur} \quad \textbf{(4-8)}$$

Based on the changes in the performance parameters presented in Figure 4-5, the value of the factor $(\dot{m}_{in} + \dot{m}_f - \dot{m}_{bl})$ remains almost constant. However, the temperature difference across the turbine reduces since it is calculated by eq. (4-2), and the turbine efficiency decreases. Thus, under the discussed fault, the power provided by the turbine decreases. As regards the compressor power consumption, it is calculated by eq. (4-7) and based on the changes in the APU performance parameters in Figure 4-5, it is observed that the decrease in the inlet mass flow is much lower compared to the increase in the temperature difference across the compressor. Thus, the compressor power consumption, under the turbine fault, increases. The decrease in the power provided by the turbine in combination with the increase in the compressor power consumption creates a tendency of the APU to reduce its rotational speed. However, since the controller is designed to keep the rotational speed constant, the fuel flow increases.

The compressor and turbine are mounted on the same shaft, and for this reason, a fault in one of these components affects the performance of the other, therefore it is worthwhile to compare the changes that the compressor and turbine faults impose on the APU performance. Figure 4-6 presents the changes in the symptom vector when the efficiency of each component individually is decreased by 1%.

Initially, it is noticed that even though the compressor operating point is almost the same for both faults (Figure 4-3: N1 and N2), the COT increases more under the compressor fault. This is explained due to the fact that the COT is calculated from eq. (4-1) and the compressor isentropic efficiency reduces (the Compressor Inlet Temperature (CIT) remains constant).

Another observation that can be extracted by comparing the changes in APU performance under the compressor and turbine faults (Figure 4-6) is that the TIT is almost the same for both faults, while the EGT presents a stronger increase under the turbine fault compared to the compressor fault. The TIT depends on 2 factors: the COT and the fuel flow. The COT is higher under the compressor fault,

while the fuel flow is higher under the turbine fault. The influence of the compressor and turbine faults on these parameters result in almost equal changes in the TIT for both faults. This is associated with the temperature difference across the turbine. The EGT is calculated by eq. (4-2) and it is based on the TIT and the turbine efficiency. The decreased turbine efficiency under the turbine fault results in a lower temperature difference across the turbine, and this explains the increased EGT observed under the turbine fault compared to the compressor fault.

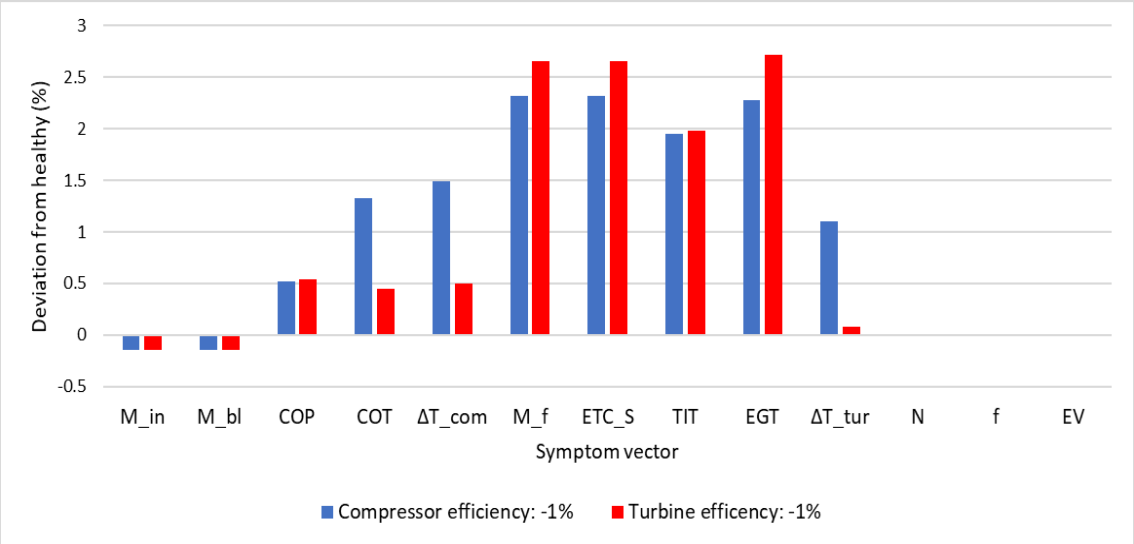

Figure 4-6 Comparison of the compressor and turbine faults

Finally, it can be observed that even though the compressor and turbine faults have the same fault severity (efficiency decrease by 1%), there is a higher increase in the fuel flow under the turbine fault. The fuel flow ensures that the turbine power matches the compressor power consumption. The compressor and turbine power are calculated by eq. (4-6) and (4-7), respectively. By comparing the magnitude of the changes in the inlet mass flow and the COT in Figure 4-6, it can be concluded that the compressor power consumption increases under both the compressor and the turbine fault. Under the compressor fault, the compressor power consumption increases, and for this reason, the fuel flow increases until the power balance between the compressor and the turbine is achieved. Under the turbine fault, the turbine power decreases (because the turbine efficiency drops) and since the turbine power must satisfy the compressor power demand,

the fuel flow rises. Moreover, as it was described in the previous paragraph, under the turbine fault the compressor power consumption also increases and this results in a further increase of the fuel flow, hence the increased fuel flow under the turbine fault.

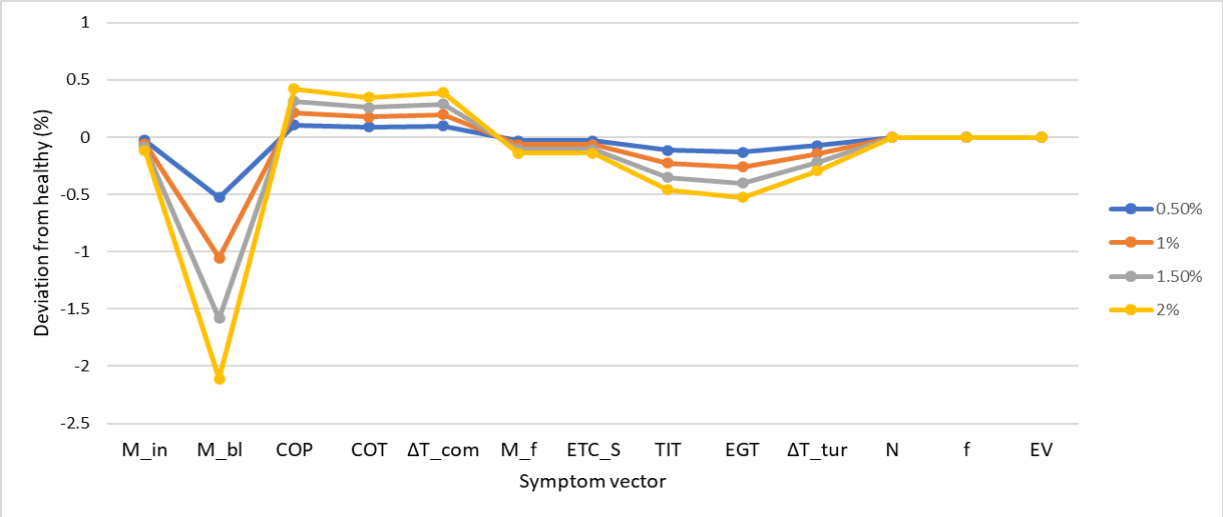

Figure 4-7 Sensitivity assessment for the LCV fault

Following the compressor and turbine faults, the effect of a sticking valve on the APU performance is investigated. Under this fault, the valve is assumed to get stuck at a position that results in reduced bleed flow compared to the operator's demand, and for this reason, the sticking valve fault is emulated by decreasing the bleed flow demand. Figure 4-7 presents the changes in the symptom vector due to the LCV's fault for various severity levels and Figure 4-3 (N3) illustrates the change of the compressor's operating point for reduced bleed flow by 1%. The sticking valve fault decreases the effective area at the compressor outlet, and this results in an increase in the pressure ratio and compressor outlet temperature. Based on the characteristics of the compressor performance map (Figure 4-3), the increase in the pressure ratio accompanies a decrease in the inlet mass flow. Since the reduction in bleed flow is more than the decrease of the inlet mass flow (Figure 4-7), the mass flow through the turbine increases and this results in a rise in turbine power. This phenomenon creates a tendency of the APU to increase its rotational speed and because the controller keeps the rotational speed constant, the fuel flow reduces.

Having concluded the investigation of the individual gas turbine faults, the effect of multiple faults in the APU performance are now discussed. By observing Figures 4-4, 4-5 and 4-7 it is noticed that the component faults discussed above have distinct features (i.e. shape of symptom vector) and can be easily identified under a single fault hypothesis. However, if multiple faults exist in the system, various fault combinations result in similar changes in the APU performance. Figure 4-8 illustrates an example of 4 different fault combinations that create similar changes in the symptom vector. These examples consider faults only in the gas turbine components and FC1-FC4 indicate their corresponding Fault Conditions. It can be seen that a fault diagnostic approach that is based on the single fault hypothesis will fail to identify the component health state in these cases since different fault combinations can result in similar fault patterns. The diagnostic technique that is proposed in this work takes into account cases where multiple faults exist in the system and the diagnostic classifiers are trained accordingly. The strengths and weaknesses of the proposed technique are discussed in Section 5.

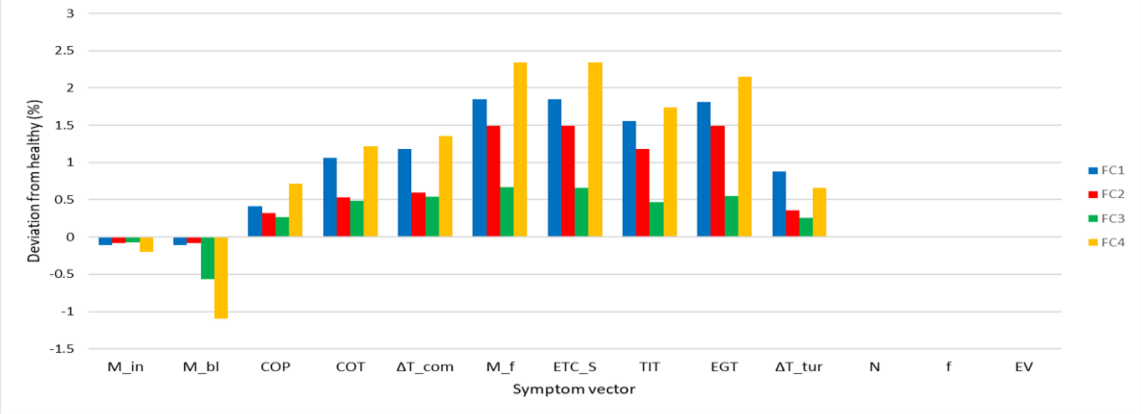

	Compressor efficiency decrease	Turbine efficiency decrease	Bleed flow decrease	SS signal bias	FMV position stuck increased from healthy state	Generator stator resistance increased
FC1	0.8%	0%	0%	0%	0%	0%
FC2	0.3%	0.3%	0%	0%	0%	0%
FC3	0.3%	0%	0.5%	0%	0%	0%
FC4	0.7%	0.3%	0.9%	0%	0%	0%

Figure 4-8 Gas turbine multiple fault combinations

4.4.2 Control and Fuel System faults

Following the gas turbine components, faults in the control and fuel system are analysed. In this section, fault modes for steady-state operation are considered for the Speed Sensor (SS) and the Fuel Metering Valve (FMV).

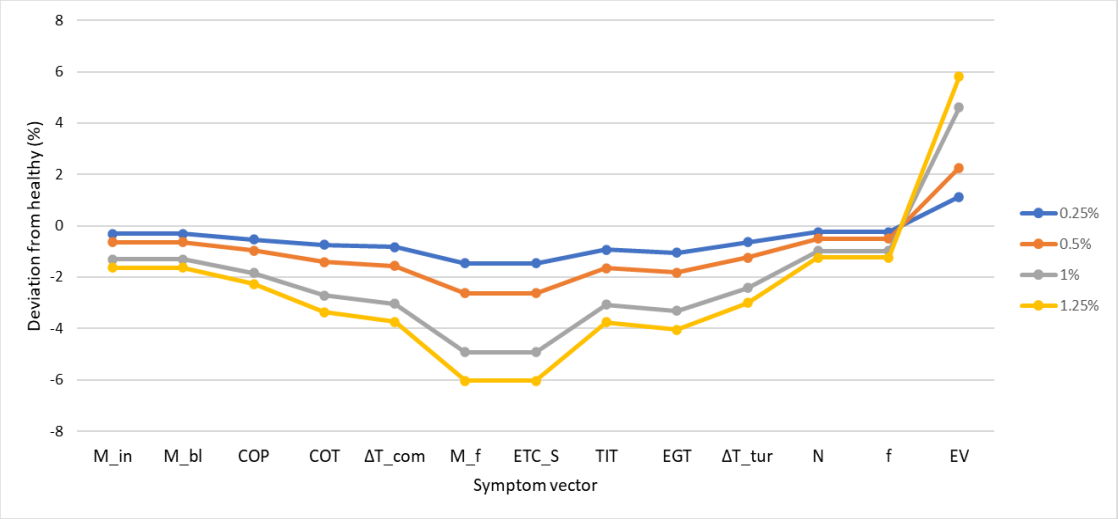

Figure 4-9 Sensitivity assessment for the speed sensor fault

As regards the SS, the simulated fault emulates a condition under which the rotational speed signal that is transferred to the APU Electronic Turbine Controller (ETC) has a constant positive bias, i.e. the actual speed is lower than that indicated. Figure 4-9 presents the corresponding changes in the symptom vector and Figure 4-3 (N4) illustrates the compressor operating point that corresponds to a 0.5% biased signal. This fault makes the controller reduce the fuel flow in order to decrease the rotational speed until the difference between the sensed rotational speed and the APU's design rotational speed (20,000 rpm) drop below a predefined threshold. This threshold sets the convergence limit of the PI controller that is used to emulate the ETC. For this reason, the change of the rotational speed under the SS fault does not match exactly with the bias injected in the SS. Under this fault, the compressor operating point moves to a lower speed line, which corresponds to a reduced inlet mass flow and pressure ratio (Figures 4-3 and 4-9). Finally, the reduced rotational speed decreases the generator's frequency, and this drives the generator's controller to increase the excitation voltage to maintain a constant output voltage.

The FMV fault replicates a sticking valve condition that keeps the fuel flow constant regardless of the controller's command. Figure 4-10 presents the changes in the symptom vector for the FMV fault, and Figure 4-3 (N5) illustrates the compressor operating point for a stuck FMV in a position that increases the fuel flow by 1% compared to the healthy state. Under this fault, since the fuel flow remains constant, the turbine power increases, and this leads to an increase in the rotational speed. The controller senses the over-speed condition and commands the FMV to close. Since the FMV does not react to the control signals, the controller dictates the FMV to become fully closed and this explains the huge difference that is observed to the "ETC_signal" parameter (Figure 4-10). The controller's behaviour is related to the fact that the FMV ignores the control signal, therefore, regardless of the fault's severity, the controller will always command the FMV to become fully close. Furthermore, the increased rotational speed drives the compressor operating point to a higher speed line that very slightly decreases the mass flow and increases the pressure ratio, as shown in Figure 4-3. Finally, the rise in the rotational speed increases the generator's frequency, which decreases the excitation voltage.

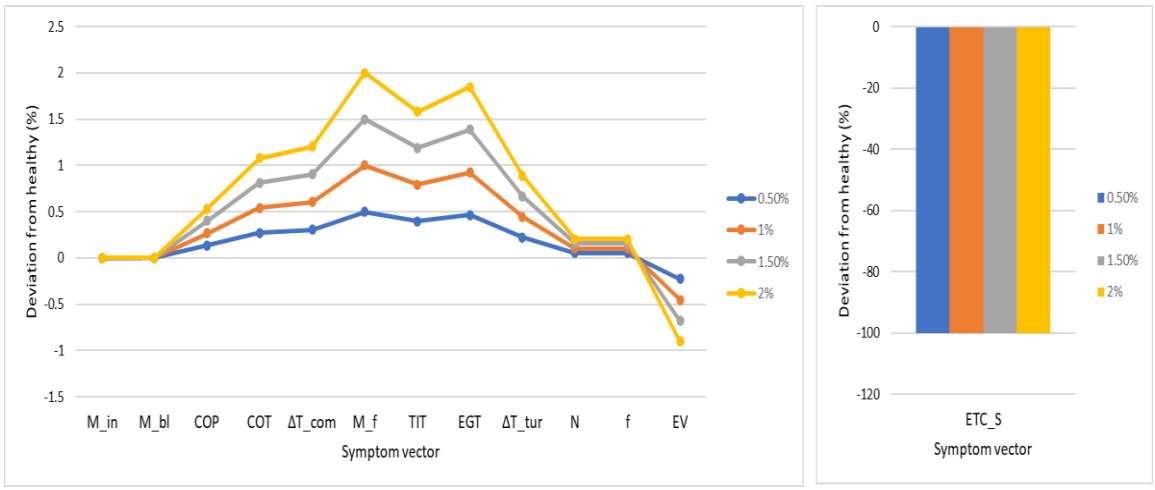

Figure 4-10 Sensitivity assessment for the FMV fault

The effects of the SS and FMV faults on the APU performance, like the gas turbine faults, are distinct and can be easily identified under single fault modes. However, when multiple faults exist in the system, the imposed changes on the symptom vector can vary and sometimes a fault can be completely masked.

These situations are presented in the examples FC5-FC7 that are illustrated in Figure 4-11. Initially, the test case FC5 (Figure 4-11) is considered. In this test case, the compressor and turbine efficiencies are decreased by 1%, and the FMV is stuck in a position that allows 0.5% more fuel flow compared to the healthy state. Under this fault combination, the constant fuel flow is not enough to drive the gas turbine's rotational speed up to its rated value, due to the compressor and turbine degradation. The controller senses an under-speed condition and commands the FMV to open. This example demonstrates that the FMV fault can result in over-speed or under-speed conditions depending on the health state of the other components.

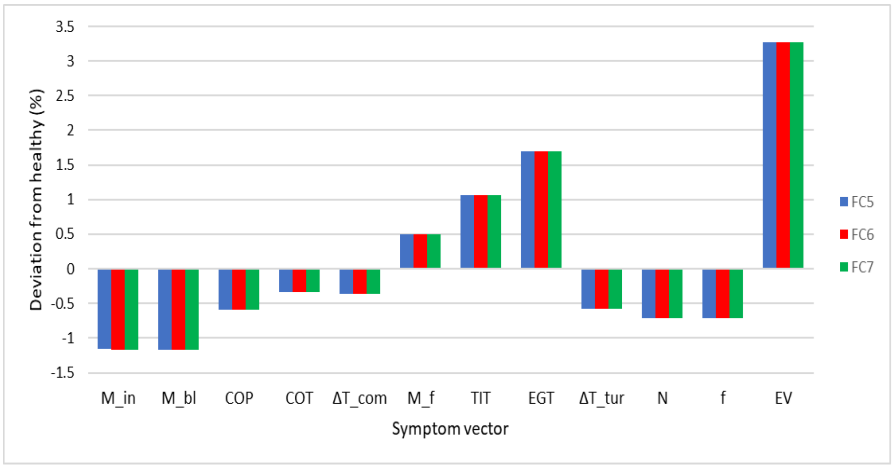

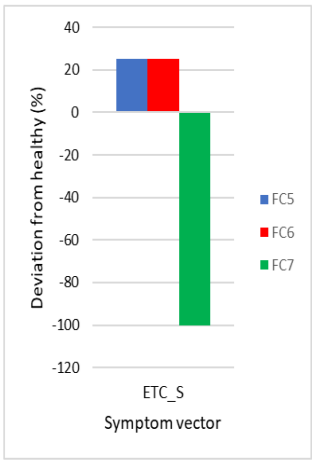

	Compressor efficiency decrease	Turbine efficiency decrease	Bleed flow decrease	SS signal bias	FMV position stuck increased from healthy state	Generator stator resistance increased
FC5	1%	1%	0%	0%	0.5%	0%
FC6	1%	1%	0%	0.2%	0.5%	0%
FC7	1%	1%	0%	0.8%	0.5%	0%

Figure 4-11 Fault combination that can mask the SS fault

The example FC6 considers a test case that includes the faults described in FC5 supplemented with a fault in the SS. It is observed that the changes imposed on the symptom vector for FC6 are identical with the changes that correspond to FC5; hence the SS fault is completely masked. This occurs because, as it was explained above, the faults in FC5 create an under-speed condition and the

severity of the SS fault in FC6 is not strong enough to stimulate an over-speed. Therefore, the addition of a SS fault with low severity to FC5 does not affect the symptom vector, because the fuel flow remains constant (the FMV is stuck) and the controller's command corresponds to an under-speed condition. In a test case that the SS fault severity is strong enough to create an over-speed condition, as seen in the example in FC7, the controller commands the opposite reaction compared to the previous test cases, hence the SS fault can be identified.

4.4.3 Generator fault

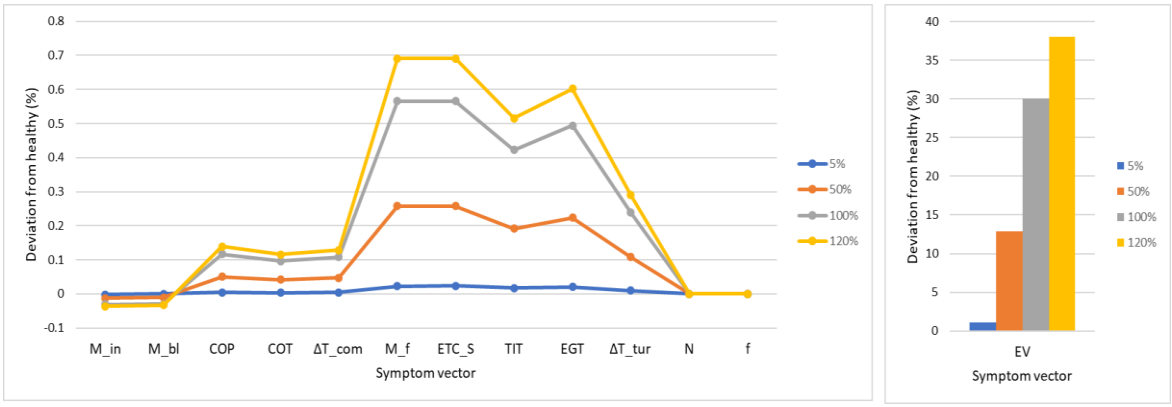

Figure 4-12 Sensitivity assessment for the generator fault

The failure modes that can be developed in an electric generator are numerous and can affect both the electrical part and the mechanical part of the generator. For this work, a simple electrical fault that simulates the increase in the stator's resistance is considered. Under this fault, the generator's output voltage presents a tendency to decrease. The generator's controller increases the excitation voltage (EV), which generates a magnetic flux to keep the output voltage constant. The increased EV results in an increase in the armature voltage, which in turn leads to an increase in power demanded from the gas turbine's shaft.

Figure 4-12 presents the changes imposed on the symptom vector under the generator fault, corresponding to 4 different levels of degradation. It is observed that the influence of the generator fault on the gas turbine parameters increases as the stator resistance rises. However, the changes remain small even when the fault severity increases by 120%. This phenomenon is associated with the fact

that the change in the electrical power demand due to the generator fault is very minor compared with the pneumatic power extracted, 7-8% from Table 4-3.

Table 4-3 Comparison of the generator power with the pneumatic power

	Pneumatic Power (kW)	Generator power imposed on the gas turbine's shaft (kW)	$\frac{P_{gen}}{P_{bl}}$	Deviation from healthy (%)
Healthy	533.54	35.53	0.07	0.00
Fault: 5%	535.28	35.72	0.07	0.19
Fault: 50%	533.74	37.42	0.07	5.28
Fault: 100%	533.96	39.65	0.07	11.50
Fault: 120%	534.07	40.59	0.08	14.13

The test case that corresponds to an increase in the stator resistance by 120% is used as a working example and, based on that, it can be observed that the increase from healthy by 14.13% leads to minor changes in the gas turbine characteristics. More specifically, the maximum change is observed in the fuel flow and the minimum change in the inlet mass flow. The only parameter that has a significant reaction under the generator fault is the excitation voltage, which increases by 38%. The excitation voltage is adjusted by the generator's controller and depends only on the gas turbine rotational speed and the generator's health state. Fault combinations that result in changes in the rotational speed affect the excitation voltage. Therefore, under such conditions, the generator's health state can be misclassified. Figure 4-13 presents an example of two fault combinations that have similar fault patterns. For FC8 the generator is healthy, and for FC9 the generator's internal resistance is increased by 3%. It is observed that both fault modes cause almost identical changes in the symptom vector. These phenomena create ambiguities in the generator's diagnosis. This will be discussed more thoroughly in Section 5.

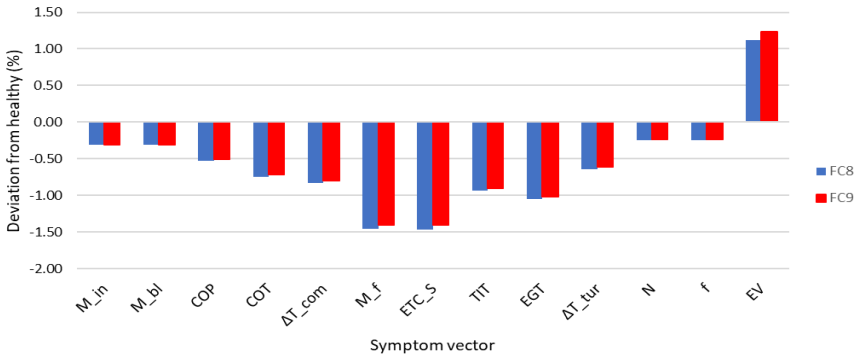

	Compressor efficiency decrease	Turbine efficiency decrease	Bleed flow decrease	SS signal bias	FMV position stuck increased from healthy state	Generator stator resistance increase
FC8	0%	0%	0%	0%	0.25%	0%
FC9	0%	0%	0%	0%	0.24%	1%

Figure 4-13 Fault combinations that result in ambiguity in the generator fault diagnosis

4.4.4 Definition of the degradation range for components considered in the diagnostic analysis

The definition of the degradation range for each component that will be considered in the diagnostic analysis is driven by two major factors: the safety-critical parameters must remain within their limits, and the injected faults should impose changes on the symptom vector parameters that are of the same order of magnitude.

As regards the analysis that is considered in this paper, the relevant safety parameters are the Exhaust Gas Temperature (EGT), which must be below 620 °C, and the rotational speed, which must be between 19,000 rpm and 21,000 rpm. The faults that increase the EGT are the compressor, turbine, FMV and generator. Based on the sensitivity assessment of these faults, the EGT reaches its maximum value when the compressor, the turbine and the generator are degraded.

The fault severity that is selected for these components, in order to keep the EGT within its limit, is 1% decrease in the efficiency of the compressor and turbine and

5% increase in the generator's stator resistance. As regards the LCV, SS and FMV faults, their degradation ranges are selected in such a way that their influence on the symptom vector is of the same order of magnitude compared with the components mentioned above. Therefore, their fault severity is selected to be: 1% reduced bleed flow for the LCV, 0.5% bias for the SS and 1% increased position for the FMV.

4.5 Diagnostic analysis

The ultimate aim of this project is to develop a diagnostic technique that can diagnose APU component faults. The diagnostic technique that is proposed in this paper uses a classification algorithm to identify each component's health state (healthy or faulty). As has been discussed in Section 4, the diagnosis of component health state under multiple faults is a challenging task, because many times different component faults result in similar fault patterns, even if the correct sensor signals are chosen for the symptom vector. The diagnostic technique that is proposed in this work aims to train diagnostic classifiers to recognise component health state under single or multiple faults.

In order to achieve this, instead of training each classifier under the single fault hypothesis, a training strategy that considers 4 different scenarios regarding the system health state (Table 4-2) is used. The fault scenarios that are considered, apart from the single fault hypothesis (Scenario 1), are the simultaneous existence of multiple component faults (Scenarios 2 and 3), and the possibility that all components have a level of degradation (Scenario 4). Thus, each classifier is trained to recognise the health state of the component under investigation while the other components can be healthy or have various fault combinations. Therefore, each classifier is able to identify unique fault features for each component fault and this allows the diagnosis of different faults that impose similar changes to the APU performance.

Data for training and testing the diagnostic classifiers are generated from the Boeing 747 APU model that has been discussed throughout this paper, and the corresponding boundary conditions that are presented in Section 4. The simulation data are then processed by supervised classification algorithms that

are included in the Matlab classification learner toolbox [35]. The algorithms that are included in Matlab are well-known classifiers (e.g. Support Vector Machine, k-nearest neighbour) and for this reason, their mathematical description is not provided in this paper. For each component under investigation, the simulation data that corresponds to the four scenarios of Table 4-1 is used to train all available classifiers, and the one that demonstrated the best classification results is selected. The classifier that is chosen for each component is shown in Table 4-2.

Training of each classification algorithm is conducted by considering the different system health scenarios in Table 4-1. 100 different simulation cases of each scenario are used to train the classifiers (4x2 scenarios from Table 4-1, 800 simulations in total). The component degradation severity for each simulation is randomly selected from the degradation range that is presented in Table 4-2. For Scenario 2, 20 faulty test cases are considered for each component (20x5 components, 100 cases in total). Finally, the component health state under Scenario 3 can be either healthy or faulty, with equal probability, for each simulation case.

The proposed methodology is tested against data corresponding to single and multiple faults for the 4 different Test Scenarios that are extracted from Table 4-1, as described below:

- Test Scenario 1 – Datasets that correspond to single faults for each component - 25 test cases for each component fault, 25 (test cases) x 6 (components) = 150 (total test cases), Figure 4-14.
- Test Scenario 2 – Datasets under which some components are healthy, while others are faulty - 25 test cases randomly generated, Figure 4-15.
- Test Scenario 3 – Datasets in which all components are faulty - 25 test cases randomly generated, Figure 4-16.
- Test Scenario 4 – Datasets in which only one component is healthy while all other components are faulty - 25 test cases for each component, 25 (test cases) x 6 (components) = 150 (total test cases), Figure 4-17.

The datasets that correspond to Test Scenarios 1-4 have been generated independently from the datasets that are used for training. The diagnostic results, for each component, are presented in the confusion matrices in Figures 4-14 – 4-17 that compare the simulated health state (vertical axis) with the classifiers' predictions (horizontal axis). For example, the symbol “GEN-H” corresponds to the generator being healthy and “GEN-F” corresponds to the generator being faulty; Figure 4-14d shows that a healthy generator has been classified correctly 18 times but misdiagnosed (as faulty) 7 times. Correct classification cases are positioned on the matrix diagonal and are shown in green. The false positives (cases diagnosed as faulty but actually healthy) and false negatives (diagnosed as healthy but actually faulty) are shown in rose and blue, respectively. To complete the table, the test cases that have an increased number of misclassifications are highlighted in yellow and are discussed in the rest of this section.

4.5.1 Test Scenario 1: single fault cases

The ability of the proposed method to detect single faults by running Test Scenario 1 is presented in Figure 4-14. Each matrix (a-f) shows the result of a single fault being classified by each individual classifier. A perfect result would be that all the classifiers showed their components as healthy, except the one fault that was being examined, which would classify all 25 cases as faulty. The results show that the compressor, LCV, SS and FMV classifiers have perfect accuracy,

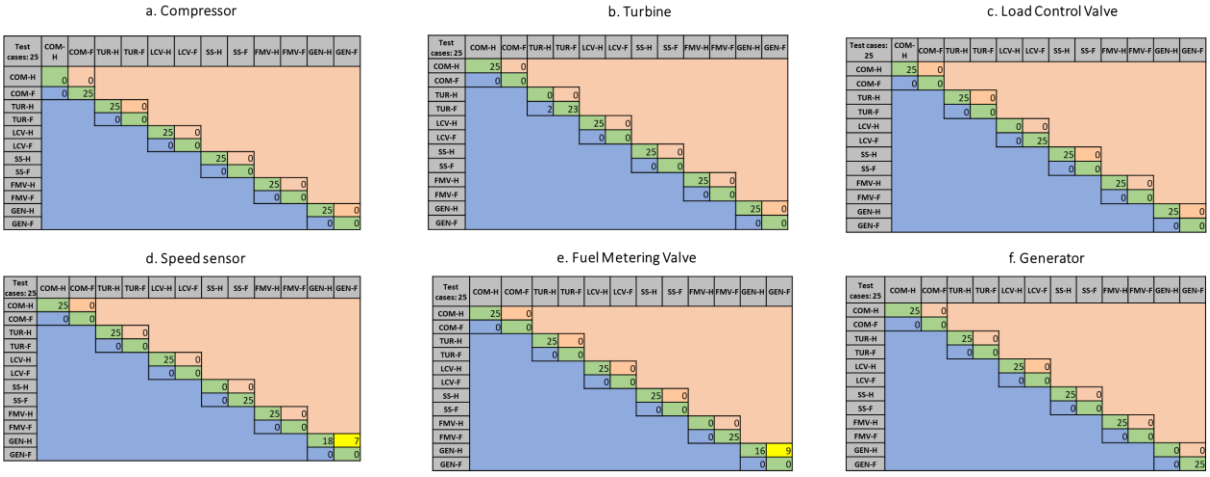

Figure 4-14 Diagnostic results for single faults

while the turbine has 2 false negatives (Figure 4-14b). The generator classifier presents false alarms when the SS or the FMV is faulty (Figures 4-14d, e).

The misclassifications for the turbine are attributed to the fact that the existence of multiple faults in the gas turbine components (compressor, turbine, and LCV) result in similar fault patterns, as it was shown in Section 4.1 (Figure 4-8). Therefore, under specific fault combinations, the gas turbine component classifiers can result in erroneous classifications. However, the diagnostic results show that, in most test cases, the compressor, turbine, and LCV classifiers can distinguish unique fault features that correspond to each component fault and can accurately diagnose the components health state under single faults. The ability of the proposed method to identify the health state of these components, even though their faults cause similar changes to the symptom vector, relies on the training strategy that takes into account the existence of multiple faults in the system.

As regards the SS classification results, a fault in the speed sensor results in a reduction in the rotational speed and, as seen in Section 4.2, this is a fault characteristic that corresponds only to the SS, hence the perfect classification. The perfect accuracy of the FMV fault is related to the fact that under this fault the control signal has a huge deviation compared to the healthy case, as seen in the sensitivity assessment (Section 4.2), and this is a unique fault characteristic for the FMV fault. As is also discussed in Section 4.2, the high deviation of the controller signal under the FMV fault is independent of the fault severity and appears for single or multiple fault cases. Thus, due to this fault characteristic, the FMV health state can be easily identified.

The generator health state is mostly diagnosed correctly but fails for test cases that correspond to SS or FMV faults (Figures 4-14d and e). As discussed in Section 4.3 the generator fault only imposes a noticeable change on the Excitation Voltage (EV), its influence on all other performance parameters being small. The EV is regulated by the generator's control unit to maintain constant output voltage, and its value depends on the generator's frequency and the armature voltage (Section 3.4, eq. (4-1) – (4-3)). As a consequence, fault

conditions that result in changes to the generator's frequency, even if the generator is healthy, will cause changes to the EV. Both the SS and the FMV faults change the generator frequency and so can be confused with a genuine generator fault. Put another way, Figure 4-9 shows a single SS fault, and Figure 4-12 a single generator fault. In the case of both the SS and generator being faulty, one of the training data scenarios which may have been labelled as a generator fault, then it is very difficult to tell the difference between this type of generator fault and a single SS fault of a higher degradation level. The same reasoning follows for the FMV case. This is a direct result of the training method chosen. If training had been performed only on single fault data, then the classifiers would have identified each fault without error.

4.5.2 Test Scenario 2: components either healthy or faulty

The diagnostic classifiers are next tested against datasets that correspond to multiple faults; Figure 4-15 presents the diagnostic results that correspond to Test Scenario 2. Under this testing scenario, there are 25 test cases in which all components could be either healthy or faulty with equal probability. Out of the 150 conditions (25x6 components), the generated cases correspond to 84 healthy components and 66 faulty ones.

Test cases: 25	COM-H	COM-F	TUR-H	TUR-F	LCV-H	LCV-F	SS-H	SS-F	FMV-H	FMV-F	GEN-H	GEN-F
COM-H	16	0										
COM-F	1	8										
TUR-H			15	0								
TUR-F			1	9								
LCV-H					12	0						
LCV-F					0	13						
SS-H							10	3				
SS-F							0	12				
FMV-H									14	0		
FMV-F									0	11		
GEN-H											7	7
GEN-F											6	5

Figure 4-15 Diagnostic results for multiple faults

The results in Figure 4-15 show that the compressor and turbine both have 1 false negative, while the LCV and FMV classifiers have perfect diagnostic accuracy. The good diagnostic results for the gas turbine components under multiple faults is attributed to the training strategy that considers multiple fault

combinations. The misclassifications that are observed are associated with the fact that these gas turbine faults can sometimes impose very similar changes on the APU performance, as explained in Section 4.1.

The SS and generator classifiers demonstrate lower accuracy. The SS classifier has 3 false positives, but no false negatives, showing that the SS classifier can recognise a fault, but can also result in false positives under specific fault conditions. These cases correspond to those in which the compressor, turbine and FMV are faulty. As was seen in Section 4.2, in such cases, if the SS fault severity is low, the changes in the SS health state do not markedly affect the symptom vector. As a consequence, the SS classifier is not able to recognise characteristic features in the symptom vector that correspond to the SS healthy or faulty state, and hence the classifier fails.

The generator classifier has 7 false positives and 6 false negatives; hence its diagnostic results are not reliable. The unsuccessful diagnostic results for the generator's classifier are related to the fact that the changes that the generator fault imposes on the gas turbine performance are negligible and any major fault is characterised by a change in EV. Therefore, SS or FMV faults that also change the EV can cause misclassification in the generator diagnosis, as it was explained in Section 5.1.

4.5.3 Test Scenario 3: all components faulty

Identification of component faults when all components are degraded, Test Scenario 3, is investigated here. The diagnostic results presented in Figure 4-16

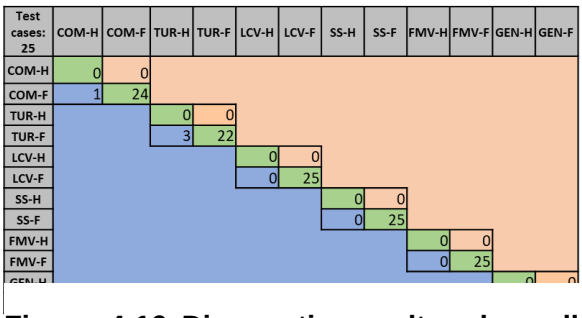

Figure 4-16 Diagnostic results when all components are degraded

show that a fault can be detected, with good accuracy, in all components apart from the generator.

More specifically, the LCV, SS and FMV have perfect fault detection accuracy, and there exists only a few false negatives for the compressor (1) and for the turbine (3). As previously discussed, the fault misclassifications for the compressor and the turbine are associated with the fact that faults in the gas turbine components result in similar changes in the APU performance. In most test cases the classifiers have accurate classification results, and this (once again) highlights the merits of the training strategy that considers multiple component faults. The unique characteristics of the SS and FMV faults, discussed in Section 5.1, are again recognised by their respective classifiers.

The generator classifier has, again, low fault detection accuracy since it has 10 false negatives, and hence the generator predictions are not trustworthy. The generator classifier fails to identify the generator's health state for the same reason that the generator diagnosis fails in Test Scenarios 1 and 2.

4.5.4 Test Scenario 4: one component healthy, all others faulty

Finally, the ability of the proposed method to identify a healthy component when all other components are degraded (Test Scenario 4) is presented in Figure 4-17. The results show that the classifiers that correspond to the compressor, turbine, LCV and FMV, can diagnose their component's health state with good

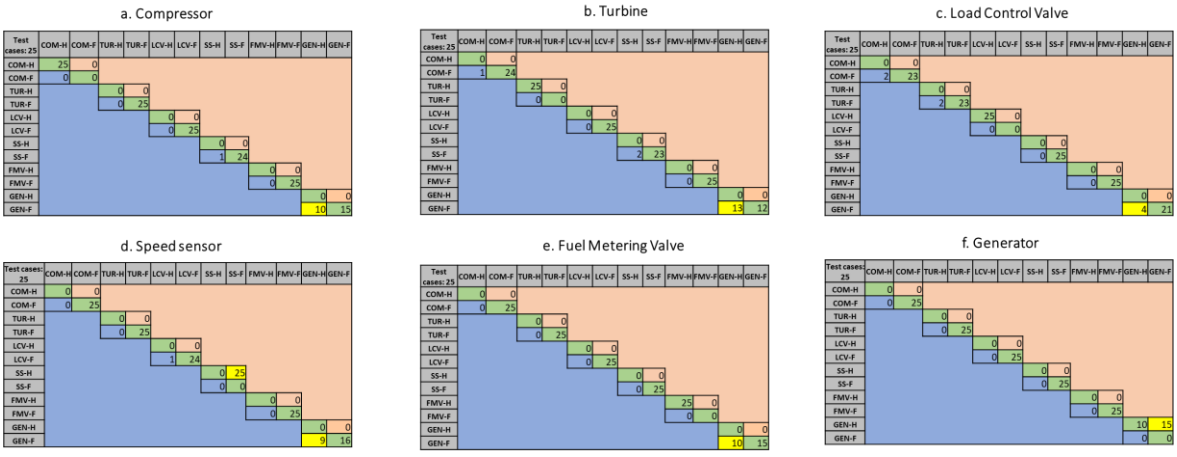

Figure 4-17 Diagnostic results when one component healthy, all others faulty

accuracy, while the SS and generator classifiers do not provide accurate predictions. Indeed, the FMV has perfect classification accuracy.

The maximum number of false negatives for the compressor, turbine, and LCV are:

- 2 each for the compressor and turbine, which correspond to the test condition where all components, apart from the LCV, are degraded (Figure 4-17c).
- 1 for the LCV, which corresponds to the test condition where all components are degraded apart from the SS (Figure 4-17d).

As has been pointed out in all the previous tests, due to the training strategy that trains the classifiers to consider the existence of multiple faults in the system, the compressor, turbine and LCV classifiers can diagnose the component's health state with a high level of accuracy for single and multiple fault conditions, even though their fault patterns are very similar. As such, the above results are seen as good.

The SS classifier cannot recognise the SS healthy state when all other components are degraded and the classification results in false alarms for all test cases (Figure 4-17 d). Under these test cases, the compressor, turbine and FMV are simultaneously degraded and, as was discussed in Section 5.2, in such cases the SS fault does not markedly influence the symptom vector. This situation does not allow the SS classifier to differentiate between healthy or faulty cases.

Finally, the generator's classifier, similarly to all the previous tests, cannot predict the generator's health state since it presents many false positives and negatives. The reason that the generator diagnosis fails when multiple faults are simultaneously degraded are the same as in the previous tests.

4.5.5 Diagnostic summary

The major findings from the diagnostics can be summarised as:

- The compressor, turbine, LCV and FMV have good classification accuracy. This is perhaps surprising as their individual degraded health results in similar changes in APU performance.
- The SS and generator classifiers do not provide reliable predictions.
- The symptom vector for these studies was chosen by engineering judgement. It could now be refined, or alternative sensors suggested, in light of these results.
- For the SS, a secondary speed sensor could be installed (redundancy) to alleviate this fault.
- For the generator, as this component is effectively de-coupled from the main gas turbine, the system diagnosis approach could be complemented with a component diagnostic approach. A sensor that provides measurement of the resistance of the generator windings can detect a fault in this component.
- The overall strategy, of training the classifiers on data sets with a mixture of faults, seems to indicate a promising way forward. In particular, the results shown as Test Scenarios 2 and 3 represent cases found in industry. The condition of a component is being examined without knowing the condition of the components around it.

4.6 Summary and Conclusions

In this paper the simulation of faults in selected components of a Boeing 747 APU is presented, and a diagnostic technique that aims to identify the health state of these components under single or multiple faults reported. The selection of the APU components is based on the most frequent component faults that have been reported by The Boeing Company and the fault mode that is simulated for each component is driven by the relevant studies in the public domain literature that discuss the component degradation mechanisms.

The aim of this work is to conduct a system level diagnostic analysis on an APU and is based on two important aspects:

- The analysis considers component faults of multiple sub-systems.
- The proposed diagnostic technique is designed to identify single and multiple faults.

Both aspects that are mentioned above, have not been sufficiently discussed by relevant studies in the public domain literature, thus, the analysis and the findings that are reported in this paper contribute to this issue.

The diagnostic technique that is proposed in this paper is able to diagnose the compressor, turbine, LCV, and FMV health state, under single and multiple faults. These faults result in similar fault patterns, and the ability of the proposed technique to identify the components health state suggests a promising way forward. The outcome of the diagnostic analysis indicates that the training of the component classifiers by considering the simultaneous existence of faults in different components is critical in the diagnosis of single and multiple faults. Also, the reasons that the SS and generator diagnosis fail are explained and based on this discussion, there are suggested ways to enhance the diagnostic results.

Finally, the results of this work suggest interesting topics that can be investigated in order to increase the system diagnostic capability. For instance, the influence of sensor noise on the symptom vector parameters would impose a further limitation on the component diagnostic. Then the ability of the diagnostic technique to distinguish between the sensors' uncertainty and the existence of component faults would be a challenging task. Also, this would set more realistic thresholds to the fault severity range. Another topic that is worthy of studying is the identification of the minimum number of sensors required to diagnose the maximum number of component faults. The answer to this question would suggest design specifications for systems that are built for fault diagnostics.

4.7 References

[1] Liu X., Liu L., Wang L., Guo Q., and Peng X., 2019, "Performance sensing data prediction for an aircraft auxiliary power unit using the optimized

extreme learning machine” *Sensors*, vol. 19, no. 18.

[2] Yabsley A. and Ibrahim Y., 2008, “Study on maintenance contribution to life cycle costs: Aircraft auxiliary power unit example” in *Proceedings of the IEEE International Conference on Industrial Technology*, Chengdu, China.

[3] Skliros C., Fakhre A., and Jennions I., 2020, “Fault Simulations and Diagnostics for a Boeing 747 Auxiliary Power Unit” *J. Eng. Gas Turbine Power*, (accepted for publication June 2020).

[4] Siebel T., Zanger J., Huber A., Aigner M., Knobloch K., and Bake F., 2018, “Experimental investigation of cycle properties, noise, and air pollutant emissions of an APS3200 auxiliary power unit,” *J. Eng. Gas Turbines Power*, vol. 140, no. 6, pp. 1–9.

[5] Gorinevsky D., Nwadiogbu E., and Mylaraswamyt D., 2002, “Model-based Diagnostics for Small-scale Turbomachines,” in *Conference of Decision and Control*, Las Vegas, Nevada.

[6] Gorinevsky D., Dittmar K., Mylaraswamy D., and Nwadiogbu E., 2002, “Model-Based Diagnostics for an Aircraft Auxiliary Power Unit,” *IEEE International Conference on Control Applications*. Glasgow, Scotland.

[7] Lei Y., Yang B., Jiang X., Jia F., Li N., and Nandi A. K., 2020, “Applications of machine learning to machine fault diagnosis : A review and roadmap,” *Mech. Syst. Signal Process.*, vol. 138.

[8] Vianna W. O. L., Gomes J. P. P., Galvão R. K. H., Yoneyama T., and Matsuura J. P., 2014, “Health monitoring of an auxiliary power unit using a classification tree,” *Proc. Annu. Conf. Progn. Heal. Manag. Soc. 2011, Montreal, Canada*.

[9] Pascoal R. M., Vianna W. O. L. L., Gomes J. P. P. P., and Galvão R. K. H. H., 2013, “Estimation of APU failure parameters employing linear regression and neural networks,” *PHM 2013 - Proc. Annu. Conf. Progn. Heal. Manag. Soc. 2013*, New Orleans, LA.

[10] Wang F., Sun J., Liu X., and Liu C., 2019, “Aircraft auxiliary power unit performance assessment and remaining useful life evaluation for predictive maintenance,” *Proc. Inst. Mech. Eng. Part A J. Power Energy*, pp. 1–13.

[11] Skliros C., Esperon Miguez M., Fakhre A., and Jennions I., 2019, “A review of model based and data driven methods targeting hardware systems diagnostics,” *Diagnostyka*, vol. 20, no. 1, pp. 3–21.

[12] Kurz R. and Brun K., “Degradation in gas turbine systems, 2001,” *J. Eng. Gas Turbines Power*, vol. 123, no. 1, pp. 70–77.

[13] Kappis W., 2013, “Impact of Degradation on the Operational Behavior of a Stationary Gas Turbine and in Detail on the Associated Compressor,” in *Turbomachinery Symposium*, Doha, Qatar.

[14] Frith P. C., 1992, “The Effect of Compressor Rotor Tip Crops,” in *International Gas Turbine and Aeroengine Congress and Exposition*, Cologne, Germany.

[15] Graf M. B. *et al.*, 1998, “Effects of non- Axisymmetric tip clearance on axial compressor performance and stability,” *J. Eng. Gas Turbines Power*, vol. 120.

[16] Frith P. C., 1992, “The effect of compressor rotor tip crops on turboshaft engine performance,” in *International Gas Turbine Aeroengine Congress and Exposition, Cologne, Germany*.

[17] Mund F. C. and Pilidis P., 2005, “Online compressor washing: A numerical survey of influencing parameters,” *Proc. Inst. Mech. Eng. Part A J. Power Energy*, vol. 219, no. 1, pp. 13–23.

[18] Fouflias D. *et al.*, 2010, “Experimental investigation of the influence of fouling on compressor cascade characteristics and implications for gas turbine engine performance,” *Proc. Inst. Mech. Eng. Part A J. Power Energy*, vol. 224, no. 7, pp. 1007–1018.

[19] Boyle R. J., 1994, “Prediction of surface roughness and incidence effects

on turbine performance," Journal of Turbomachinery, vol. 116.

[20] Diakunchak I. S., 1991, "Performance deterioration in industrial gas turbines," *J. Eng. Gas Turbines Power*, vol. 161.

[21] Shang L. and Liu G., 2011, "Sensor and actuator fault detection and isolation for a high performance aircraft engine bleed air temperature control system," *IEEE Trans. Control Syst. Technol.*, vol. 19, no. 5, pp. 1260–1268, 2011.

[22] Daigle M. J. and Goebel K., 2011, "A model-based prognostics approach applied to pneumatic valves," *Int. J. Progn. Heal. Manag.*, vol. 2, no. 2.

[23] Balaban E., Saxena A., Bansal P., Goebel K. F., and Curran S., 2009, "Modeling, detection, and disambiguation of sensor faults for aerospace applications," *IEEE Sens. J.*, vol. 9, no. 12, pp. 1907–1917.

[24] Goebel K. and Yan W., 2008, "Correcting Sensor Drift and Intermittency Faults With Data Fusion and Automated Learning," *IEEE Syst. J.*, vol. 2, no. 2, pp. 189–197.

[25] Xiao L., Meng Z., Huang X., and Ma L., 2019, "Adaptive observer based fault tolerant control for aircraft engine with sensors and actuators faults," *Chinese Control Conf. CCC*, Guangzhou, China.

[26] Balaban E., Saxena A., Bansal P., Goebel K. F., Stoelting P., and Curran S., 2009, "A diagnostic approach for electro-mechanical actuators in aerospace systems," *IEEE Aerosp. Conf. Proc.*, Big Sky, MT.

[27] Cao Y., Wang J., Xie R., and Wang X., 2015, "Fault tree analysis of electro-mechanical actuators," *Chinese Control Conf. CCC*, Hangzhou, China.

[28] Batzel T. D., Swanson D. C., and Defenbaugh J. F., 2003, "Predictive diagnostics for the main field winding and rotating rectifier assembly in the brushless synchronous generator," *IEEE Int. Symp. Diagnostics Electr. Mach. Power Electron. Drives, SDEMPED 2003, Atlanta, GA*.

[29] Batzel T. D. and Swanson D. C., 2009, "Prognostic health management of

aircraft power generators," *IEEE Trans. Aerosp. Electron. Syst.*, vol. 45, no. 2, pp. 473–483, 2009.

[30] Tantawy A., Koutsoukos X., and Biswas G., 2012, "Aircraft power generators: Hybrid modeling and simulation for fault detection," *IEEE Trans. Aerosp. Electron. Syst.*, vol. 48, no. 1, pp. 552–571.

[31] Bettocchi R., Pinelli M., Spina P. R., and Venturini M., 2007, "Artificial intelligence for the diagnostics of gas turbines - Part II: Neuro-fuzzy approach," *J. Eng. Gas Turbines Power*, vol. 129.

[32] Bettocchi R., Pinelli M., Spina P. R., and Venturini M., 2007, "Artificial intelligence for the diagnostics of gas turbines - Part I: Neural network approach," *J. Eng. Gas Turbines Power*, vol. 129.

[33] Hare J., Gupta S., Najjar N., D'Orlando P. et al., 2015, "System-Level Fault Diagnosis with Application to the Environmental Control System of an Aircraft," SAE Technical Paper 2015-01-2583, 2015, doi:10.4271/2015-01-2583.

[34] Norton J., 2015, "An introduction to sensitivity assessment of simulation models," *Environ. Model. Softw.*, vol. 69, pp. 166–174.

[35] MathWorks, "Classification Learner Documentation", accessed at June 24, 2020, https://www.mathworks.com/help/stats/classificationlearner-app.html.

5 CONCLUDING REMARKS

The development of diagnostic methods for gas turbines is an active area of research since the gas turbine engine was introduced in the aircraft. During this time the APU has, largely, been ignored. Even though many researchers have proposed various diagnostic approaches, the prompt identification of component faults in the APU is a problem that still concerns aircraft operators, manufacturer, and academics.

This situation is mainly attributed to the following reasons:

- The design characteristics for these systems are not publicly available.
- Performance data that correspond to healthy conditions as well as to known component faults, are rarely available in the public domain literature.

As a consequence, the existing diagnostic methods, are usually based on assumptions regarding the system design characteristics, as well as the influence of the component faults on the system's performance.

Also, another simplification that is usually made is related to the degradation that is developed in the components. In real-world scenarios, degradation starts to develop simultaneously in all components from the day a system is installed on the aircraft. This means that during aircraft operation, it is normal for all components to have a level of degradation. Most diagnostic approaches ignore the latter phenomenon and consider the existence of degradation in a single, or only a few components.

The existing diagnostic approaches, due to the assumptions and simplifications that are mentioned above, many times fail to correctly diagnose faults in the discussed systems. The tasks that were carried out in this Thesis aimed to address some of these gaps in the knowledge.

5.1 Project highlights

In order to conclude this Thesis, this section highlights the most important tasks that were carried out throughout this project and the most interesting ideas that were used in this research.

5.1.1 The Boeing 747 APU experimental rig

One of the major intellectual contributions of this research is the experimental investigation of a Boeing 747 APU, by discussing various aspects related with the rig development and validation, as well as the uncertainty analysis and data collection under various power settings.

The APU that is used to develop the test rig was purchased at the beginning of this project. This APU comes from a Boeing 747 aircraft that was retired and was missing maintenance logs. For this reason, this APU could not be used on an aircraft, however, it proved to be a very good platform for academic research.

An important task that was carried out in order to set up the APU rig, was the development of the control panel that is required to start, stop, and monitor the APU operation. The development of the control panel was based on the relevant information that is included in the overhaul manual. The power supply that was initially used in the control panel was not able to provide the necessary power to the electronics and this created a problem to start the APU. The fact that the power supply was responsible for the starting problem was not obvious, and for this reason, the inability of the APU to start was attributed to the control unit and the speed sensor. Finally, the problem was solved when a more powerful power supply was installed. This issue caused a delay of almost six months to the project.

Another important aspect of the rig development is related to the excitation of the electric generator. When the APU is installed on the aircraft, the generator control unit provides the appropriate excitation voltage to the generators in order to maintain the constant output voltage. However, the generator control unit was not available during the rig development, and for this reason, the excitation of the electric generator was conducted by an alternative method. The excitation voltage to the generator was provided manually by a power supply with adjustable power output. The relationship between the generator output power and the excitation voltage was established by applying various electric loads and adjusting properly the excitation voltage.

Finally, it is noted that other tasks that are related with the development of the rig, such as the initial safety inspection of the APU components and the design and installation of the inlet section and the bleed air system, required considerable time and effort.

5.1.2 The diagnostic analysis

The other important intellectual contribution of this Thesis is the development of a diagnostic technique that is able to diagnose both single and multiple component faults. The results of this analysis showed that the proposed diagnostic technique is able to identify the simultaneous existence of multiple faults in the system, even though in some cases different faults, result in similar fault patterns.

The most critical part of this technique is related to the training strategy applied to the component classifiers. Under this training strategy, each classifier is trained to recognise the health state of the component under examination, while the other components can be either healthy or faulty. This strategy has been motivated by the work conducted by Hare et al. [1] who developed a fault diagnostic technique for an aircraft ECS. The technique that was proposed in the referenced paper was properly adapted and enhanced, in order to satisfy the objectives of the case study explored in this project.

The proposed technique showed promising results in diagnosing multiple fault combinations. The discussed cases are usually found in industry; therefore, the findings of this work can be useful to aircraft operators and manufacturers.

5.2 Suggestions for future research

This research project has produced the following outcomes that can motivate future research:

- An experimental rig of a Boeing 747 APU.
- A simulation model that is calibrated against experimental data from the Boeing 747 APU rig.
- A diagnostic technique that demonstrated promising results in the identification of simultaneous component faults.

Some recommendations regarding future research that can be generated from these outcomes are given below.

An interesting topic that could be explored in a future project, is the injection of faults in selected components of the Boeing 747 APU rig. This would allow the investigation of the changes in the APU performance under the influence of these faults. Relevant studies are missing from the public domain literature; thus, the results of these experiments would provide useful insights regarding the changes in the system and component performance under faulty conditions. Also, the experimental data that correspond to faulty conditions could be used to calibrate the simulation model against component faults.

Another interesting topic for future research is the design of experiments in order to investigate the behaviour of starting stage of the APU. Similarly, to the previous approach, faults can be injected during the starting stage and changes in the relevant parameters can be identified. The observed changes in the monitored parameters can be used to create diagnostic rules for the starting stage. Also, empirical models that can simulate healthy and faulty conditions of the starting stage can be developed.

Apart from the experimental rig and the simulation model, the diagnostic analysis can also motivate future research. By taking into account the uncertainty of the parameters that are included in the symptom vector, a diagnostic technique that considers more realistic fault detection thresholds can be developed. Furthermore, the consideration of the uncertainty of the measurement in the diagnostic analysis could be used to define the requirements regarding the accuracy of the sensors.

Also, various modifications to the proposed diagnostic technique can be investigated. For instance, a comparative study can be conducted between a diagnostic technique that uses a single classifier for all component faults and the diagnostic technique that is proposed in this Thesis.

Finally, another area for further research is the identification of the minimum number of sensors that are required in order to diagnose the maximum number of faults. This topic is of great interest to aircraft manufacturers and operators since it can define the requirements for the design of new systems.

5.3 References

[1] Hare J., Gupta S., Najjar N., Orlando P. D., and Walthall R., “System-Level Fault Diagnosis with Application to the Environmental Control System of an Aircraft.” SAE Technical Paper 2015-01-2583, 2015, 2015, doi: 10.4271/2015-01-2583.

APPENDICES

Appendix A **The Boeing 747 APU Gas Turbine Simulation Model**

The Gas Turbine (GT) model used to simulate the Boeing 747 APU was developed in Simulink by leveraging the T-MATS library, which is a library of components developed by the NASA Glenn Research Centre designed to simulate thermodynamic systems. More details regarding the mathematical equations used to model the components included in the T-MATS library and the fluid properties, are reported by Chapman et al. [1] and Chapman et al. [2], and the relevant software is publicly available at GitHub [3]. This Appendix presents the architecture of the Boeing 747 APU GT model, and provides a brief description of the mathematical equations used to simulate the model's components, explains the model's convergence process and presents the methods used to modify the compressor and turbine maps, in order to simulate faults in the corresponding components. It is noted that all calculation in T-MATS are based on the Imperial Unit system, therefore the figures that present the components characteristics in this Appendix use the Imperial Unit system.

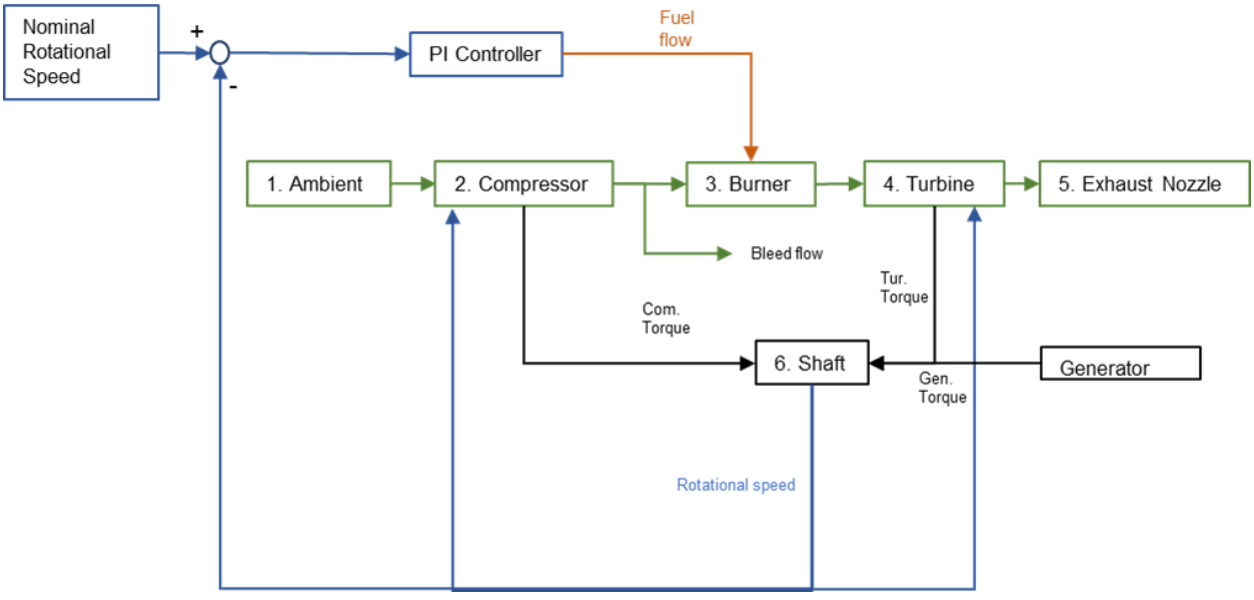

Figure A-1 The Boeing 747 Gas Turbine model schematic

The architecture of the Boeing 747 APU model is illustrated in Figure A-1. The simulation model calculates the air flow and fuel flow characteristics across the GT based on a given set of boundary conditions, which are presented in Table A-1, by using an iterative process. The model convergences to a solution when the compressor inlet mass flow rate matches the mass flow rate that corresponds to the compressor's operating point, the turbine inlet mass flow rate matches the mass flow rate that corresponds to the turbine operating point and the exhaust nozzle inlet mass flow rate matches the exhaust nozzle outlet mass flow rate. The fuel flow is adjusted in order to ensure that the APU rotational speed is maintained at its nominal value (20,000 rpm).

Table A-1 Boundary conditions for the simulation model

Boundary conditions	
1. Ambient Temperature	Environmental conditions
2. Altitude	
3. Mach n.	
4. Bleed flow	Power settings
5. Electric load	
6. Components design maps	Components characteristics
7. Components characteristics (e.g. burner pressure drop, exhaust nozzle characteristics)	

More specifically, the model's solution is calculated by a Newton-Raphson iterative solver, which calculates:

a. The compressor's operating point.
b. The turbine's operating point.
c. The inlet mass flow rate.

Independent variables

In order to minimize the differences between:

a. The compressor inlet mass flow rate and the mass flow rate that corresponds to the operating point on the compressor map.
b. The turbine inlet mass flow rate and the mass flow rate that corresponds

Dependent variables

to the operating point on the turbine map.

c. The exhaust nozzle inlet mass flow rate and the exhaust nozzle outlet mass flow rate.

The APU is a constant speed GT and in order to ensure that the rotational speed remains constant, a Proportional – Integral (P-I) controller monitors the rotational speed and adjusts the fuel flow in order to maintain the APU rotational speed at its nominal value.

In the rest of this section, there are presented the mathematical equations used to simulate the model's components according to the sequence shown in Figure A-1.

1. Ambient

Based on appropriate look-up tables in T-MATS, the "Ambient" block calculates the airflow characteristics (mass flow rate corrected for Standard Day conditions, enthalpy, temperature and pressure) at the APU inlet, according to the given boundary conditions (altitude, Mach number and the value of inlet mass flow calculated by the N-R iterative solver).

2. Compressor

The air flow characteristics calculated by the "Ambient" block, enter the compressor. The compressor characteristics are defined by the compressor map, which provides a relationship between the mass flow rate (corrected for Standard Day conditions), the pressure ratio, the isentropic efficiency and the rotational speed. The compressor map characteristics are defined by appropriate tables as shown in Figure A-2.

In order to create a compressor map that approximates the real compressor's characteristics, the compressor characteristics are calibrated appropriately. In order to conduct the compressor's calibration, the mass flow rate table, pressure ratio table and isentropic efficiency table, that correspond to an initial compressor map estimate, are

multiplied by appropriate scalars (scaling factors) in order to create a compressor map that corresponds to the real compressor's characteristics. The original compressor map for the Boeing 747 APU, as reported by Davenport [4] (Figure A-3), was used as the initial compressor map estimate. The scaling factors used in the simulations in this Thesis are presented in Table A-2. The method used to select the appropriate scaling factors is presented in Chapter 3. As regards the rotational speed, a proper scalar is used to associate the nominal rotational speed (20,000 rpm) with the 100% speed line on the compressor map. The scaled compressor map that is used in the simulation model is illustrated in Figure A-4.

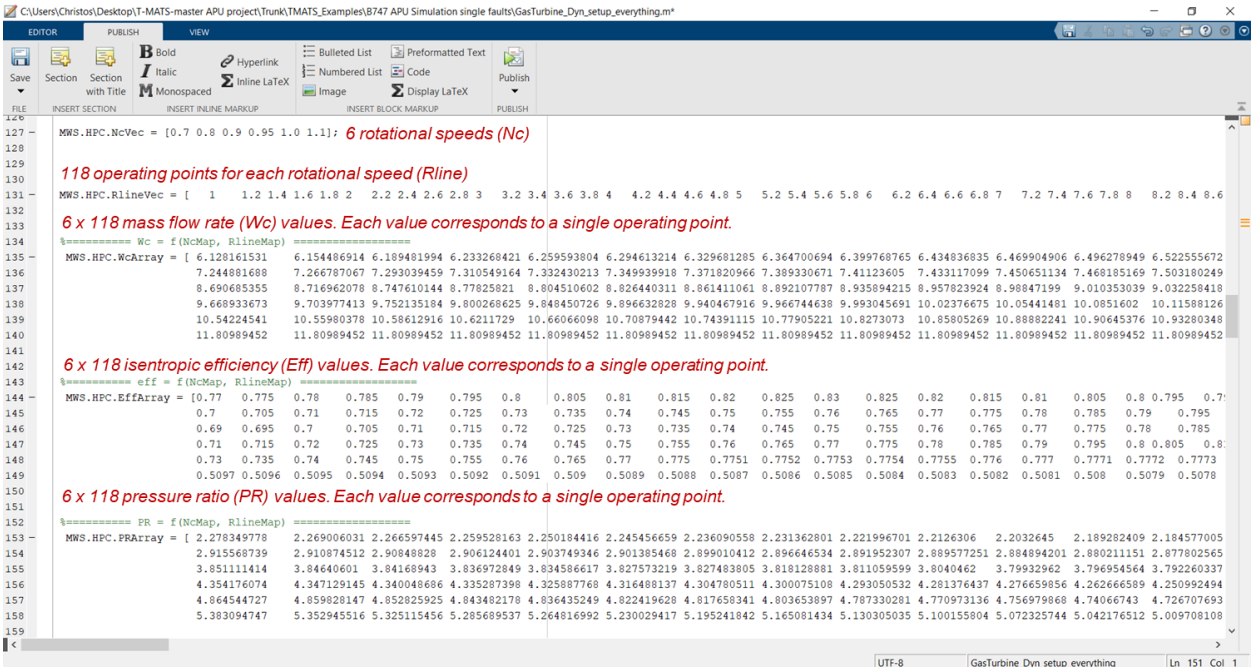

Figure A-2 Compressor performance characteristics

Faults can be injected into the compressor by modifying the compressor map characteristics. This is achieved by multiplying the scaled mass flow rate table, pressure ratio table and isentropic efficiency table (Figure A-2) with relevant scalars (health parameters), which are symbolised by $\dot{m}_{hp\_com}$, PR_{hp_com}, η_{hp_com} respectively. The value of each health parameter ranges from 0 to 1 and results in a homogenous decrease in the mass flow rate, pressure ratio and isentropic efficiency of the compressor map. For example, when $\dot{m}_{hp\_com} = 1$, $PR_{hp\_com} = 1$ and $\eta_{hp\_com} = 0.99$, there is emulated a fault

condition that results in a 1% decrease in the isentropic efficiency, while the mass flow rate and pressure ratio characteristics are not affected.

Table A-2 Compressor map Scaling Factors and Health Parameters

Parameter	Scaling Factor Definition	Scaling Factor used in the simulations	Health Parameter
Mass flow rate	$SF\_MF_{com} = \frac{MF_{com\_final}}{MF_{com\_initial}}$	2.152635	$\dot{m}_{hp\_com}$
Pressure ratio	$SF\_PR_{com} = \frac{PR_{com\_final} - 1}{PR_{com\_initial} - 1}$	0.686552	PR_{hp_com}
Isentropic Efficiency	$SF\_EFF_{com} = \frac{EFF_{com\_final}}{EFF_{com\_initial}}$	0.913536	η_{hp_com}

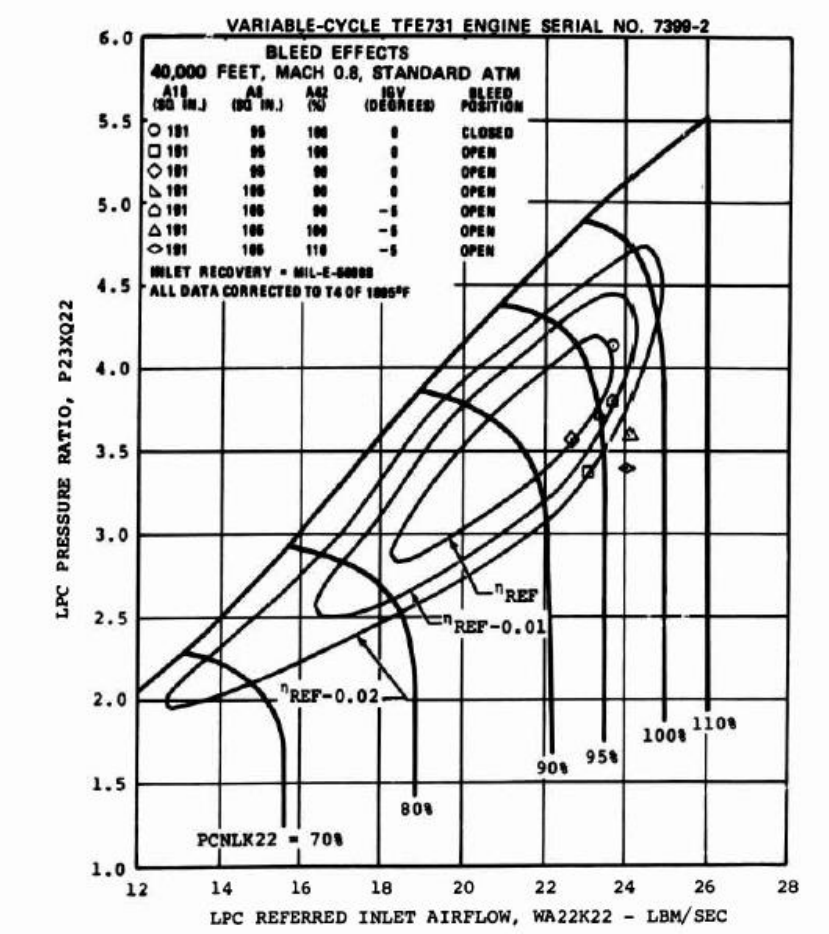

Figure A-3 Original compressor map for the Boeing 747 APU as reported by Davenport [4]

The compressor inputs are:

- The compressor's inlet air flow characteristics (corrected mass flow rate: $\dot{m}_{com\_in}$, enthalpy: $h_{com\_total\_in}$, temperature: $T_{com\_total\_in}$, pressure: p_{com_in}).
- The operating point on the compressor map (corrected mass flow rate: $\dot{m}_{com\_map}$, pressure ratio: PR_{com}, isentropic efficiency: η_{com_isen} and rotational speed: N).
- The health parameters ($\dot{m}_{hp\_com}, PR_{hp\_com}, \eta_{hp\_com}$).

The airflow characteristics at the compressor output are calculated by the relationships presented below.

Based on the inlet air flow enthalpy ($h_{com\_total\_in}$) and the isentropic efficiency that corresponds to the compressor operating point (η_{com_isen}), the outlet flow enthalpy ($h_{com\_total\_out}$) is calculated, according to eq. (A-1).

$$h_{com\_total\_out} = \frac{h_{com\_isen\_out} - h_{com\_total\_in}}{\eta_{com\_isen}} - h_{com\_total\_in} \quad \textbf{(A-1)}$$

It is noted that the compressor's outlet isentropic (ideal) enthalpy ($h_{com\_isen\_out}$) is calculated based on look-up tables in T-MATS.

The power consumed by the compressor (P_{com}) is calculated by eq. (A-2) and depends on the enthalpy difference across the compressor and the inlet mass flow rate ($\dot{m}_{com\_in}$)

$$P_{com} = \dot{m}_{com\_in} * (h_{com\_total\_out} - h_{com\_total\_in}) \quad \textbf{(A-2)}$$

The torque that is provided by the APU shaft to the compressor ($Torque_{com}$) is calculated by the compressor's power consumption (P_{com}) divided by the rotational speed (N) as shown in eq. (A-3).

$$Torque_{com} = \frac{P_{com}}{N} \quad \textbf{(A-3)}$$

The outlet air flow pressure (p_{com_out}) is calculated based on the inlet air flow pressure (p_{com_in}) and the pressure ratio that corresponds to the operating point on the compressor map (PR_{com_final}) according to eq. (A-4).

$$p_{com\_out} = p_{com\_in} * PR_{com} \quad \textbf{(A-4)}$$

Finally, it is noted that the bleed mass flow ($\dot{m}_{bleed}$) is extracted at the compressor outlet and consequently, the mass flow that is used in the combustion process ($\dot{m}_{bur\_in}$) is calculated according to eq. (A-5).

$$\dot{m}_{bur\_in} = \dot{m}_{com\_in} - \dot{m}_{bleed} \quad \textbf{(A-5)}$$

The aim of the Newton-Raphson iterative solver is to match the mass flow rate at the compressor's inlet ($\dot{m}_{com\_in}$) with the mass flow rate corresponding to the compressor's operating point ($\dot{m}_{com\_map}$). Therefore, the compressor's operating point is updated at each iteration step, until the difference between the two mass flow rates drops below a predefined threshold.

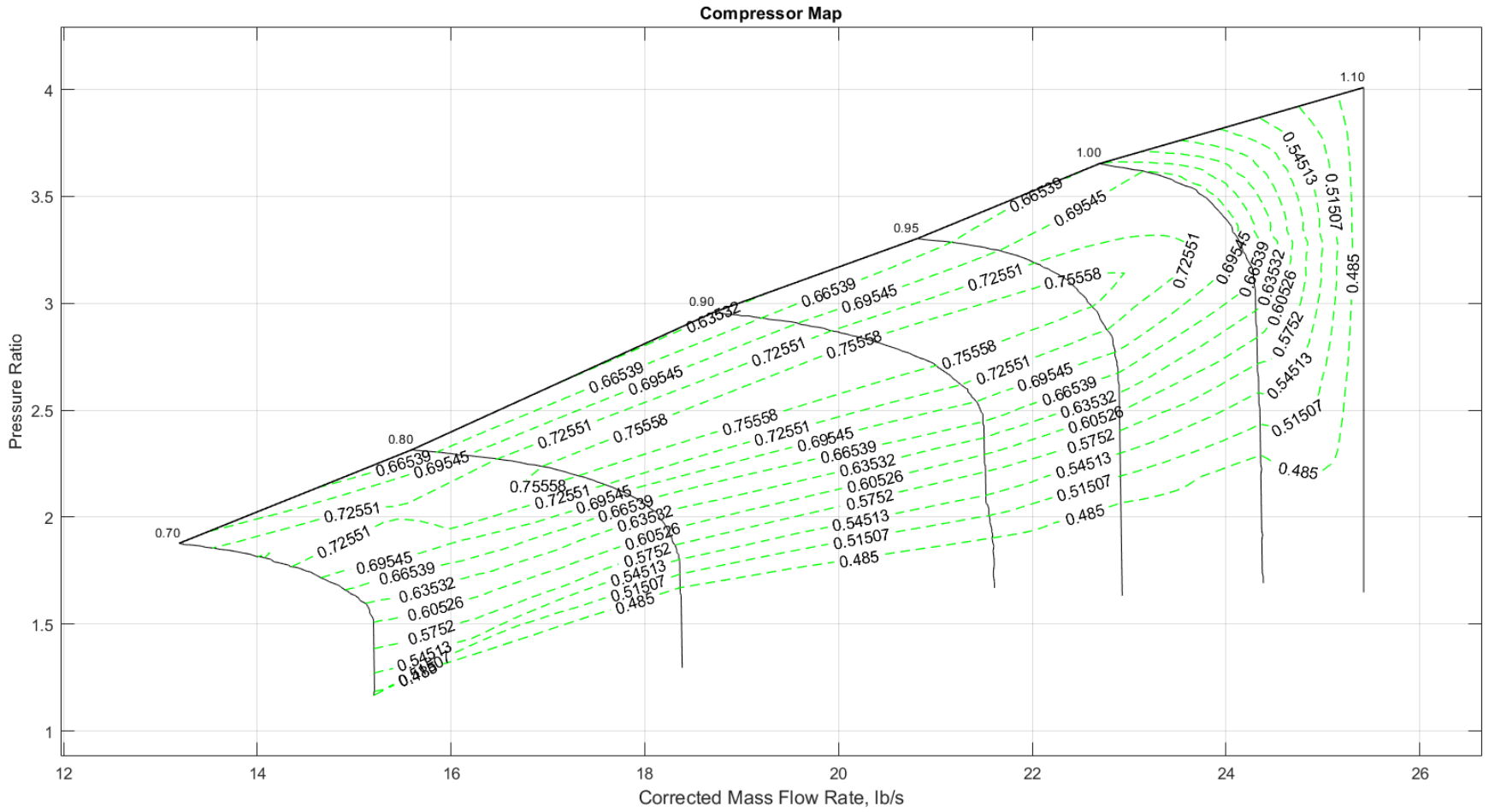

Figure A-4 Scaled compressor performance map used in the Boeing 747 APU model

3. Burner

Following the compressor, the air flow enters the burner. In this component, the air flow mixes with the fuel flow and the combustion process takes place. The burner calculates the increase in the gas flow enthalpy and the pressure drop across the combustion chamber. The burner's outlet enthalpy is based on the burner's inlet enthalpy ($h_{bur\_total\_in} = h_{com\_total\_out}$), the burner's inlet mass flow ($\dot{m}_{bur\_in}$), the fuel flow ($\dot{m}_f$), the fuel's Lower Heating Value (H_f), and the mass flow that exits the burner ($\dot{m}_{bur\_out} = \dot{m}_{bur\_in} + \dot{m}_f$) according to eq. (A-6).

$$h_{bur\_total\_out} = \frac{\dot{m}_{bur\_in} * h_{bur\_total\_in} + \dot{m}_f * H_f * \eta_{bur}}{\dot{m}_{bur\_out}} \quad \textbf{(A-6)}$$

The burner's outlet pressure depends on the burner's input pressure and the pressure drop across the burner according to eq. (A-7).

$$p_{bur\_out} = p_{bur\_in} * (1 - Burner\ pressure\ drop) \quad \textbf{(A-7)}$$

The pressure drop across the burner is selected in order the experimental data match the simulations, as described in Chapter 3.

4. Turbine

The gas flow that exits the burner enters the turbine. The turbine characteristics are defined by the turbine map which provides a relationship between the mass flow rate (corrected for Standard Day conditions), the pressure ratio, the isentropic efficiency and the rotational speed. The turbine map characteristics are defined by appropriate tables as shown in Figure A-5.

Similarly with the compressor, appropriate scalars (scaling factors) are used to modify the mass flow rate, pressure ratio and efficiency tables of an initial turbine map estimate in order to approximate the real turbine characteristics. The estimates for the mass flow rate, pressure ratio and isentropic efficiency for the turbine map were sought from turbine performance characteristics for 2-stage axial turbines as reported by Snyder and Thurman [5] (Figure A-6). The method used to select the appropriate scaling factors is

presented in Chapter 3. The scaling factor used to modify the turbine map are presented in Table A-3. As regards the rotational speed, a proper scalar associates the nominal rotational speed (20,000 rpm) with the 100% speed line on the turbine map. The scaled turbine map is presented in Figure A-7.

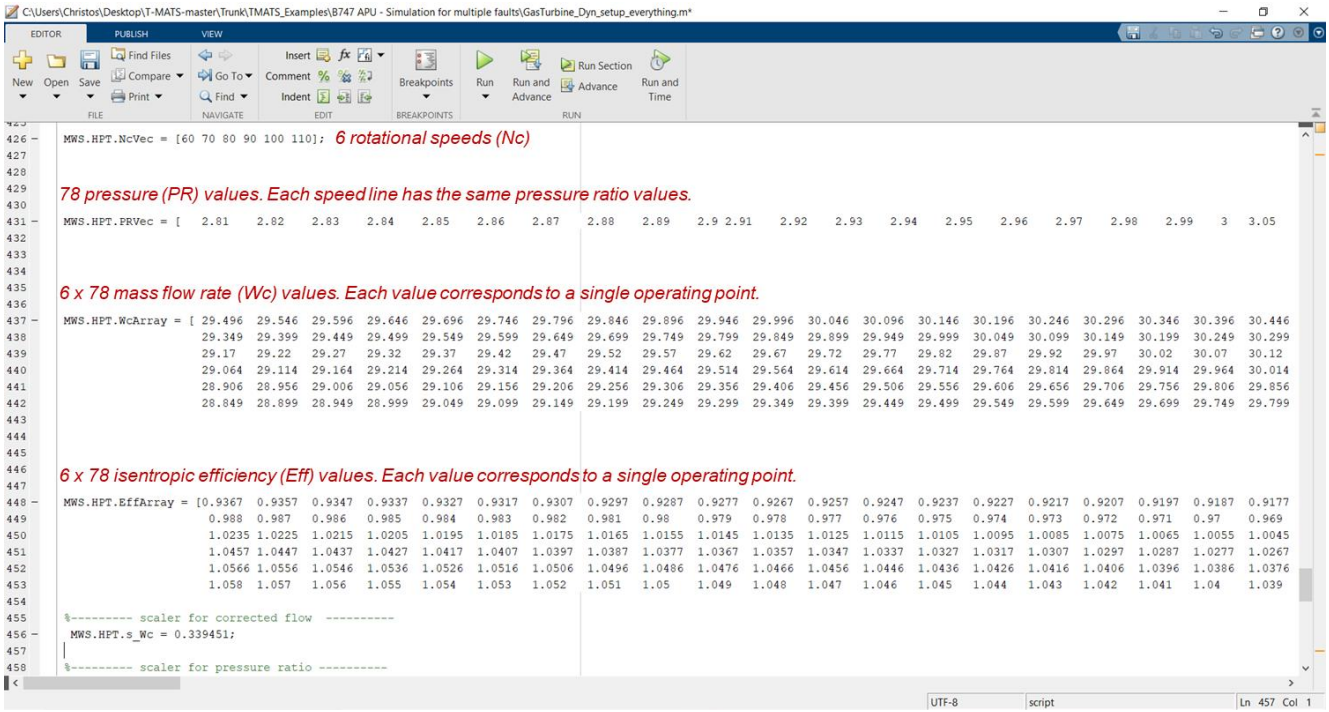

Figure A-5 Compressor performance characteristics

Fault conditions can be simulated into the turbine by modifying the turbine map characteristics. This is achieved by multiplying the scaled mass flow rate table and isentropic efficiency table (Figure A-5) with relevant scalars (health parameters), which are symbolised with $\dot{m}_{hp\_tur}$, η_{hp_tur} respectively. The value of each health parameter ranges from 0 to 1 and results in a homogenous decrease in the mass flow rate and isentropic efficiency of the turbine map. For example, when $\dot{m}_{hp\_tur} = 1$ and $\eta_{hp\_tur} = 0.99$, there is emulated a fault condition that results in a 1% decrease in the isentropic efficiency, while the mass flow rate and pressure ratio characteristics are not affected.

The inputs to the turbine are:

- The turbine's inlet flow characteristics (corrected mass flow rate: $\dot{m}_{tur\_in}$, enthalpy: $h_{tur\_total\_in}$, temperature: $T_{tur\_total\_in}$, pressure: p_{tur_in}).

- The operating point on the turbine map (corrected mass flow rate: $\dot{m}_{tur\_map}$, pressure ratio: PR_{tur}, isentropic efficiency: η_{tur_isen} and rotational speed: N).
- The turbine's health parameters ($\dot{m}_{hp\_tur}, \eta_{hp\_tur}$).

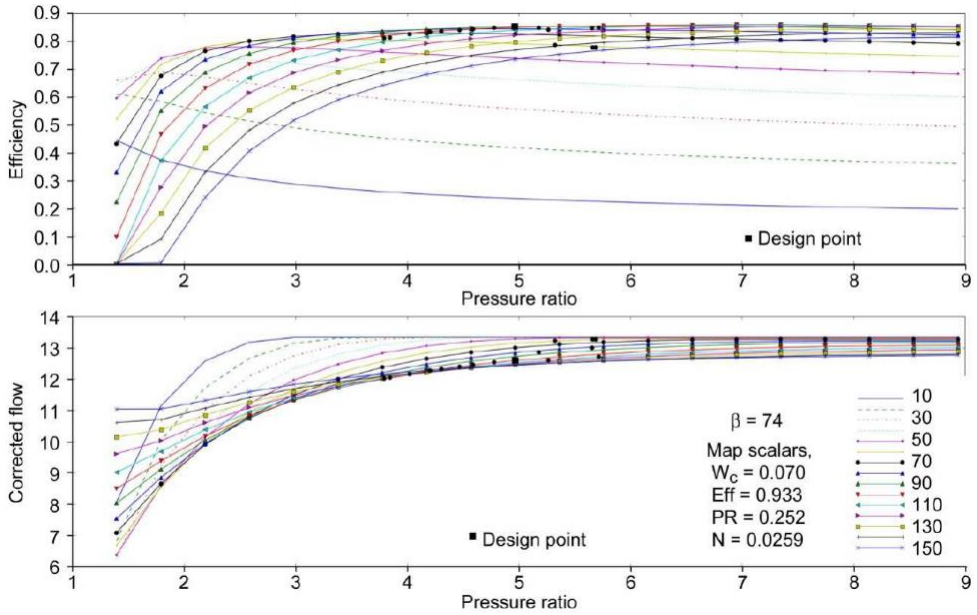

Figure A-6 Initial estimate for the turbine map taken from Snyder and Thurman [5]

The airflow characteristics at the turbine output are calculated by the relationships presented below.

The turbine outlet enthalpy ($h_{tur\_total\_out}$) is calculated based on the turbine's inlet enthalpy ($h_{bur\_total\_out} = h_{tur\_total\_in}$) and the isentropic efficiency that corresponds to the turbine's operating point ($\eta_{tur\_isen\_map}$), according to eq. (A-8).

$$h_{tur\_total\_out} = \left(h_{tur\_isen\_out} - h_{tur\_total\_in}\right) * \eta_{tur\_isen} + h_{tur\_total\_in} \qquad \textbf{(A-8)}$$

It is noted that the isentropic (ideal) enthalpy at the turbine's outlet ($h_{tur\_isen\_out}$) is calculated by look-up tables in T-MATS.

The power provided by the turbine to the APU shaft, depends on the enthalpy difference across the turbine, the isentropic efficiency that corresponds to the turbine's operating point and the turbine inlet mass flow ($\dot{m}_{tur\_in} = \dot{m}_{bur\_out}$) according to eq. (A-9).

$$P_{tur} = \left(h_{tur\_total\_in} - h_{tur\_isen\_out}\right) * \eta_{tur\_isen} * \dot{m}_{bur\_out} \quad \textbf{(A-9)}$$

Finally, the torque provided by the turbine to the APU shaft depends on the turbine's power (P_{tur}) and the rotational speed (N), according to eq. (A-10).

$$Torque_{tur} = \frac{P_{tur}}{N} \quad \textbf{(A-10)}$$

Table A-3 Turbine map Scaling Factors and Health Parameters

Parameter	Scaling Factor Definition	Scaling Factor used in the simulations	Health Parameter
Mass flow rate	$SF\_MF_{com} = \frac{MF_{com\_final}}{MF_{com\_initial}}$	0.339451	$\dot{m}_{hp\_tur}$
Pressure ratio	$SF\_PR_{com} = \frac{PR_{com\_final} - 1}{PR_{com\_initial} - 1}$	0.975059	N/A
Isentropic Efficiency	$SF\_EFF_{com} = \frac{EFF_{com\_final}}{EFF_{com\_initial}}$	0.83558196	η_{hp_tur}

The turbine's outlet pressure (p_{tur_out}), is calculated according to eq. (A-11) and depends on the turbine inlet pressure ($p_{tur\_in} = p_{bur\_out}$) and the pressure ratio that corresponds to the turbine's operating point (PR_{tur}).

$$p_{tur\_out} = \frac{p_{tur\_in}}{PR_{tur}} \quad \textbf{(A-11)}$$

As stated in the beginning of this section, the Newton-Raphson solver aims to minimize the difference between the value of mass flow rate that enters the turbine ($\dot{m}_{tur\_in}$) and the value of the mass flow rate that corresponds to the turbine's operating point ($\dot{m}_{tur\_map}$). Thus, at each step of the iterating process, the turbine's operating point is updated until the difference between the turbine inlet mass flow and the mass flow rate that corresponds to the turbine's operating point drops below a predefined threshold.

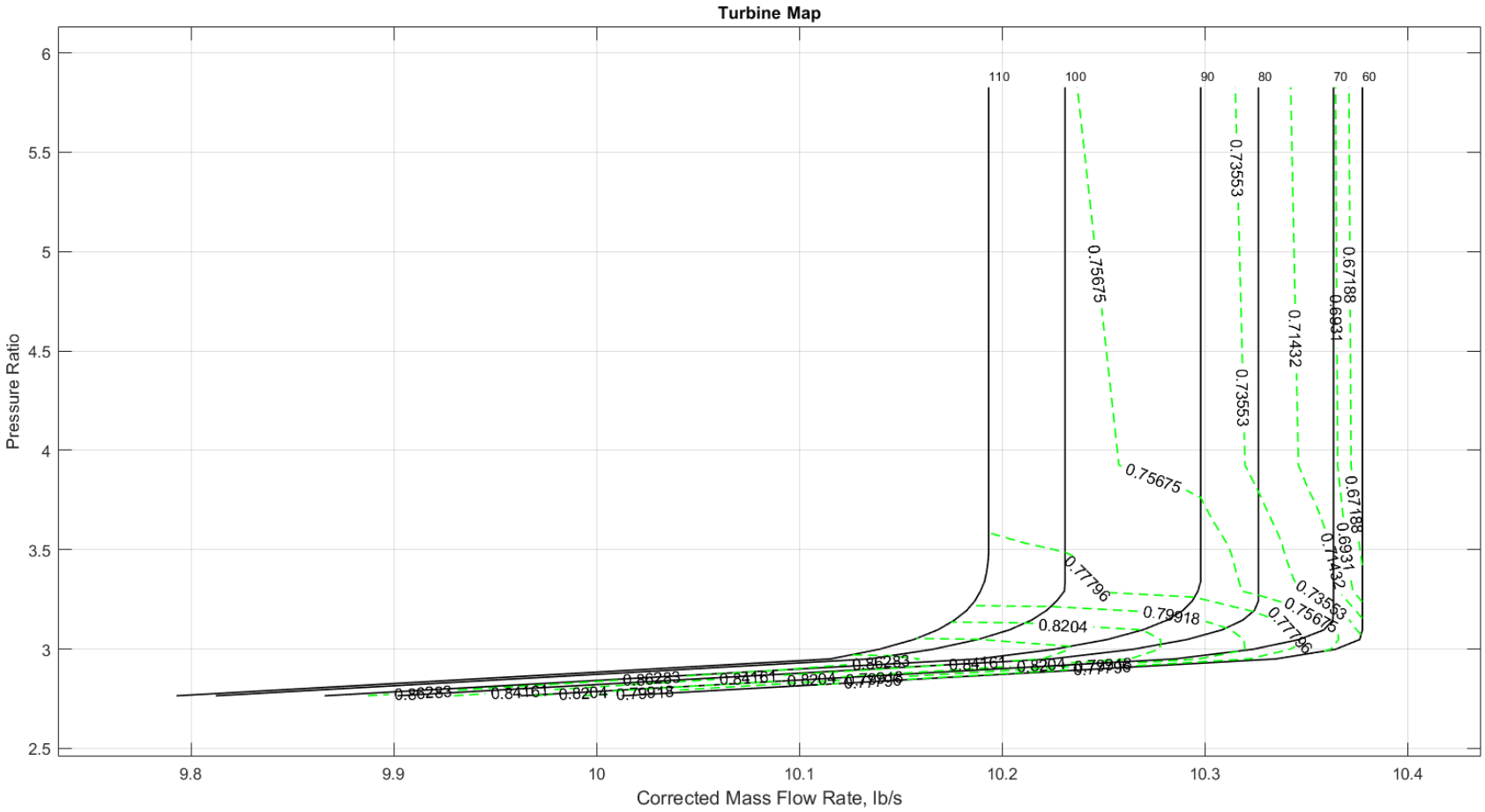

Figure A-7 Scaled turbine performance map used in the Boeing 747 APU model

5. Exhaust Nozzle

The gas flow characteristics at the turbine outlet are used by the exhaust nozzle in order to calculate the mass flow that exits the nozzle. Based on the comparison between the mass flow rate at the nozzle inlet ($\dot{m}_{noz\_in} = \dot{m}_{tur\_in}$) and the mass flow rate calculated at the nozzle outlet ($\dot{m}_{noz\_out}$), the Newton-Raphson solver updates the value of the inlet mass flow rate used to calculate the air flow characteristics at the "Ambient" block.

The mass flow rate at the nozzle outlet ($\dot{m}_{noz\_out}$) depends on the nozzle's throat area (A_{th}), the flow velocity at the throat (v_{th}) and the gas density (ρ) and is calculated according to eq. (A-12).

$$\dot{m}_{noz\_out} = \rho * v_{th} * A_{th} \quad \textbf{(A-12)}$$

The gas flow velocity at the nozzle's throat area depends on the difference between the total (h_{th_total}) and static (h_{th_static}) enthalpy at the throat according to eq. (A-13).

$$v_{th} = \sqrt{2 * \left(h_{th\_total} - h_{th\_static}\right) * g * J} \quad \textbf{(A-13)}$$

In eq. (A-13), g is the acceleration due to gravity and J is Joule's constant.

The throat's static enthalpy is calculated by look-up tables in T-MATS, by taking into account the flow characteristics at the nozzle's inlet. The density of the gas flow is calculated based on the pressure and temperature at the turbine's outlet.

The nozzle's throat area is a characteristic of the nozzle's geometry and the identification of this parameter is based on the experimental data that correspond to the APU under investigation. The methodology followed to select the value of the nozzle throat area used in this Thesis is described in Chapter 3.

6. APU shaft

The APU shaft transfers the torque produced by the turbine, to the compressor and the other power consuming components (e.g. generator). The shaft's

acceleration ($\dot{N}$) is calculated according to eq. (A-14) and depends on the sum of the torques on the APU shaft.

$$\dot{N} = \frac{60 * (Torque_{com} + Torque_{tur} + Torque_{gen})}{2 * \pi * (Shaft\ Inertia)} \quad \textbf{(A-14)}$$

If the sum of torques does not equal to zero, then the shaft is accelerating or decelerating, and consequently the rotational speed deviates from its nominal value. In such cases, the P-I controller increases or decreases the fuel flow appropriately, in order to maintain the APU rotational speed at its nominal value.

Finally, based on the iterative process presented above, when the differences between:

- the mass flow rate at the exhaust nozzle inlet and mass flow rate at the exhaust nozzle outlet,
- the compressor inlet mass flow and the mass flow that corresponds to the compressor's operating point,
- and the turbine inlet mass flow and the mass flow that corresponds to the turbine's operating point

drop below a predefined threshold, the Newton-Raphson solver converges to a solution and the air flow and fuel flow parameters take their final values according to the relationships presented throughout this Appendix.

A.1 References

[1] Chapman, J. W., Lavelle, T. M., Litt, J. S., and T. H., Guo, "A Process for the Creation of T-MATS Propulsion System Models From NPSS Data," National Aeronautics and Space Administration, Cleveland, OH, Report No.NASA/TM-2014-218409.10.2514/6.2014-3931

[2] Chapman, J. W., Lavelle, T. M., May, R. D., Litt, J. S., and T. Guo, "Propulsion System Simulation Using the Toolbox for the Modeling and Analysis of Thermodynamic Systems", July 28-30, 2014, 50th AIAA/ASME/SAE/ASEE Joint Propulsion Conference, Cleveland, OH.

[3] NASA 2020, https://github.com/nasa/T-MATS, accessed at: 18 Oct 2020

[4] Davenport, W. R., 1974, “Impact of Turbine Modulation on Variable-Cycle Engine Performance—Phase IV: Additional Design and Fabrication Engine Modification, Engine Modification and Altitude Test Part IIIb,” AiResearch Manufacturing Company of Arizona, Phoenix, Arizona, Report No. F33615-71-C-1625.

[5] Snyder, C. A., Thurman, D. R., 2010, “Gas Turbine Characteristics for a Large Civil Tilt-Rotor (LCTR),” National Aeronautics and Space Administartion, Ohio, USA, Report No. NASA/TM-2010-216089.